The Passage of Fast Electrons Through Matter

Adam P. Sorini

A dissertation submitted in partial fulfillment of
the requirements for the degree of

Doctor of Philosophy

University of Washington

2008

Program Authorized to Offer Degree: Physics

University of Washington
Graduate School

This is to certify that I have examined this copy of a doctoral dissertation by

Adam P. Sorini

and have found that it is complete and satisfactory in all respects,
and that any and all revisions required by the final
examining committee have been made.

Chair of the Supervisory Committee:

_____

John J. Rehr

Reading Committee:

_____

John J. Rehr

_____

Gerald T. Seidler

_____

Gerald A. Miller

Date: _____

In presenting this dissertation in partial fulfillment of the requirements for the doctoral degree at the University of Washington, I agree that the Library shall make its copies freely available for inspection. I further agree that extensive copying of this dissertation is allowable only for scholarly purposes, consistent with "fair use" as prescribed in the U.S. Copyright Law. Requests for copying or reproduction of this dissertation may be referred to Proquest Information and Learning, 300 North Zeeb Road, Ann Arbor, MI 48106-1346, 1-800-521-0600, to whom the author has granted "the right to reproduce and sell (a) copies of the manuscript in microform and/or (b) printed copies of the manuscript made from microform."

Signature_____

Date_____

University of Washington

Abstract

The Passage of Fast Electrons Through Matter

Adam P. Sorini

Chair of the Supervisory Committee:
Professor John J. Rehr
Physics

This work regards the passage of fast electrons through matter, and in particular how electrons scatter and lose energy within a solid. The basic quantum theory of these scattering processes was first considered in the early- to mid-20th century by Bohr, Bethe, Fermi, and others. This work extends our understanding of how a relativistic electron scatters off, and loses energy to, a complex many-body system.

The main idea of this work is that it is now possible to calculate, from first-principles, the inelastic losses of relativistic electrons in condensed matter. We present *ab initio* calculations based on a real-space Green's function approach, implemented in the `FEFF8` computer program[1]. Our work focuses on three topics: Relativistic stopping power and associated loss parameters, electron energy loss spectroscopy in high energy transmission electron microscopes, and the inelastic electron scattering mixed dynamic form factor.

We calculate, for the first time, *ab initio* stopping powers and inelastic mean free paths in real materials. The stopping powers are calculated over a broad energy range, from ten eV to above ten MeV. We also present the first *ab initio* calculations of the "mean excitation energy".

We develop a relativistic theory of inelastic electron scattering, based on *ab initio* calculations of dielectric response, and the generalized Lorenz gauge. Using our relativistic dielectric theory, we calculate the EELS magic angle ratio for boron nitride and for graphite. In these anisotropic materials we find large relativistic corrections to the magic angle for

high energy electron microscopes. We also predict and calculate large deviations in the EELS magic angle from the relativistic vacuum predictions in the low energy-loss regime. Finally, we present calculations of mixed dynamic form factor.

TABLE OF CONTENTS

LIST OF FIGURES

LIST OF TABLES

ACKNOWLEDGMENTS

A great many people have helped me complete this dissertation and my degree. First, my most sincere thanks go to my advisor, John Rehr. John gave me many great ideas for projects to work on, he was always very supportive of my work, and he taught me a lot of physics. Second, my thanks to my other advisor, Zachary Levine, who also gave me support and help with physics even though he lives 3000 miles away. Another thank you goes to my next-door neighbors Josh and Micah for helping me understand FEFF and also for letting me borrow dielectric functions and staples. Thanks to my next-next-door neighbors Mat and Greg for kindly putting up with my riddles, and putting together CM journal club. Thanks to the other journal clubbers: Wei Chen, Doug Faust, Eric Deyo, Dima Pesin, Marcel den Nijs, and Anton Andreev. Of course, I would be remiss if I didn't offer my sincere thanks to my parents for their love and support during graduate school and otherwise. I'm also thankful for the people who lay foundations for my magic angle and stopping power work, namely: P. Schattschneider, B. Jouffrey, C. Hebert, J. M. Fernández-Varea, and F. Salvat. In addition, a lot of work on calculating EELS spectra with FEFF has been done by Kevin Jorissen, which I have found very useful. I've benefited from collaboration with so many people that any list is bound to miss some. But, here's an attempt to thank even more people who helped me along the way: Tim Fister, Jerry Seidler, Joe Bradley, Ken Nagle, Eric Shirley, Cedric Powell, Aleksi Soininen, Hadley Lawler, Fernando Vila, Hans Bichsel, Jerry Miler, Ed Stern, Larry Yaffe, Matt Luzum, Rob Johnson, Brian Smigielski, Cihan Akcay, Matt Kerr, Mike Marino, Lola Sorini, and Jason Dexter. I should also love to thank Miss Christina Rohlik for putting up with me during the process of writing this thesis; she has helped me a great deal, but never with physics. Finally, I thank the National Institute for Standards and Technology for support of this work.

Chapter 1

INTRODUCTION

1.1 Historical Introduction

In 1912, Niels Bohr was busy at the Cavendish Laboratory working for Ernest Rutherford. Perhaps somewhat bored[17] with taking data in Rutherford's lab, Bohr decided to improve on some earlier work due to Darwin (*the* Darwin's grandson) regarding the theory of how alpha-particles lose energy while passing through matter.

Bohr felt that Darwin's theory "wasn't quite right mathematically"[17] and so he wrote his own, now classic, paper[18] on stopping power. He obtained a result depending a single parameter (called k) which he was forced to compute numerically. The numerical calculation was presumably a painfully tedious one, but Bohr did the calculation by hand, and found

$$k \approx 1.123 \ . \tag{1.1}$$

In less than the twinkling of an eye the computer program Mathematica tells us more exactly[1]

$$k \approx 1.122918967 \ . \tag{1.2}$$

This historical anecdote illustrates a few interesting points. One point is that the problem of calculating stopping powers in particular, and electronic losses in general, has a long and impressive history that involves some of the greatest physicists of the 20th century. The other point is that sometimes ordinary mortals like us can gain a small advantage over the old masters like Bohr[18, 19, 20] and Bethe[21] and Fermi[7], because we have more powerful computers.

---

[1] Actually, we can do even better–the exact value is $2/e^{\gamma}$, where γ is the Euler-Mascheroni constant.

By the way, the title of this thesis is an allusion to the title of a paper[21] by Bethe. In that paper Bethe presents one of the first calculations of electronic stopping power based on quantum mechanics.

1.2 Goals

Early theoretical work was at a loss to describe, from first principles, the effect of real condensed matter systems on the scattering of electrons. The calculations necessary for a proper description are numerically intense and have only become possible in recent years with the advent of modern high-powered computers.

The goal of this work is the calculation, from first-principles, of inelastic losses of relativistic electrons in condensed matter. To that end we have completed work on a number of different projects, presented in Chapters 3, 4, and 5. All this work relies on a real-space multiple-scattering Green's function approach implemented in the FEFF8[1] computer program, which is most well-known for theoretical calculations of x-ray absorption. This work extends that well-established and useful Green's function technology from calculations for x-rays to relativistic electrons. A version of the `FEFF8` program for calculating relativistic dipole EELS spectra has recently been developed by Kevin Jorissen[22]. The very useful work done by Jorissen is completely separate from our work on relativistic EELS; we calculate a screened relativistic EELS magic angle, not dipole spectra.

We present novel relativistic broad-spectrum calculations of the "stopping power" and "inelastic mean free path" applicable to relativistic and non-relativistic electrons. These calculations are the first *ab initio* calculations of this type. In addition we also calculate, from first-principles, the "mean excitation energy" for five different solids: aluminum, silicon, copper, silver, and gold. The mean excitation energy is an important "parameter" from the relativistic theory of stopping. Historically, this "parameter" is interesting because it is where Bethe hid all of the difficult many-body quantum mechanics. The mean excitation energy is difficult to calculate from first-principles because it depends on the broad-spectrum response of the material.

In this work we also develop a relativistic *ab initio* theory of the EELS magic angle that includes the effects of dielectric screening. Using this relativistic dielectric theory we

calculate the EELS magic angle for boron nitride and graphite. The EELS magic angle is an important parameter used in transmission electron microscopy of anisotropic materials. Our calculations show large relativistic corrections to the non-relativistic magic angle for high energy microscopes, in agreement with experiment. We also predict and calculate large corrections to the magic angle in the low energy-loss regime where dielectric response is large.

Formally, all of the above calculations may be considered as reductions (energy moments, for example) of a linear response function called the "mixed dynamic form factor" (MDFF). The MDFF is a generalization of van Hove's "dynamic form factor" (DFF). We present *ab initio* calculations of the MDFF (which may be reduced to the DFF) within the framework of real-space multiple-scattering Green's function theory. Additionally, our work on EELS may also be of interest in the field of non-resonant inelastic x-ray scattering (NRIXS). The reason is due to the fact that both of these spectroscopies determine the "dynamic form factor" (DFF) of the system (see Eqs. 1.7 and 1.9), at least within the Born approximation. However, in order to correctly interpret and compare spectra from these two different spectroscopies an account must taken of the relativistic effects in EELS. Recently, an extension of the `FEFF` program was developed for calculating NRIXS spectra via the DFF[23]. We utilized this program, and the relationship between NRIXS and EELS, in our work on the MDFF.

1.3 Dissertation Overview

This dissertation is organized as follows: In Chapter 1 the motivation, goals and overview are presented. Chapter 1 also briefly introduces and describes three interesting spectroscopies; In Chapter 2 we present an assortment of basic theory to which we will refer back from subsequent chapters. We feel this chapter is useful because the next two chapters are based on published journal articles[24, 25] and do not include detailed information about basic material; In Chapter 3 we present an *ab initio* approach for calculating the stopping power and inelastic mean free path associated with electrons traversing a solid. We also present calculations (for a variety of solids) which span a broad spectral range from low incident electron kinetic energies (circa the plasma energy) up to and including the case of relativistic

electron incident kinetic energies; In Chapter 4 we consider relativistic effects in electron microscopy. We start from a fully relativistic theory and show how to properly include transverse field effects which are often ignored in condensed matter theory. Interesting relativistic effects which occur in anisotropic materials are investigated. In particular the electron energy-loss "magic angle" is calculated, including relativistic corrections, for a variety of materials; In Chapter 5 we present numerical calculations of the mixed dynamic form factor for a few materials; In Chapter 6 we give our concluding remarks; In the Appendix we give details regarding the computer programs we developed in order to perform the numerical calculations presented in this thesis.

1.4 Overview of Spectroscopies

This thesis is about spectroscopy–in particular electron energy-loss spectroscopy (EELS). But, formally, the expression for the EELS cross-section is quite similar to the cross-section for a number of other spectroscopies. This formal similarity is due to an underlying physical similarity, namely, that the system which gets kicked is the same regardless of what does the kicking. Here we compare and contrast three different spectroscopies: x-ray absorption (XAS), EELS, and non-resonant inelastic x-ray scattering (NRIXS).

1.4.1 XAS

The electric field of an x-ray can be used to "kick" an electron in a sample of condensed matter. The sample electron feels a force ("kick"), and thus a change of momentum, parallel to the polarization. Formally, this kick is due to a coupling between the electron and the x-ray (of angular frequency ω) which may[2] be taken to have the form

$$H_{\text{int}} = -E_0 \hat{\epsilon} \cdot \hat{\mathbf{d}} \tag{1.3}$$

where $\hat{\epsilon}$ is a unit vector specifying the polarization of the x-ray, and $\hat{\mathbf{d}}$ is the dipole operator

$$\hat{\mathbf{d}} = -e \sum_{i=1}^{N} \hat{\mathbf{r}}_i \ ,$$

[2]This is hardly obvious, nor correct in all situations. We choose this simple form for the coupling for illustrative purposes.

where $-e$ is the charge[3] of the electron. The quantity E_0 is the magnitude of the x-ray electric field. The "hat" on the polarization indicates that it is a unit vector. The "hat" on the dipole operator indicates that it is an operator.

From the interaction of Eq. (1.3) we obtain the cross-section for absorption from the ground state $|\Psi_0\rangle$ of the Hamiltonian H_0 by application of Fermi's golden rule[26]

$$\sigma(\omega) = \frac{4\pi^2\omega}{c} \sum_m |\langle\Psi_m| \hat{\epsilon}^* \cdot \hat{\mathbf{d}} |\Psi_0\rangle|^2 \delta(E_0 + \hbar\omega - E_m) \,, \tag{1.4}$$

where $\hbar$ is the reduced Planck constant and c is the speed of light. Eq. (1.4) can be rewritten as

$$\sigma(\omega) = \frac{2\pi\omega}{\hbar c} \int dt e^{i\omega t} \langle\Psi_0| \hat{d}_{\hat{\epsilon}}(t) \hat{d}^\dagger_{\hat{\epsilon}}(0) |\Psi_0\rangle \,, \tag{1.5}$$

where

$$\hat{d}_{\hat{\epsilon}}(t) = e^{i\hat{H}t/\hbar} \hat{\epsilon} \cdot \mathbf{d} e^{-i\hat{H}t/\hbar} \,.$$

1.4.2 EELS

Electrons can "kick" other electrons just as well as x-rays. Again this "kick" results in an amount $\hbar\mathbf{q}$ of momentum being transfered to the sample. In EELS the kick is due to a coupling between the electrons which may[4] be taken to have the form

$$H_{\text{int}} = \frac{4\pi e^2}{q^2 \mathcal{V}} \hat{n}^\dagger_{\mathbf{q}} \,, \tag{1.6}$$

where $\mathcal{V}$ is a normalization volume[5] for the probe electron and where $\hat{n}^\dagger_{\mathbf{q}}$ is the density fluctuation operator

$$\hat{n}^\dagger_{\mathbf{q}} = \sum_{i=1}^{N} e^{i\mathbf{q}\cdot\hat{\mathbf{r}}_i} \,.$$

---

[3] We use gaussian units where the dimensions of e^2 are energy times length.

[4] This is hardly obvious, nor correct in all situations. We choose this simple form for the coupling for illustrative purposes.

[5] The golden rule formula contains a probe-electron phase-space factor which cancels one factor of the normalization volume. The other normalization volume factor is canceled by the probe-electron incident flux factor.

From the interaction of Eq. (1.6) we obtain the cross-section for scattering from the ground state $|\Psi_0\rangle$ of the Hamiltonian H_0 by application of Fermi's golden rule[26]

$$\frac{d\sigma}{d(\hbar\omega)d\Omega} = \frac{k_f}{k_0}\left(\frac{2me^2}{(\hbar q)^2}\right)^2 \sum_m \left|\langle\Psi_m| n_{\mathbf{q}}^\dagger |\Psi_0\rangle\right|^2 \delta(E_0 + \hbar\omega - E_m) \,, \tag{1.7}$$

where $\hbar\omega$ is the energy lost by the probe electron scattered into solid angle Ω, and where m is the mass of the electron. Eq. (1.7) can be rewritten as

$$\frac{d\sigma}{d(\hbar\omega)d\Omega} = \frac{k_f}{2\pi\hbar k_0}\left(\frac{2me^2}{(\hbar q)^2}\right)^2 \int dt e^{i\omega t} \langle\Psi_0| \hat{n}_{\mathbf{q}}(t)\hat{n}_{\mathbf{q}}^\dagger(0) |\Psi_0\rangle \ .$$

For small $q = |\mathbf{q}|$ and non-zero energy-loss this can be rewritten as

$$\frac{d\sigma}{d(\hbar\omega)d\Omega} = \frac{q^2 k_f}{2\pi\hbar k_0}\left(\frac{2me}{(\hbar q)^2}\right)^2 \int dt e^{i\omega t} \langle\Psi_0| \hat{d}_{\hat{q}}(t)\hat{d}_{\hat{q}}^\dagger(0) |\Psi_0\rangle \ ,$$

which, apart from the prefactor, is quite similar to Eq. (1.5).

1.4.3 NRIXS

An x-ray may be scattered as well as absorbed. Just as in the EELS case, the scattering results in a "kick" to the sample. The kick imparts momentum $\hbar\mathbf{q}$ and energy $\hbar\omega$ to the sample. Here, the energy transfered to the sample $\hbar\omega$ is equal to the difference $\hbar(\omega_i - \omega_f)$ of incoming and outgoing x-ray energies. In non-resonant x-ray scattering, the kick is due to a coupling which may[6] be taken to have the form

$$H_{\text{int}} = \frac{2\pi\hbar e^2}{m\mathcal{V}\sqrt{\omega_i\omega_f}} \hat{\epsilon}_i \cdot \hat{\epsilon}_f^* n_{\mathbf{q}}^\dagger \,, \tag{1.8}$$

where $\hat{\epsilon}_i$ and $\hat{\epsilon}_f$ are the incoming and outgoing x-ray polarizations, respectively.

From the interaction of Eq. (1.8) we obtain the cross-section for scattering from the ground state $|\Psi_0\rangle$ of the Hamiltonian H_0 by application of Fermi's golden rule[26]

$$\frac{d\sigma}{d(\hbar\omega)d\Omega} = \frac{\omega_f}{\omega_i}\left(\frac{e^2}{mc^2}\right)^2 |\hat{\epsilon}_i \cdot \hat{\epsilon}_f^*|^2 \sum_m |\langle\Psi_m| \hat{n}_{\mathbf{q}}^\dagger |\Psi_0\rangle|^2 \delta(E_0 + \hbar\omega - E_m) \,, \tag{1.9}$$

where the similarity with Eq. (1.7) is apparent. Eq. (1.9) can also be rewritten as

$$\frac{d\sigma}{d(\hbar\omega)d\Omega} = \frac{\omega_f}{2\pi\hbar\omega_i}\left(\frac{e^2}{mc^2}\right)^2 |\hat{\epsilon}_i \cdot \hat{\epsilon}_f^*|^2 \int dt e^{i\omega t} \langle\Psi_0| \hat{n}_{\mathbf{q}}(t)\hat{n}_{\mathbf{q}}^\dagger(0) |\Psi_0\rangle \ .$$

---

[6] This is hardly obvious, nor correct in all situations. We choose this simple form for the coupling for illustrative purposes.

Thus, NRIXS, just like all the other spectra, can be written in terms of a two-particle correlation function

$$\langle \Psi_0 | \, \hat{n}_{\mathbf{q}}(t) \hat{n}^{\dagger}_{\mathbf{q}}(0) \, | \Psi_0 \rangle = \int d^3x d^3x' e^{i\mathbf{q}\cdot(\mathbf{x}-\mathbf{x}')} \, \langle \Psi_0 | \, \hat{\psi}^{\dagger}(\mathbf{x},t) \hat{\psi}(\mathbf{x},t) \hat{\psi}^{\dagger}(\mathbf{x}',0) \hat{\psi}(\mathbf{x}',0) \, | \Psi_0 \rangle \ .$$

For non-interacting particles in orbitals $|i\rangle$ having energies λ_i, where the ground state is a Slater determinant made up of the lowest N orbitals, this correlation function can be written as

$$\sum_{i \leq N} \sum_{j > N} \langle i | \, e^{i\mathbf{q}\cdot\hat{\mathbf{r}}} \, | f \rangle \, \langle f | \, e^{-i\mathbf{q}\cdot\hat{\mathbf{r}}} \, | i \rangle \, e^{i(\lambda_i - \lambda_j)t} \ . \tag{1.10}$$

Chapter 2

BASIC THEORY

2.1 Electromagnetism

In this section we review the relevant classical electromagnetism that underlies many of the ideas presented in this thesis. Our system of electrostatic units is defined and various response functions are introduced. The concept of a "generalized Lorenz gauge", which will be applied to calculations later in this thesis, is also introduced. We also introduce the classical stopping power.

2.1.1 Dielectric Response

Nearly the entire content of this thesis will revolve around the linear response of condensed matter systems (briefly, "the system") to electromagnetic fields. Thus we begin with a brief review of the dielectric[27] theory of linear response. Within the framework of linear response, the "electric field"[28] (**E**) and the "electric displacement" (**D**) are related by

$$D_i = \epsilon_{ij} E_j \ , \tag{2.1}$$

where we have introduced the "dielectric tensor" ϵ_{ij}. The spatial and temporal dependence of the dieletric tensor have been suppresed in Eq. (2.1) pending a discussion of causality.

2.1.2 Maxwell's Equations

Ignoring the difference between **B** and **H** we now write down, for completeness and to set notation, the basic equations of electrodynamics[28, 29, 30]:

$$\nabla \cdot \mathbf{B} = 0 \ , \tag{2.2}$$

$$\nabla \times \mathbf{E} = -\frac{1}{c}\frac{\partial \mathbf{B}}{\partial t} \ , \tag{2.3}$$

$$\nabla \times \mathbf{B} = \frac{4\pi \mathbf{j}_{\rm tot}}{c} + \frac{1}{c}\frac{\partial \mathbf{E}}{\partial t} \ , \tag{2.4}$$

$$\nabla \cdot \mathbf{E} = 4\pi\rho_{\text{tot}} \ , \tag{2.5}$$

where we employ the Gaussian system of units here and throughout this thesis.

Because the system under consideration is electrically neutral on the whole (neglecting any "external" charge we may inject) we immediately separate the "polarization" charge and current (ρ and $\mathbf{j}$, respectively) from the "external" charge and current (ρ_{ext} and $\mathbf{j}_{\text{ext}}$, respectivly);

$$\rho_{\text{tot}} = \rho + \rho_{\text{ext}} \ , \tag{2.6}$$

$$\mathbf{j}_{\text{tot}} = \mathbf{j} + \mathbf{j}_{\text{ext}} \ . \tag{2.7}$$

We next introduce the "polarization" $\mathbf{P}$ by the following definitions[29]:

$$\rho = -\nabla \cdot \mathbf{P} \ , \tag{2.8}$$

$$\mathbf{j} = \frac{\partial \mathbf{P}}{\partial t} \ . \tag{2.9}$$

The physical interpretation of the polarization is that it is the dipole moment per unit volume[29, 27].

From Maxwell's equations, $\frac{\partial \rho_{\text{tot}}}{\partial t} = -\nabla \cdot \mathbf{j}_{\text{tot}}$. From Eqs. (2.8) and (2.9), so too does the continuity equation hold for the polarization density and polarization current. And thus so too does the continuity equation hold for the "external" charge and "external" current.

Using Eqs. (2.8) and (2.9), We may now rewrite Maxwell's equations in the form

$$\nabla \cdot \mathbf{B} = 0 \ , \tag{2.10}$$

$$\nabla \times \mathbf{E} = -\frac{1}{c}\frac{\partial \mathbf{B}}{\partial t} \ , \tag{2.11}$$

$$\nabla \times \mathbf{B} = \frac{4\pi \mathbf{j}_{\text{ext}}}{c} + \frac{1}{c}\frac{\partial \mathbf{D}}{\partial t} \ , \tag{2.12}$$

$$\nabla \cdot \mathbf{D} = 4\pi\rho_{\text{ext}} \ , \tag{2.13}$$

where

$$\mathbf{D} \equiv \mathbf{E} + 4\pi\mathbf{P} \ . \tag{2.14}$$

Within the context of linear response, we define the polarizability tensor α_{ij} as the proportionality constant between the polarization and the electric field

$$P_i = \alpha_{ij} E_j \ , \tag{2.15}$$

so then

$$\epsilon_{ij} = \delta_{ij} + 4\pi\alpha_{ij} \ . \tag{2.16}$$

We define conductivity tensor σ_{ij} as the proportionality constant between the polarization current and the electric field

$$j_i = \sigma_{ij} E_j \ . \tag{2.17}$$

It is also possible to relate σ_{ij} to α_{ij} and to ϵ_{ij}; each of the three contain all the information about the sample available within the framework of linear response.

We will also find it useful to define a response function which relates the external potential (the potential for $\mathbf{D}$) to the system density. This definition is most useful when we can ignore the transverse part of the electric field and thus consider only electric potentials. In this case

$$\mathbf{E} = -\nabla\phi \ , \tag{2.18}$$

$$\mathbf{D} = -\nabla\phi_{\text{ext}} \ , \tag{2.19}$$

$$\phi = \epsilon^{-1}\phi_{\text{ext}} \tag{2.20}$$

and

$$\rho = \chi\phi_{\text{ext}} \ , \tag{2.21}$$

where

$$\epsilon^{-1} = 1 + v\chi \ . \tag{2.22}$$

In the above equations spatial and temporal indices are still suppressed, and v is the Coulomb potential. For example, in momentum space we have

$$\epsilon^{-1}_{\mathbf{q},\mathbf{q}'}(\omega) = \delta_{\mathbf{q},\mathbf{q}'} + \frac{4\pi}{q^2}\chi_{\mathbf{q},\mathbf{q}'}(\omega) \ . \tag{2.23}$$

2.1.3 Gauge Fields

It is somewhat amusing that for our field of interest (energy-loss spectroscopy) we can concentrate entirely on just a single Maxwell equation

$$\nabla \times \mathbf{B} = \frac{4\pi}{c}\mathbf{j}_{\text{ext}} + \frac{1}{c}\frac{\partial \mathbf{D}}{\partial t} \ , \tag{2.24}$$

rather than four different equations. This is so because we obviate the two source-free Maxwell equations by introducing gauge fields ϕ and $\mathbf{A}$ via

$$\mathbf{E} = -\nabla\phi - \frac{1}{c}\frac{\partial \mathbf{A}}{\partial t} \tag{2.25}$$

$$\mathbf{B} = \nabla \times \mathbf{A} \ , \tag{2.26}$$

and then we note that (for $\omega \neq 0$) the remaining Maxwell equation is just the longitudinal part of Eq. (2.24).

It is well-known that the gauge fields are not specifed entirely by Eqs. (2.25) and (2.26), but rather there is a residual "gauge freedom". We can exploit this gauge freedom in an interesting way when dealing with condensed matter by using auxiliary information about the sample. In order to see how best to exploit our gauge freedom let us rewrite Eq. (2.24) in terms of the gauge fields and also Fourier transform with respect to space and time. We obtain

$$\left(\delta^{ij}q^2 - q^i q^j\right) A_j = \frac{4\pi}{c} j^i_{\text{ext}} - \frac{i\omega}{c}\epsilon^{ij}\left(-iq_j\phi + \frac{i\omega}{c}A_j\right) \ .$$

Here we have used the following Fourier transform conventions:

$$A_i(\mathbf{q},\omega) \equiv \int d^3x dt e^{-i\mathbf{q}\cdot\mathbf{x}+i\omega t} A_i(\mathbf{x},t) \ , \tag{2.27}$$

and similarly for other functions. The inversion of Eq. (2.27) is given by

$$A_i(\mathbf{x},t) \equiv \int \frac{d^3q}{(2\pi)^3}\frac{d\omega}{2\pi} e^{+i\mathbf{q}\cdot\mathbf{x}-i\omega t} A_i(\mathbf{q},\omega) \ . \tag{2.28}$$

For the case when the dielectric tensor is diagonal

$$\epsilon^{ij} = \delta^{ij}\epsilon \ ,$$

we have

$$\left(q^2 - \frac{\omega^2}{c^2}\epsilon\right) A^i - q^i\left(\mathbf{q}\cdot\mathbf{A} - \frac{\omega\epsilon}{c}\phi\right) = \frac{4\pi}{c}\mathbf{j}_{\text{ext}} \ ,$$

which suggests that we choose the gauge where

$$\mathbf{q}\cdot\mathbf{A} = \frac{\omega\epsilon}{c}\phi \ .$$

This is known as the "generalized Lorentz [sic] gauge"[29] or the "generalized Lorenz gauge". When in vacuum, where $\epsilon = 1$, the generalized Lorenz gauge reduces to the usual Lorenz gauge.

In the generalized Lorenz gauge we thus have

$$\mathbf{A} = \frac{4\pi}{c}\mathbf{j}_{\text{ext}}\frac{1}{q^2 - \epsilon\omega^2/c^2} ,$$

and

$$\phi = \frac{4\pi}{\epsilon}\rho_{\text{ext}}\frac{1}{q^2 - \epsilon\omega^2/c^2} .$$

2.1.4 Classical Stopping

As a quick example, consider the electric field due to a swiftly moving "delta-electron". That is, consider

$$\rho_{\text{ext}}(\mathbf{r}, t) = \delta(\mathbf{r} - \mathbf{v}_0 t) ,$$

for constant $\mathbf{v}_0$. In this case the scalar potential is

$$\phi = -\frac{4\pi e}{\epsilon}2\pi\delta(\mathbf{q}\cdot\mathbf{v}_0 - \omega)\frac{1}{q^2 - \epsilon\omega^2/c^2} ,$$

and the vector potential is

$$\mathbf{A} = -\frac{4\pi e}{c}\mathbf{v}_0 2\pi\delta(\mathbf{q}\cdot\mathbf{v}_0 - \omega)\frac{1}{q^2 - \epsilon\omega^2/c^2} = \frac{\mathbf{v_0}}{c}\epsilon\phi ,$$

and thus the electric field is

$$\mathbf{E}(\mathbf{q}, \omega) = -4\pi e i 2\pi\delta(\mathbf{q}\cdot\mathbf{v}_0 - \omega)\frac{\left(\mathbf{v}_0\frac{\omega}{c^2} - \frac{\mathbf{q}}{\epsilon}\right)}{q^2 - \omega^2/c^2\epsilon} . \tag{2.29}$$

When a fast electron passes by another charged object we usually think that most of the momentum transfered to the other object is perpendicular to the path. This is because the force exerted parallel to the path "on the way in" is nearly canceled "on the way out". However, the total force on the delta-electron parallel to the incident direction is not zero. In fact, the force parallel to the path is just what we would like calculate–the classical stopping power. The total field $\mathbf{E}$ takes into account the response of the sample electrons via the dielectric constant. These electrons will slow the delta-electron and we can easily

find the stopping power by simply evaluating the magnitude of the force in the incident direction at the location of the delta-electron.

$$S \equiv -\frac{\delta W}{\delta x} = -\mathbf{v}_0 \cdot \mathbf{F}/v_0 = \frac{e}{v_0}\mathbf{v}_0 \cdot \mathbf{E}(\mathbf{x} = \mathbf{v}_0 t, t) \ , \tag{2.30}$$

where the apparent time-dependence on the right hand side (RHS) of the equation actually drops out due to the uniform motion of the delta-electron. Explicitly, we plug into Eq. (2.30) using Eq. (2.29) and find

$$S = \frac{e^2 i}{2v_0^2\pi^2}\int d^2q_\perp d\omega \frac{\omega}{\epsilon(\omega)}\frac{\left(1-\epsilon\beta^2\right)}{\left(q_\perp^2 + \omega^2/v_0^2(1-\epsilon\beta^2)\right)} \ ,$$

where $\beta \equiv v_0/c$, and where we pause to emphasise and forshadow (see Chapter 4) the appearance of the factor

$$h(\omega) \equiv (1 - \epsilon v_0^2/c^2) \equiv (1 - \epsilon\beta^2) \ ,$$

which reduces to the usual "relativistic gamma" for $\epsilon = 1$ and reduces to 1 in the non-relativistic limit. Continuing now with the evaluation of the classical stopping power we have to cut off the momentum integral at $q_\perp^2 \equiv q_c^2$. The integral must be cut off because it is (logarithmically) divergent. The divergence comes from the fact that we assume the classical continuum electrodynamic description of the force on the point charge holds for all wavelengths (all values of $\mathbf{q}$). This is not actually true since large values of momentum transfer occur for collisions in which the delta-electron passes very close to a single atom. Thus in these situation the continuum description does not hold. After cutting off the momentum integral we find

$$S = \frac{\omega_p^2 e^2}{v_0^2}\left(\log\left(\frac{q_c v_0}{I}\right) - \frac{i}{2\pi\omega_p^2}\int d\omega \frac{\omega}{\epsilon}h(\omega)\log(h(\omega)/(1+\omega^2 h/q_c^2 v_0^2))\right) \ , \tag{2.31}$$

where ω_p^2 is the "plasma frequency"

$$\frac{\pi}{2}\omega_p^2 = -\int_0^\infty d\omega\omega \mathrm{Im}(1/\epsilon) \ ,$$

and I is the "mean excitation energy"

$$-\log(I) = \frac{\int_0^\infty d\omega\omega\log(\omega)\mathrm{Im}(1/\epsilon)}{\pi\omega_p^2/2} \ ,$$

and where we used

$$\int d\omega \frac{\omega}{\epsilon}(1-h)\log(\omega_c^2/\omega^2) = 0 \ .$$

The final term in Eq. (2.31) can be simplifed by taking $q_c \to \infty$ to find

$$\frac{\omega_p^2 e^2}{v_0^2}\frac{-i}{2\pi\omega_p^2}\int d\omega \frac{\omega}{\epsilon} h\log(h) \ ,$$

which is zero in the non-relativistic limit.

Eq. (2.31) is about as far as we can go without invoking quantum mechanics to determine the cutoff q_c. One exception is for the case of a heavy (of mass M) non-relativistic incident particle, for which we set $h = 1$ and $q_c = 2Mv_0$ to find the expected expression

$$S_{\rm heavy,non-relativistic} = \frac{\omega_p^2 e^2}{v_0^2}\log(2Mv_0^2/I) \ .$$

But, even this expression is worthless without knowledge of the "parameter" I which must be calculated using quantum mechanics. This parameter is calculated in Chapter (3). For rough estimates one can often get away with $I = 10Z$ electron volts[31, 32], where Z is the atomic number of the elements making up the sample.

2.2 Causality and Linear Response

Here we give a brief discussion of causality and its practical applications to electron energy-loss spectroscopy. The discussion is presented from both a dielectric and a quantum mechanical point of view. The electronic Hamiltonian is introduced as well as various relevant "interaction" terms. Fermi's golden rule is stated and discussed for relevant cases. We also give a number of properties and definitions pertaining to correlation functions.

2.2.1 Dielectric Response

It may come as a surprise that the dielectric tensor (defined in the previous section) is *not* a response function. By this we mean that the dielectric tensor does not, in general, respect causality[33, 34]; the dielectric tensor gives the response to the *total* field, which cannot, in general, be controlled externally. On the other hand, the *inverse* dielectric tensor is a true response function;

$$\epsilon_{ij}^{-1}(t) = 0 \qquad \text{if} \ \ t < 0 \tag{2.32}$$

regardless of the other suppressed arguments. Here, we have written the inverse dielectric tensor as a function of a single time argument. This is possible due to temporal homogeneity which we shall see explicitly and formally later on.

Because of Eq. (2.32) we can write the Fourier transform of the inverse dielectric tensor

$$\epsilon_{ij}^{-1}(\omega) \equiv \int_{-\infty}^{\infty} dt e^{i\omega t} \epsilon_{ij}^{-1}(t) = \int_{0}^{\infty} dt e^{i\omega t} \epsilon_{ij}^{-1}(t) \tag{2.33}$$

as an integral over only positive times. From the above equation we see that the convergence of the integral on the right hand side is only improved if ω is analytically continued into the upper-half complex-plane (UHP). Thus, $\epsilon^{-1}(\omega)$ is analytic in the UHP as a result of causality.

Now it is time to unveil the other arguments of the inverse dielectric function and to specify when the dielectric function can be regarded as a response function. In general, we have

$$E_i(\mathbf{x}, t) = \int dt' d^3x' \epsilon_{ij}^{-1}(\mathbf{x}, \mathbf{x}'; t - t') D_j(\mathbf{x}', t') \ . \tag{2.34}$$

For simplicity of presentation we specialize to a homogeneous system for which the dielectric function depends only on the difference between position arguments. Then, Fourier transforming with respect to space and time, we have

$$E_i(\mathbf{q}, \omega) = \epsilon_{ij}^{-1}(\mathbf{q}, \omega) D_j(\mathbf{q}, \omega) \ . \tag{2.35}$$

The quantities ω and $\mathbf{q}$ refer to the frequency and wavevector of the perturbing field, respectively. Thus, $\mathbf{q} = 0$ means that the perturbing field is of infinite wavelength.

In the $\mathbf{q} = 0$ case, it turns out, the dielectric function may also be considered as a response function along with the inverse dielectric function. This can be understood physically[34]; the dielectric function determines response to an external *potential* whereas the inverse dielectric function determines response to an external *charge*. It is only in the infinite wavelength limit that we can truly control, and let the system respond to, an external potential (e.g., a system fixed in between a parallel-plate capacitor). In order to control an external potential with finite wavelength, slabs of metal (capacitor plates) would have to be embedded in the system itself which is not allowable. On the other hand we can shoot

in an external probe charge which has Fourier components at all wavelengths to which the system will respond.

So, we expect on physical grounds that necessarily at $q = 0$ the dielectric function has no poles in the UHP. We show this by proving that the ($q = 0$) *inverse* dielectric function has no zeros in the UHP. To this end one may consider the integral

$$\int_C \frac{dw}{\epsilon^{-1}} \frac{d\epsilon^{-1}}{d\omega} \ , \tag{2.36}$$

where the contour is a large semi-circle in the UHP. This integral is proportional to the number of zeros minus the number of poles of the inverse dielectric function in the UHP. Or, since it has no poles, Eq. (2.36) is proportional to the number of zeros of ϵ^{-1} in the UHP. We proceed to show that Eq. (2.36) is equal to zero.

The integral in Eq. (2.36) is equal to an integral in the complex ϵ^{-1} plane

$$\int_{C'} \frac{d\epsilon^{-1}}{\epsilon^{-1}} \ , \tag{2.37}$$

where the contour C' does not encircle the origin.[1] An example of the contour C' is shown for the specific case of aluminum nitride in Fig. (2.1). Thus the integral is zero and the $q = 0$ inverse dielectric function has no zeros or poles in the UHP and thus similarly the $q = 0$ dielectric function has no zeros or poles in the UHP.

2.2.2 Quantum Mechanics

The basic problem in quantum mechanics[35, 36, 37, 38], whether relativistic or non-relativistic, whether field-theoretical or not, is the solution of the time-dependent Schrödinger equation

$$\hbar \frac{\partial \left|\Psi\right\rangle}{\partial t} = -i\hat{H}(t) \left|\Psi\right\rangle \ , \tag{2.38}$$

[1] This relies on the fact that $\mathrm{Im}(\epsilon(\omega)) > 0$ if $\omega > 0$, which is a result of the fact that the system gets hotter when irradiated.[29] Actually, it is not obvious how to show this for general systems, but for the systems considered in this thesis which have real magnetic permeability the arguments given in Ref. [29] are adequate. See also the sentence following Eq. (2.68). The proof of the causal nature of the dielectric function for $\mathbf{q} = 0$ also relies on $\epsilon(\mathbf{0}, 0)$ being real and positive, which can be thought of as due to the empirical fact that when a dielectric material is introduced into a parallel plate capacitor with fixed plate charge the potential difference drops.[27] From an atomic perspective this last point is obvious from the fact that "opposites attract" and thus the static polarization is parallel rather than anti-parallel to the electric field.

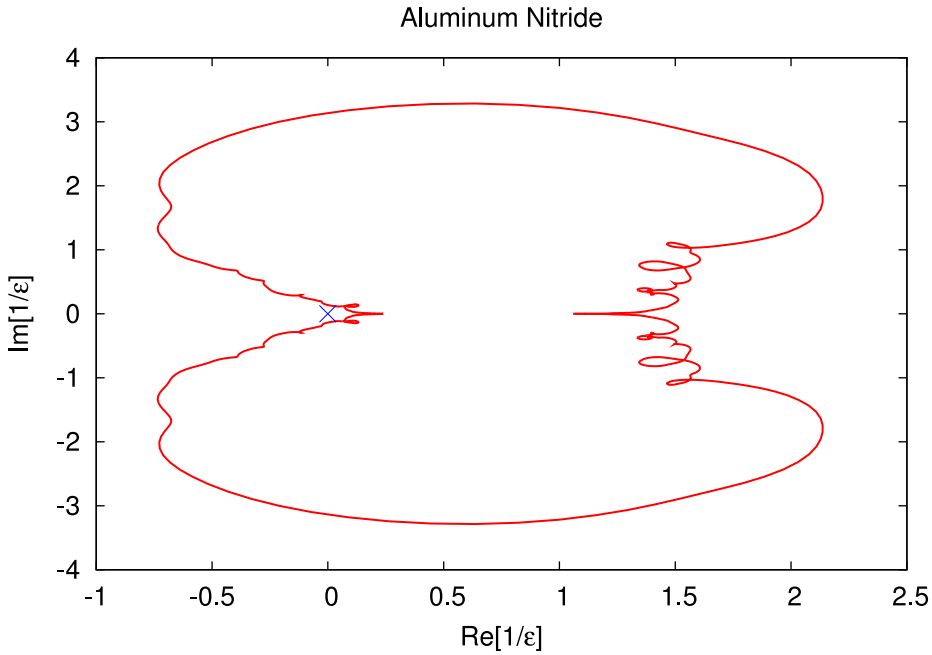

Figure 2.1: The contour C' of Eq. (2.37) for the specific case of aluminum nitride. Note that, although the contour is very complicated, it never encircles the pole at the origin, indicated by the blue 'X'.

where $\hbar$ is the reduced Planck constant, and where $\hat{H}(t)$ is the total Hamiltonian of the system under consideration which may be explicitly time-dependent due to external interactions. The appropriate Hamiltonian may usually[2] be obtained by taking the classical Hamiltonian of the corresponding classical system and replacing the dynamical variables ($\mathbf{r}$ and $\mathbf{p}$) of each particle with operators ($\mathbf{r}$ and $\mathbf{p}$). In this work we will often denote operators and their corresponding classical variables with the exact same notation. This is a lamentable, yet standard, practice. When the difference between operators and numbers is not obvious from context we will include a "hat" $\hat{}$ on the operator. Other observables are obtained in the same way as the Hamiltonian and are thus represented by Hermitian operators. In general these operators may have explicit time dependence, but in many important cases the operators of interest are not explicitly time dependent. The expectation value of such an operator $\hat{X}$ is then given by

$$X(t) = \langle \Psi(t) | \hat{X} | \Psi(t) \rangle \ . \tag{2.39}$$

An example of an important operator in the study of condensed matter is the N-body[39] electronic Hamiltonian, which we denote as H_0^s

$$H_0^s = \sum_{i=1}^{N} \left(\frac{1}{2} \frac{p_i^2}{m_e} + v_{\text{ext}}(\mathbf{r_i}) + \frac{1}{2} \sum_{j \neq i} \frac{e^2}{|\mathbf{r}_i - \mathbf{r}_j|} \right) + \dots \ , \tag{2.40}$$

where the p_i are the electron momentum operators, the r_i are the electron position operators, m_e is the mass of the electron, e^2 is the squared charge of the electron[3], and $v_{\text{ext}}(\mathbf{x})$ is a time-independent "external" potential which makes the system inhomogeneous. For example, if we consider the "external" potential to be composed of a monatomic lattice of point nuclei having charge Ze then we have

$$v(\mathbf{x}) = -\sum_{\mathbf{R}} \frac{Ze^2}{|\mathbf{x} - \mathbf{R}|} \ , \tag{2.41}$$

[2]Unfortunately, this is not always the case as we can easily see by considering a physical quantity such as spin, which has no classical counterpart. Apparently, there may exist terms in the quantum Hamiltonian (such as spin terms) which vanish as $\hbar \to 0$.

[3]Remember that we use Gaussian units whereas in S. I. units $e^2 \to q^2/4\pi\epsilon_0$, where q is called the "charge" in S.I. units. The physics, however, is simply that the Coulomb potential is e^2/r which tells us all we need to know.

where $\{\mathbf{R}\}$ is the set of lattice vectors.

From now on we choose our units such that $m_e = e = \hbar = 1$. Except for different conventions regarding the sign of e (which we define as positive), this choice of units is known as "(Hartree) atomic units". The atomic unit of energy is called the "Hartree" ($1H \approx 27.2\text{eV}$). The atomic unit of length is called the "Bohr" ($1B \approx 0.529\text{Å}$). Other units can be derived, but don't have special names. For example, the atomic unit of time is $\hbar/(27.2\text{eV}) \approx 0.0242\text{fs}$.

We have included an explicit ellipsis in Eq. (2.40) to indicate that the given terms on the RHS are by no means complete. However, the terms that we have written are the most important terms for a study of most condensed matter phenomena. For example, our approximation of a fixed "external" lattice is equivalent to completely disregarding the intereaction of phonons and electrons. We certainly could introduce a kinetic term for the nuclei and thus treat the $\mathbf{R}$ as dynamical quantum variables. Very often we do not have to use the RHS of Eq. (2.40) explicitly. If we ever do need an explicit expression for H_0^s then we can just use the RHS of Eq. (2.40) without the ellipsis as a first approximation.

One other thing that is missing from Eq. (2.40) is the "transverse" interaction between the electrons. That is, the electrons are only allowed to interact via a "longitudinal"[4] Coulomb force. This missing interaction is most important for the case of relativistic electrons. This oversight will be explicitly remedied in our Chapter on EELS and the Magic Angle.

If we consider a closed system then the Hamiltonian H of Eq. (2.38) is a function only of the operators $\mathbf{r}$ and $\mathbf{p}$ of each particle in the system and is not explictly time-dependent. Although we may always redefine what we mean by the "system" in order make sure H has no explicit time-dependence, it is not always convenient to do so.

2.2.3 Interaction Picture

If we are interested in doing perturbation theory, it is convenient to define wave functions and operators in the so-called "interaction picture". In this picture we consider our Hamiltonian

[4]We say "longitudinal" because the field can be written as the gradient of a scalar, thus the Fourier transform is proportional to the wave-vector.

to be split into a sum of two parts

$$H(t) = H_0 + V(t) \ ,$$

where H_0 is called the "unperturbed" Hamiltonian and is often time-independent and $V(t)$ is called the perturbation which may or may not be explicitly time-dependent. For example, if we are interested in treating the interaction of a system with an external time-dependent field then $V(t)$ has the same time-dependence as the field. Or, if we are interested in treating internal inter-particle interactions in perturbation theory then V is time-independent.

In the interaction picture we define a wave function

$$\left|\Psi^I(t)\right\rangle = e^{iH_0 t} \left|\Psi(t)\right\rangle \ ,$$

which satisfies

$$\frac{\partial \left|\Psi^I(t)\right\rangle}{\partial t} = -iV^I(t) \left|\Psi^I(t)\right\rangle \ , \tag{2.42}$$

where

$$V^I(t) \equiv e^{iH_0 t} V(t) e^{-iH_0 t} \ ,$$

may have both explicit and implicit time-dependence. In general, operators in the interaction picture are defined as

$$X^I = e^{iH_0 t} X e^{-iH_0 t} \ .$$

Since Eq. (2.42) is linear in the time-derivative we may write down the unique solution at all times if we know the wave-function at a single instant in time (t_0). This is done as follows, we integrate both sides of Eq. (2.42) from t_0 to t giving an integral equation

$$\left|\Psi^I(t)\right\rangle = \left|\Psi^I(t_0)\right\rangle - i \int_{t_0}^{t} dt' V^I(t') \left|\Psi^I(t')\right\rangle \ .$$

We then substitute the expression on the RHS into the last term on the RHS giving

$$\left|\Psi^I(t)\right\rangle = \left|\Psi^I(t_0)\right\rangle - i \int_{t_0}^{t} dt' V^I(t') \left(\left|\Psi^I(t_0)\right\rangle - i \int_{t_0}^{t'} dt'' V^I(t'') \left|\Psi^I(t'')\right\rangle \right) \ .$$

Repeating this procedure ad infinitum we obtain

$$\left|\Psi^I(t)\right\rangle = T\left(e^{-i\int_{t_0}^{t} dt' V^I(t')} \right) \left|\Psi^I(t_0)\right\rangle \ , \tag{2.43}$$

where T is Dyson's "time-ordering operator" which rearranges operators according to their time argument with later times on the left.

A very useful special case of Eq. (2.43) is when the interaction picture wave-function is known to coincide with an eigenstate of the unperturbed Hamiltonian at the initial time (which we take to be $t_0 = -\infty$). In particular, if the interaction picture wavefunction is known to equal the ground state of the unperturbed Hamiltonian $|\Psi_0\rangle$ we then have

$$\left|\Psi^I(t)\right\rangle = T\left(e^{-i\int_{-\infty}^{t} dt' V^I(t')}\right)|\Psi_0\rangle \ . \tag{2.44}$$

Typically, we will consider perturbations which are turned on at $t = -\infty$. Interestingly, we could even treat inter-particle interactions in this way, even though it does not make much physical sense to "turn off" those interactions[40].

2.2.4 Fermi's Golden Rule

Fermi's golden rule[26] (number 2) is a useful first-order result for calculating "transition rates". We give a brief and reckless derivation here, with the promise that the end result is correct. We give a more careful derivation of the cross-section formula for EELS in a later Section.

For now, we simply expand Eq. (2.44) to lowest order and find

$$\left|\Psi^I(t)\right\rangle = |\Psi_0\rangle - i\int_{-\infty}^{t} dt' V^I(t')\,|\Psi_0\rangle \ . \tag{2.45}$$

Here we have assumed that the interaction gets turned on in the distant past (i.e., at $t = -\infty$). To implement this formally we replace the interaction

$$V(t) \to V(t)e^{\delta t} \ ,$$

where δ is a positive infinitesimal.

Then the probability amplitude that the state evolves into an eigenstate $|\Psi_m\rangle \neq |\Psi_0\rangle$ of the unperturbed Hamiltonian at time t is given to linear order as

$$A_{0\to m\neq 0} = -i\int_{-\infty}^{t} dt e^{i(E_m - E_0)t' + \delta t'} \langle\Psi_m|\, V(t')\,|\Psi_0\rangle \ , \tag{2.46}$$

where the time-dependence of $V(t)$ is due to explicit time-dependence of the interaction (if there is any). One of the most important cases is when V is not explicitly time dependent. In this case we have

$$A_{0\to m} = -i \langle \Psi_m | V | \Psi_0 \rangle \frac{e^{t(\delta + i(E_m - E_0))}}{\delta + i(E_m - E_0)} \tag{2.47}$$

and so the transition probability is

$$P_{0\to m} = | \langle \Psi_m | V | \Psi_0 \rangle |^2 \frac{e^{2\delta t}}{|E_0 - E_m + i\delta|^2} \ .$$

The transition rate $R = dP/dt$ is thus

$$2\delta | \langle \Psi_m | V | \Psi_0 \rangle |^2 \frac{e^{2\delta t}}{|E_0 - E_m + i\delta|^2} \ ,$$

which equals zero (because of the infinitesimal) unless $E_0 = E_m$. In fact, since

$$\lim_{\delta \to 0} 2\delta \frac{1}{|x + i\delta|^2} = 2\pi\delta(x) \ ,$$

where the $\delta(x)$ on the RHS is Dirac's delta function, we have

$$R_{-\to m} = 2\pi | \langle \Psi_m | V | \Psi_0 \rangle |^2 \delta(E_0 - E_m) \ , \tag{2.48}$$

which is the correct expression for the rate to lowest order in V.

But–hey! Where did the time dependence go in Eq. (2.48)? Well, it went away in the limit that δ went to zero. But, if there is no time dependence then how come I can't take $\lim_{t\to\infty} \lim_{\delta\to 0}$[5] in Eq. (2.47) to end up with

$$A_{0\to m} = (-2\pi i)\delta(E_0 - E_m) | \langle \Psi_m | V | \Psi_0 \rangle |^2 \ ,$$

and the patently absurb

$$P_{0\to m} = (2\pi)\delta(E_0 - E_m) | \langle \Psi_m | V | \Psi_0 \rangle |^2 (2\pi)\delta(0) \ ?$$

Well, we can do this, as long as we "interpret" $(2\pi)\delta(0)$ as the total time of interaction, thus returning to us the correct result of Eq. (2.48). However, this "interpretation" of $2\pi\delta(0)$

[5] In that order. I.e., from right to left. cf., also Eq. (2.46) in this section. Also, in the next section cf. Eqs. (2.81) and (2.82) and the comment following those Eqs.

seems rather dishonest, doesn't it? It is just this type of dishonesty which we wish to avoid in our derivation of the cross-section for EELS in Section (2.3.1) on scattering.

We also note here that it is simple to take into account external fields with time variation $e^{-i\omega t}$ by replacing Eq. (2.48) with

$$R_{0\to m} = 2\pi |\langle \Psi_m | V | \Psi_0 \rangle|^2 \delta(E_0 + \omega - E_m) \ , \tag{2.49}$$

which can be understood if we imagine that there is some quantity in the initial state with an energy $\hbar\omega$ which does not appear in the final state. I.e., energy supplied by the field and "absorbed" by the system.

2.2.5 Linear Response and Correlation Functions

In this section we derive an expression for the inverse dielectric function in terms of the so-called "retarded density correlation function". The correlation function is also often called a "Green's function". We will continue to use the phrase "correlation function" in this section and reserve the phrase "Green's function" for a quantity to be defined later. We often use the symbol χ for correlation functions and the symbol G for Green's functions. We have no good reasons for this overuse of symbols other than history and habit.

The density correlation function is a useful quantity because the imaginary part is directly measurable by a variety of scattering experiments, most notably for us: electron energy-loss spectroscopy (EELS) and non-resonant inelastic x-ray scattering (NRIXS).

The retarded correlation function for an arbitrary bosonic operator $\hat{X}$ is defined as[41, 42]

$$\chi^{(X)}_{\rm ret}(t-t') \equiv -i\theta(t-t') \langle 0 | [X(t), X^\dagger(t')] | 0 \rangle \ , \tag{2.50}$$

where the † symbol represents Hermitian conjugation and the time-dependence is governed by the Hamiltonian of the system

$$X(t) \equiv e^{iH_0^s t} X e^{-iH_0^s t} \ , \tag{2.51}$$

where we take H_0^s to be given by Eq. (2.40) for definiteness. Of course, the time-dependence of correlation functions (and Green's functions) may be defined with respect to any Hamiltonian we like. However, the dependence of the correlation function on the time-difference $t - t'$ as in Eq. (2.50) will only occur if the Hamiltonian is not explictly time dependent.

In Eq. (2.50), the state $|0\rangle$ is taken as the ground state of the system (the lowest energy eigenstate of H_0^s). This expectation value is appropriate when working with a system at zero temperature, or at temperatures much lower than the typical excitation energy scale. For the most part, since we are concerned with electronic excitations whose typical scale is on the order of electron-volts and temperatures whose typical scale is on the order of room temperature, we can get away with considering the zero temperature correlation function.

The definition of the retarded correlation function for an arbitrary fermionic operator is the same as Eq. (2.50), but with the commutator replaced by an anticommutator. We are also often interested in the "time-ordered" correlation function

$$\chi^{(X)}(t-t') \equiv -i \langle 0| T(X(t)X^\dagger(t')) |0\rangle \ , \tag{2.52}$$

where T is the "time-ordering" symbol.

The specific retarded correlation function which we will be able to relate to the inverse dielectric function is the retarded correlation function for the density operator

$$\chi(\mathbf{r},\mathbf{r}',t-t') \equiv -i\theta(t-t') \langle 0| [\hat{n}(\mathbf{r},t),\hat{n}(\mathbf{r}',t')] |0\rangle \ , \tag{2.53}$$

where

$$\hat{n}(\mathbf{r}) = \sum_{i=1}^{N} \delta(\mathbf{r}-\hat{\mathbf{r}}_i) \ . \tag{2.54}$$

We will see later that scattering experiments are typically able to measure a certain retarded correlation function that is easily related to Eq. (2.53). This useful correlation function is given by

$$\chi(\mathbf{q},t-t') \equiv -i\theta(t-t') \langle 0| [\hat{n}_{\mathbf{q}}(t),\hat{n}^\dagger_{\mathbf{q}}(t')] |0\rangle \ , \tag{2.55}$$

where

$$\frac{1}{\mathcal{V}}\hat{n}^\dagger_{\mathbf{q}} \equiv \frac{1}{\mathcal{V}} \int d^3r e^{i\mathbf{q}\cdot\mathbf{r}} \hat{n}(\mathbf{r}) = \frac{1}{\mathcal{V}} \sum_{i=1}^{N} e^{i\mathbf{q}\cdot\hat{\mathbf{r}}_\mathbf{i}} \tag{2.56}$$

is the density fluctuation operator (i.e., for non-zero $\mathbf{q}$ this operator gives fluctuation about the $\mathbf{q}=0$ density $N/\mathcal{V}$). The correlation function $\chi(\mathbf{q},t)$ is the diagonal element of

$$\chi(\mathbf{q},\mathbf{q}';t) \equiv \int d^3r d^3r' e^{-i\mathbf{q}\cdot\mathbf{r}} e^{i\mathbf{q}'\cdot\mathbf{r}'} \chi(\mathbf{r},\mathbf{r}'\ t) \ . \tag{2.57}$$

There is a relationship, which we will presently introduce, between the imaginary part of the inverse dielectric function and the retarded density correlation function. This relationship is often called the "fluctuation-dissipation theorem" (for electronic excitations) because it relates "fluctuations" in the electron density ($n_{\mathbf{q}}$) to the "dissipative" part of a dielectric response function ($\mathrm{Im}[\epsilon^{-1}]$).[6]

Also, in this section we will ignore the effects of transverse electromagnetic fields which is a very good approximation for the large part of condensed matter theory. We will return to include the transverse fields later when we discuss high-energy EELS in Chapter (4).

Ignoring transverse fields means that we can write the total Hamiltonian of the system (characterized by Hamiltonian H_0^s) and the external electric potential $\phi_{\mathrm{ext}}(\mathbf{r},t)$ as

$$H = H_0^s + V(t) \ , \tag{2.58}$$

with

$$V(t) = (-e)\sum_{i=1}^{N}\phi_{\mathrm{ext}}(\mathbf{r_i},t) = (-1)\int d^3r\hat{n}(\mathbf{r})\phi_{\mathrm{ext}}(\mathbf{r},t) \ . \tag{2.59}$$

Here we are interested in perturbation theory in the external time-dependent potential V and so the "interaction picture" is defined with respect to H_0^s. In the interaction picture we have

$$V^I(t) \equiv e^{iH_0^s t}V(t)e^{-iH_0^s t} = (-1)\int d^3r\hat{n}^I(\mathbf{r},t)\phi_{\mathrm{ext}}(\mathbf{r},t) \ . \tag{2.60}$$

We again use the expansion of Eq. (2.44) to linear order

$$\left|\Psi^I(t)\right\rangle = |0\rangle - i\int_{-\infty}^{t} dt' V^I(t')\,|0\rangle \ , \tag{2.61}$$

where $|0\rangle$ is the ground state of H_0^s.

The density of the system (denoted by the same symbol as the density operator, but

---

[6]The term "dissipative" can be justified by considering the explicit energy absorbed via Eq. (2.59) and $< \partial V/\partial t >$, or by Fermi's golden rule for the absorption[43].

with no "hat") is then given to linear order in V by

$$\begin{aligned} n(\mathbf{r},t) &= \left\langle \Psi^I(t)\right| \hat{n}^I(\mathbf{r},t) \left|\Psi^I(t)\right\rangle \\ &= \langle 0|\, \hat{n}(\mathbf{r})\, |0\rangle + i\int_{-\infty}^{t} dt' \,\langle 0|\, [V^I(t'), \hat{n}^I(\mathbf{r},t)]\, |0\rangle \\ &= n_0(\mathbf{r}) + i\int_{-\infty}^{t} dt' \int d^3r' \,\langle 0|\, [\hat{n}^I(\mathbf{r},t), \hat{n}^I(\mathbf{r}',t')]\, |0\rangle\, \phi_{\rm ext}(\mathbf{r}',t') \\ &= n_0(\mathbf{r}) + i\int_{-\infty}^{\infty} dt' \int d^3r' \theta(t-t') \,\langle 0|\, [\hat{n}^I(\mathbf{r},t), \hat{n}^I(\mathbf{r}',t')]\, |0\rangle\, \phi_{\rm ext}(\mathbf{r}',t') \\ &= n_0(\mathbf{r}) - \int dt' d^3x' \chi(\mathbf{x},\mathbf{x}',t-t')\phi_{\rm ext}(\mathbf{x}',t') \;, \end{aligned} \tag{2.62}$$

where the last equality follows from the definition of the retarded correlation function in Eq. (2.53).

Thus

$$\rho(\mathbf{q},\omega) \equiv (-e) n(\mathbf{q},\omega) = (-1)^2 \int d^3q' \chi(\mathbf{q},\mathbf{q}',\omega)\phi_{\rm ext}(\mathbf{q}',\omega) \;, \tag{2.63}$$

which gives a linear relation between the external electric potential and the induced density. For finite ω, the zeroth order term is zero since the equilibrium density does not change with time. For a homogeneous system Eq. (2.63) reduces to

$$\rho(\mathbf{q},\omega) = \chi(\mathbf{q},\omega)\phi_{\rm ext}(\mathbf{q},\omega) \;. \tag{2.64}$$

The function $\chi(\mathbf{q},\mathbf{q}';\omega)$ is the Fourier transform with respect to time of $\chi(\mathbf{q},\mathbf{q}';t)$. Thus, using Eqs. (2.57) and (2.53)we have

$$\begin{aligned} \chi(\mathbf{q},\mathbf{q}',\omega) &= -i\int_{-\infty}^{\infty} dt e^{i\omega t}\theta(t) \,\langle 0|\, \left[n_{\mathbf{q}}(t), n^\dagger_{\mathbf{q}'}\right]\, |0\rangle \\ &= -i\int_0^{\infty} dt \sum_m e^{-\delta t} e^{i\omega t} \Big(\langle 0|\, n_{\mathbf{q}}\, |m\rangle\, e^{i(E_0-E_m)t}\, \langle m|\, n^\dagger_{\mathbf{q}'}\, |0\rangle \\ &\qquad\qquad - \langle 0|\, n^\dagger_{\mathbf{q}'}\, |m\rangle\, \langle m|\, n_{\mathbf{q}}\, |0\rangle\, e^{i(E_m-E_0)t} \Big) \\ &= i\sum_m \left(\frac{\langle 0|\, n_{\mathbf{q}}\, |m\rangle\, \langle m|\, n^\dagger_{\mathbf{q}'}\, |0\rangle}{-\delta + i\omega + i(E_0-E_m)} - \frac{\langle 0|\, n^\dagger_{\mathbf{q}'}\, |m\rangle\, \langle m|\, n_{\mathbf{q}}\, |0\rangle}{-\delta + i\omega + i(E_m-E_0)} \right) \;. \end{aligned} \tag{2.65}$$

Taking the diagonal element of the above equation we have

$$\chi(\mathbf{q},\omega) = \sum_m \left|\langle m|\, n^\dagger_{\mathbf{q}}\, |0\rangle\right|^2 \left(\frac{1}{E_0+\omega-E_m+i\delta} - \frac{1}{E_m+\omega-E_0+i\delta} \right) \;. \tag{2.66}$$

And, finally, taking the imaginary part of the above equation, and taking E_0 as the ground state energy, we have

$$\mathrm{Im}\left[\chi(\mathbf{q},\omega)\right] = -\pi \sum_m \left|\langle m|\, n^\dagger_{\mathbf{q}}\, |0\rangle\right|^2 \delta(E_0 + \omega - E_m)\ , \tag{2.67}$$

which is never positive.

Using Eq. (2.22) to relate χ and ϵ^{-1} we see that

$$-\mathrm{Im}\left[\epsilon^{-1}(\mathbf{q},\omega)\right] = -\frac{4\pi}{q^2}\mathrm{Im}\left[\chi(\mathbf{q},\omega)\right]\ , \tag{2.68}$$

which is never negative. Also, we can see from Eq. (2.68) that the imaginary part of the dielectric function is never negative. The quantity $-\mathrm{Im}\epsilon^{-1}(\mathbf{q},\omega)$ is often called the "energy loss function" (ELF) or even the "EELS spectrum". It is so called because, within the first born approximation (FBA), the EELS cross-section is given by Eq. (1.7). And, on comparison of with Eqs. (2.67) and (2.68), Eq. (1.7) is is seen to be the same as

$$\frac{d\sigma}{d\Omega d\omega} = \frac{k_f}{k_i}\frac{1}{\pi^2 q^2}\mathrm{Im}(\frac{-1}{\epsilon(\mathbf{q},\omega)})\ . \tag{2.69}$$

Thus, within the FBA, EELS can directly measure the dielectric function. This is described in more detail in the next section. For future reference, we note here that in the case of high energy EELS $k_i^2 >> \omega$. Thus in

$$\frac{qdq}{k_i^2} = d\cos(\theta)\left(1 - \frac{\omega}{v_0 k_i} + \ldots\right)\ , \tag{2.70}$$

the $O(\omega/v_0 k_i)$ term can be ignored. In this case, and for an azimuthally symmetric differential cross-section, Eq. (2.69) can be rewritten as

$$\frac{d\sigma}{dqd\omega} = \frac{2}{\pi q k_i^2}\mathrm{Im}(\frac{-1}{\epsilon(q,\omega)})\ . \tag{2.71}$$

2.3 High Energy Electron Scattering

In this Section we present a well-founded derivation of the double differential EELS scattering cross-section. Along with this we also introduce the necessary "Green's functions", "T-matrices" and "form-factors".

2.3.1 Scattering and Cross-Sections

The general theory of scattering is given in a number of good textbooks[44, 45, 46, 47]. Thus, we can restrain ourselves here to just a brief treatment for the specific case of EELS. Our goal in this section is to derive a well-known formula from first principles and without recourse to intellectually dishonest tricks such as squared delta-functions, etc. We beg the forgivness of experts for the inclusion of our take on this well-known material. In our defense, the specific case of EELS is particularly cute and streamlined mostly due to the fact that only one simple wavepacket (for the probe) must be introduced.

Also, this subsection serves the purpose of naturally introducing a number of important quantities such as: the "Green's function", the "T-matrix", and the "Dynamic Form Factor" (DFF).

In the case of EELS we are interested in a system composed of a "probe" and a "sample" (the "sample" being the same as the "system" of previous sections). We consider the sample to be at rest at the origin. The sample eigenfunctions are already localized in space thanks to the "external" potential. The sample eigenfunctions are normalizable and describe physical states; we do not need wave packets for the sample. On the other hand, the probe is a free particle whose description requires wavepackets. In this section we consider the probe to be non-relativitistic. This limitation is removed in subsequent chapters.

The total Hamiltonian for EELS is just that of the sample, the probe, and their interaction

$$H = H_0^s + \frac{p^2}{2} + v_{\text{ext}}(\mathbf{r}) + \sum_{i=1}^{N} \frac{1}{|\mathbf{r} - \mathbf{r_i}|} \ , \tag{2.72}$$

where H_0^s is from Eq. (2.40), $\mathbf{p}$ is the momentum of the probe, and $\mathbf{r}$ is the position of the probe. Because we are interested in initial- and final-states in which the probe is greatly separated from the sample we write

$$H = H_0 + V \ , \tag{2.73}$$

where

$$H_0 = H_0^s + p^2/2 \ ,$$

and

$$V = v_{\text{ext}}(\mathbf{r}) + \sum_{i=1}^{N} \frac{1}{|\mathbf{r} - \mathbf{r_i}|} \ . \tag{2.74}$$

Thus, eigenfunctions of H_0 are direct products of plane-waves $|\mathbf{k}\rangle$ and sample eigenfunctions $|m\rangle$

$$H_0 \, |\mathbf{k}\rangle \, |m\rangle = (\frac{k^2}{2} + E_m) \, |\mathbf{k}\rangle \, |m\rangle \ ,$$

where E_m is the energy of the sample.

To treat the incident probe correctly we form a wave packet to localize the probe electron in space. That is, we write the $(t = 0)$ free wave-function of the system as

$$W_{\mathbf{k}_i,m}(\mathbf{r}, \mathbf{r_1}, \ldots, \mathbf{r_N}) \equiv e^{i\mathbf{k}_i \cdot \mathbf{r}} w(\mathbf{r}) \phi_m(\mathbf{r_1}, \ldots, \mathbf{r_N}) \ , \tag{2.75}$$

where $w(\mathbf{r})$ is some small "blob" localized about the origin in position space. The state we have written in Eq. (2.75) is similar to the standard (dishonest) incident state $e^{i\mathbf{k_i} \cdot \mathbf{r}} \phi_m$ except that we have included the blob to localize the probe. Thus, we expect that the quantity $\mathbf{k_i}$ will be interpreted as the initial momentum of the probe.

The state in Eq. (2.75) may also be written as

$$|W_{\mathbf{k_i},m}\rangle = \int \frac{d^3k}{(2\pi)^3} w(\mathbf{k}) \, |\mathbf{k_i} + \mathbf{k}\rangle \, |m\rangle \ , \tag{2.76}$$

where $w(\mathbf{k})$ is the Fourier transform of $w(\mathbf{r})$ which has been chosen such that particle is localized in momentum space. In Eq. (2.75) we use the convention $\langle \mathbf{x}|\mathbf{k}\rangle = e^{i\mathbf{x}\cdot\mathbf{k}}$ which is perfectly appropriate, but often not convenient. If we instead choose the normalization $\langle \mathbf{x}|\mathbf{k}\rangle = e^{i\mathbf{x}\cdot\mathbf{k}}/\sqrt{\mathcal{V}}$ then the only thing that changes is that Eq. (2.76) must be multiplied by $\sqrt{\mathcal{V}}$.

It is possible to adequately (within the requirements of a given experiment) satisfy both the requirements of localization in position and momentum as long as we do not require extreme localization in both simultaneously.

Also, although our resourceful experimentalist friends can probably figure out how to localize the probe and shoot it at the sample, they probably can not figure out how to prepare an arbitrary eigenstate of the sample. Thus, in practice, $m = 0$ in Eq. (2.76) for the incident packet.

If we evolve the free wave-packet with the free Hamiltonian we find

$$W_{\mathbf{k_i},0}(\mathbf{r},\mathbf{r_1},\ldots,\mathbf{r_N};t) \approx e^{i\mathbf{k_i}\cdot\mathbf{r}-itk^2/2} w(\mathbf{r}-\mathbf{v_i}t) e^{-iE_0 t}\phi_0(\mathbf{r_1},\ldots,\mathbf{r_N}) \ ,$$

where $\mathbf{v_i} = \mathbf{k_i}/m = \mathbf{k_i}$ which justifies the expected interpretation of $\mathbf{k_i}$. Further, we know that in this scattering experiment the system is well separated and well described by the free packet for any time in the distant past. In our scattering experiment (where the true Hamiltonian is H) the actual state of the system at an aribtrary time t is thus given by

$$|\Psi(t)\rangle = e^{-iH(t-(-\tau))} e^{-iH_0(-\tau)} |W_{\mathbf{k_i},0}\rangle = e^{-iHt} \left(e^{-iH\tau} e^{iH_0\tau}\right) |W_{\mathbf{k_i},\mathbf{0}}\rangle \ , \tag{2.77}$$

where τ is a time which is large enough that the free probe wave-packet has a negligible overlap in space with the ground state wavefunction of the system.

The quantity in the parenthesis in Eq. (2.78) can be rewritten as

$$e^{-iH\tau} e^{iH_0\tau} = 1 - i\int_{-\tau}^{0} dt' e^{iHt'} V e^{-iH_0 t'} \ ,$$

where V is the interaction potential defined via Eq. (2.74).

Thus we have

$$\begin{aligned} |\Psi(t)\rangle &= e^{-iHt}\left(1 - i\int_{-\tau}^{0} dt' e^{iHt'} V e^{-iH_0 t'}\right) |W_{\mathbf{k_i},0}\rangle \\ &= e^{-iHt}\left(1 - \lim_{\delta\to 0} i\int_{-\tau}^{0} dt' e^{\delta t'} e^{iHt'} V e^{-iH_0 t'}\right) |W_{\mathbf{k_i},0}\rangle \\ &= e^{-iHt}\left(1 - \lim_{\delta\to 0} i\int_{-\infty}^{0} dt' e^{\delta t'} e^{iHt'} V e^{-iH_0 t'}\right) |W_{\mathbf{k_i},0}\rangle \ . \end{aligned} \tag{2.78}$$

The second equality above follows from the fact that we may interchange the limit and the integration. The third equality follows from the fact that V gives zero when it acts on the well separated free wave-packet. I.e., for large τ the probe wave-packet is localized about $\mathbf{r} \approx -\mathbf{v}_i\tau$ which is very far from the (localized) sample. Thus V, which is a function only of the probe/sample separation, acting on the wave-packet vanishes. In fact, this was the reason we chose the particular separation of H into $H_0 + V$ that we did.

If we substitute the expansion Eq. (2.76) of the wave-packet in terms of free eigenfunc-

tions into Eq. (2.78) we find

$$\begin{aligned} |\Psi(t)\rangle &= e^{-iHt}\int \frac{d^3k}{(2\pi)^3} w(\mathbf{k}) \left(1 - \lim_{\delta\to 0} i\int_{-\infty}^{0} dt' e^{\delta t'} e^{iHt'} V e^{-iE_I(\mathbf{k})t'}\right) |\mathbf{k_i}+\mathbf{k}\rangle\,|0\rangle \\ &= e^{-iHt}\int \frac{d^3k}{(2\pi)^3} w(\mathbf{k}) \left(1 + G(E_I(\mathbf{k}))^+ V\right) |\mathbf{k_i}+\mathbf{k}\rangle\,|0\rangle \ , \end{aligned} \tag{2.79}$$

where $E_I(\mathbf{k}) \equiv E_0 + (\mathbf{k_i}+\mathbf{k})^2/2$ and where (sound the trumpets) we have introduced the "retarded Green's function"

$$G(E)^+ \equiv \lim_{\delta\to 0} \frac{1}{E - H + i\delta} \ ,$$

where the limit is taken from above. This quantity turns out to be a very useful tool in the study of a great many branches of physics. We will discuss the Green's function in more detail in the next section. But for now we are content to simply state (and use) the well-known property[7]

$$G(E)^+ V = G(E)_0^+ T(E) \ ,$$

where $G_0(E)^+$ is the retarded free Green's function

$$G_0(E)^+ = \lim_{\delta\to 0} \frac{1}{E - H_0 + i\delta} \ ,$$

and $T(E)$ is the aptly named "T-matrix"

$$T(E) = V + VG(E)^+ V \ . \tag{2.80}$$

As the time t grows large we may ask for the probability amplitude to be in the state $e^{-iH_0 t}\,|\mathbf{k_f}\rangle\,|n\rangle$. Here, we assume that $|\mathbf{k_f}\rangle\,|n\rangle \neq |\mathbf{k_0}\rangle\,|0\rangle$.[8] This amplitude is independent of t for large t (as expected) for the same reason that the RHS of Eq. (2.78) was independent

---

[7] which is proved by applying algebra to the definitions of $G(E)$, $G_0(E)$ and $T(E)$

[8] But not necessarily $|n\rangle \neq |0\rangle$. I.e., we can still treat elastic scattering, just not in the forward direction. Although, our focus here will turn out to be inelastic scattering.

of τ for large τ. The scattering amplitude is thus

$$\begin{aligned}
A &= \lim_{t\to\infty} \langle n| \langle \mathbf{k_f}| e^{iH_0 t} |\Psi(t)\rangle \\
&= \lim_{t\to\infty} \langle n| \langle \mathbf{k_f}| e^{iH_0 t} e^{-iHt} \int \frac{d^3k}{(2\pi)^3} w(\mathbf{k}) \left(1 + G_0^+ T\right) |\mathbf{k_i} + \mathbf{k}\rangle |0\rangle \\
&= \lim_{t\to\infty} \langle n| \langle \mathbf{k_f}| e^{iE_F t} \int \frac{d^3k}{(2\pi)^3} w(\mathbf{k}) e^{-iE_I(\mathbf{k})t} \left(1 + G_0^+ T\right) |\mathbf{k_i} + \mathbf{k}\rangle |0\rangle \\
&= \lim_{t\to\infty} \int \frac{d^3k}{(2\pi)^3} w(\mathbf{k}) e^{-i(E_I(\mathbf{k})-E_F)t} \lim_{\delta\to 0} \frac{1}{E_I(\mathbf{k}) - E_F + i\delta} \langle n| \langle \mathbf{k_f}| T |\mathbf{k_i} + \mathbf{k}\rangle |0\rangle \\
&= \int \frac{d^3k}{(2\pi)^3} w(\mathbf{k}) (-2\pi i) \delta(E_F - E_I(\mathbf{k})) \langle n| \langle \mathbf{k_f}| T |\mathbf{k_i} + \mathbf{k}\rangle |0\rangle \ , \qquad (2.81)
\end{aligned}$$

where $E_F \equiv E_n + k_f^2/2$, and where we have used the fact that $(1 + G_0^+ T) |\mathbf{k_i} + \mathbf{k}\rangle |0\rangle$ is an eigenfunction of the full Hamiltonian with eigenvalue $E_I(\mathbf{k})$. We have also used

$$\lim_{t\to\infty} \lim_{\delta\to 0} e^{-ixt} \frac{1}{x + i\delta} = (-2\pi i)\delta(x) \ . \qquad (2.82)$$

The amplitude contains a Dirac delta function. But, because of the wave-packet, we don't have the square of a delta-function when we square the amplitude to find the probability. The delta functions will have different arguments due to the spread of the incident probe-momentum. We will find, upon squaring the amplitude, a term like

$$\begin{aligned}
\delta(E_F - E_I(\mathbf{k}))\delta(E_F - E_I(\mathbf{k}')) &\approx \delta(E_F - E_I(0))\delta(E_I(\mathbf{k}) - E_I(\mathbf{k})) \\
&\approx \delta(E_F - E_I(0))\delta(\mathbf{v_i} \cdot (\mathbf{k} - \mathbf{k})) \ , \qquad (2.83)
\end{aligned}$$

which is resonable since $E_F - E_I(0)$ is just $(E_n + k_f^2/2) - (E_0 + k_i^2/2)$ and we expect conservation of energy. In the rest of this section we denote $E_I(0)$ by E_I.

The scattering probability is thus

$$\begin{aligned}
P &= |A|^2 \\
&= \int \frac{d^3k}{(2\pi)^3} w(\mathbf{k})(-2\pi i)\delta(E_F - E_I(\mathbf{k}))\, \langle \mathbf{k_f}| \langle n| T |\mathbf{k_i}+\mathbf{k}\rangle |0\rangle \\
&\quad \times \int \frac{d^3k'}{(2\pi)^3} w^*(\mathbf{k}')(2\pi i)\delta(E_F - E_I(\mathbf{k}'))\big(\langle \mathbf{k_f}| \langle n| T \left|\mathbf{k_i}+\mathbf{k}'\right\rangle |0\rangle\big)^* \\
&\approx (2\pi)\delta(E_F - E_I)|\, \langle \mathbf{k_f}| \langle n| T |0\rangle |\mathbf{k_i}\rangle\, |^2 \int \frac{d^3k}{(2\pi)^3}\frac{d^3k'}{(2\pi)^3} w(\mathbf{k})w^*(\mathbf{k}')(2\pi)\delta(\mathbf{v_i}\cdot(\mathbf{k}-\mathbf{k}')) \\
&= (2\pi)\delta(E_F - E_I)|\, \langle \mathbf{k_f}| \langle n| T |0\rangle |\mathbf{k_i}\rangle\, |^2 \int_{-\infty}^{\infty} dt \left| \int \frac{d^3k}{(2\pi)^3} w(\mathbf{k}) e^{it\mathbf{v_i}\cdot\mathbf{k}} \right|^2 \\
&= (2\pi)\delta(E_F - E_I)|\, \langle \mathbf{k_f}| \langle n| T |0\rangle |\mathbf{k_i}\rangle\, |^2 \frac{1}{v_0}\left[\int_{-\infty}^{\infty} dz |w(0,0,z)|^2\right] , \qquad (2.84)
\end{aligned}$$

where the incident beam direction is taken as the z-axis. The term in braces in Eq. (2.84) is just the number of probe electrons[9] per unit area. Thus the quantity

$$\frac{P}{\int_{-\infty}^{\infty} dz |w(0,0,z)|^2} \equiv \frac{P}{n^1_{\text{probe}}} , \qquad (2.85)$$

is independent of the particular details of the probe wave-packet. Eq. (2.85) has units of area, and is called the "cross-section" for scattering. The last equality just defines the quantity $n^1_{\text{probe}} = \int dz |w(0,0,z)|^2$.

Over the course of an actual experiment a large number of probe particles are fired at the sample (which may or may not itself consist of a large number of approximately independent "molecular" particles). But each probe particle is taken to be independent of the other probe particles. And each "molecular" particle is by definition independent of the other molecular particles. Thus, also in this case the cross-section is given by Eq. (2.85). I.e.,

$$\sigma \equiv \frac{P}{n^1_{\text{probe}}} = \frac{1}{v_0}(2\pi)\delta(E_0 + \omega - E_n)|\, \langle \mathbf{k_f}| \langle n| T |0\rangle |\mathbf{k_i}\rangle\, |^2 , \qquad (2.86)$$

where we have also defined the "energy-loss"

$$\omega \equiv k_i^2/2 - k_f^2/2 .$$

Eq. (2.86) is a sensible[10] formula in light of the following remarks: Imagine that a large

[9] There is only one probe electron, but the phrase "number of probe electron" sounds silly. Really we should say, "number of probe electrons per unit area per probe electron."

[10] I.e., can be made sense of in vivid classical terms.

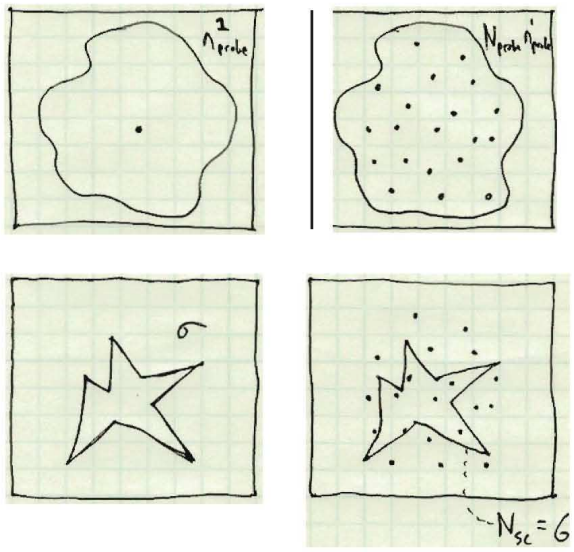

Figure 2.2: An artist's depiction of scattering six incident particles (out of 20 total) by an unknown area σ along with the depiction of various other quantities of interest (see text).

number N_{probe} of probe particles are shot at the sample. In this case one can think about how the distribution of probe particles "looks" as viewed down the incident axis. The distribution one "sees" is just $N_{\text{probe}} \int dz|w|^2 \equiv N_{\text{probe}} n^1_{\text{probe}}$. Probe particles are scattered because the sample takes up some area perpendicular to the incident axis. This "sample area" is of course unknown and is just what we call the cross-section σ. Thus, see Fig. (2.2), the number of scattered particles is $N_{\text{scattered}} = N_{\text{probe}} n^1_{\text{probe}} \sigma$. If we prefer to describe the entire sample as a collection of N_A independent scatters then it makes sense to define the cross-section per scatter ($\sigma_A N_A \equiv \sigma$) rather than for the whole sample. I.e., $N_{\text{scattered}} = N_{\text{probe}} n^1_{\text{probe}} \sigma_A N_A$. The cross-section is then

$$\sigma_A = \frac{N_{\text{scattered}}}{N_{\text{probe}} N_{\text{A}} n^1_{\text{probe}}} \ ,$$

which is the same as Eq. (2.86) since $N_{\text{scattered}} = N_{\text{probe}} P N_A$. Also we note here that the division of the sample into independently scattering "atoms" or "molecules" is not necessary, but is often convenient.

From the above description of the scattering process we might think that we can only gain information about the overall "size" of the sample. But, still speaking classically, we

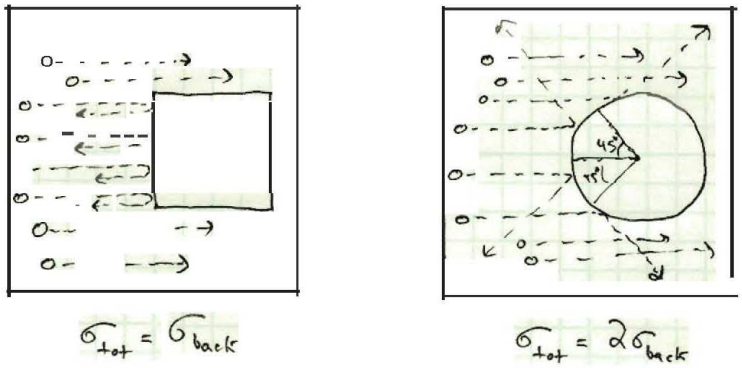

Figure 2.3: Comparison of the total cross-section to the backscattering cross-section for a classical hard-sphere versus a square. The *total* cross-sections are (apparently) nearly equal, but the relative size of the *backscattering* cross-section tells us that the two shapes differ.

can also learn about the "shape" of the sample by considering not just the total cross-section, but the cross-section as a function of angle. As a blunt example, we could compare the total cross-section to the back-scattering cross-section for the case of a sphere and a square. This is done in Fig. (2.3). Thus, we can learn not only about the "size" via the total cross-section, but also about the "shape" via the differential cross-section as a function of angle.

Finally, for the case of scattering into within d^3k_f of $\mathbf{k_f}$, and into any final state of the sample, we can write down the very useful formula for the EELS cross-section:

$$d\sigma = \mathcal{V}\frac{d^3k_f}{(2\pi)^3}\sum_n \frac{\mathcal{V}}{v_0}(2\pi)\delta(E_0+\omega-E_n)|\left\langle \mathbf{k_f}\right|\left\langle n\right|T\left|0\right\rangle\left|\mathbf{k_i}\right\rangle|^2 , \tag{2.87}$$

where we have introduced a normalization volume $\mathcal{V}$ for the plane-waves such that

$$\langle \mathbf{x}|\mathbf{k}\rangle = \frac{1}{\sqrt{\mathcal{V}}}e^{i\mathbf{k}\cdot\mathbf{x}} .$$

In Eq. (2.87), the first factor of $\mathcal{V}$ comes from counting plane-wave states in a box, and the second factor of $\mathcal{V}$ comes from the fact that we have changed our normalization conventions for $\langle \mathbf{x}|\mathbf{k}\rangle$ relative to Eq. (2.75). Of course, the normalization drops out at the end of any calculation because there is a factor of $1/\mathcal{V}$ in the T-matrix element now.

We are also now in a position to state the main point of this section: the only thing that is really difficult to calculate in the theory of scattering is the quantity

$$\langle \mathbf{k_f} | \langle n | T | 0 \rangle | \mathbf{k_i} \rangle \ , \tag{2.88}$$

everything else in this section really just deals with the quantum kinematics. The kinematics will go through in almost exactly the same way for any type of scattering and so we will usually just be interested in matrix elements such as Eq. (2.88). However, the connection to experiment is through Eq. (2.87).

In order to obtain a simple and useful formula for the EELS cross-section we make the "First Born Approximation" (FBA) which consists of replacing T by it's first term in Eq. (2.80). I.e., $T \to V$. In this case Eq. (2.87) becomes

$$\begin{aligned} d\sigma^{(\mathrm{FBA})} &= \mathcal{V}\frac{d^3k_f}{(2\pi)^3}\sum_n \frac{\mathcal{V}}{v_0}(2\pi)\delta(E_0+\omega-E_n)\left|\langle \mathbf{k_f}|\langle n|\left(v_{\mathrm{ext}}(\mathbf{r})+\sum_{i=1}^{N}\frac{1}{|\mathbf{r}-\mathbf{r_i}|}\right)|0\rangle|\mathbf{k_i}\rangle\right|^2 \\ &= \frac{d^3k_f}{(2\pi)^3}\sum_n \frac{1}{v_0}(2\pi)\delta(E_0+\omega-E_n)\left|\langle n|\int d^3x e^{i(\mathbf{k_i}-\mathbf{k_f})\cdot\mathbf{x}}\sum_{i=1}^{N}\frac{1}{|\mathbf{x}-\mathbf{r_i}|}|0\rangle\right|^2 \\ &= \frac{d^3k_f}{(2\pi)^3}\sum_n \frac{1}{v_0}(2\pi)\delta(E_o+\omega-E_n)\left(\frac{4\pi}{q^2}\right)^2\left|\langle n|\sum_{i=1}^{N}e^{i\mathbf{q}\cdot\mathbf{r_i}}|0\rangle\right|^2 , \end{aligned} \tag{2.89}$$

where the second equality holds only for inelastic scattering[11]. The third equality introduces the definition

$$\mathbf{q} \equiv \mathbf{k_i} - \mathbf{k_f} \ . \tag{2.90}$$

Using the definition of ω, we can write

$$d^3k_f = d\Omega dk_f k_f^2 = d\Omega d\omega k_f^2/v_f \ ,$$

and thus

$$\begin{aligned} \left(\frac{d\sigma}{d\Omega d\omega}\right)^{(\mathrm{FBA})} &= \frac{k_f^2}{v_f v_0}\frac{4}{q^4}\sum_n\left|\langle n|\sum_{i=1}^{N}e^{i\mathbf{q}\cdot\mathbf{r_i}}|0\rangle\right|^2\delta(E_0+\omega-E_n) \\ &= \frac{k_f^2}{v_f v_0}\frac{4}{q^4}S(\mathbf{q},\omega) \\ &= \frac{k_f}{k_0}\frac{4}{q^4}S(\mathbf{q},\omega) \ , \end{aligned} \tag{2.91}$$

[11] By "inelastic" we mean that the state of the sample changes. I.e., $n \neq 0$

where the final (seemingly trivial) equality is displayed as a reminder of the fact that this is a non-relativistic result; the standard relativistic extension of this calulation is achieved by replacing $m \to m\gamma$ in Eq. (2.91). Unfortunately (and amusingly), this procedure can be difficult when using atomic units (where $m = 1$) unless we remember that the DDCS is proportional to m^2, as evidenced by the penultimate expression in Eq. (2.91).

The EELS cross-section within the FBA is a very important tool, especially when it comes to calculating the stopping power (CSP) and inelastic mean free path (IMFP) of electrons in condensed matter. Even though the FBA fails in many circumstances, the calculation of the stopping power is especially resiliant against failure because it involves the integrated cross-section. The unusually large range of validity of the FBA for calculating the CSP can also be seen *a posteriori* from the explicit numerical calculations of Chapter (3).

2.3.2 Green's functions, Correlation, and all that

In the preceding sections we have introduced the definition of the retarded Green's function

$$G(E)^+ \equiv \frac{1}{E - H + i\delta} \,, \tag{2.92}$$

as well as the definition of the retarded correlation function

$$\chi(\mathbf{x}, \mathbf{x}'; t) = -i\theta(t) \left\langle 0 \right| \left[X(t), X^\dagger(0) \right] \left| 0 \right\rangle \ . \tag{2.93}$$

Really, the correlation function should also bear indices indicating the operator X whose correlations are being measured. Also, the correlation function depends on what state $|0\rangle$ we choose to use for the expectation value.

The Green's function of Eq. (2.92) and the correlation function of Eq. (2.93) turn out to be the same when the operator $X(t)$ in Eq. (2.93) is replaced by the particle annihilation operator[48, 49, 41, 50] $\psi(\mathbf{x})$. For example, for the case when $|0\rangle$ is the particle vacuum, we have

$$\chi(\mathbf{x}, \mathbf{x}'; t) = -i\theta(t) \left\langle 0 \right| \psi(\mathbf{x}, t) \psi^\dagger(\mathbf{x}') \left| 0 \right\rangle = -i\theta(t) \left\langle \mathbf{x} \right| e^{-iHt} \left| \mathbf{x}' \right\rangle \ .$$

Whereas the Green's function (Fourier transformed) is

$$\left\langle \mathbf{x} \right| \int \frac{dE}{2\pi} e^{-iEt} G(E) \left| \mathbf{x}' \right\rangle = \int \frac{dE}{2\pi} e^{-iEt} \left\langle \mathbf{x} \right| \frac{1}{E - H + i\delta} \left| \mathbf{x}' \right\rangle = \theta(t)(-2\pi i) \frac{1}{2\pi} \left\langle \mathbf{x} \right| e^{-iHi} \left| \mathbf{x}' \right\rangle \ ,$$

which is the same thing as the correlation function. Thus, it makes no difference whether we say "Green's function" or "correlation function".

We now proceed to examine a few properties of the Green's function and introduce some terminology which we will use later.

The Green's function for $t < 0$ is given by Eq. (2.52) as

$$G(\mathbf{x}, \mathbf{x}'\ t) = i \left\langle 0 \right| \psi^\dagger(\mathbf{x}')\psi(\mathbf{x}, t) \left| 0 \right\rangle \ , \tag{2.94}$$

where we will most often be interested in the case when $|0\rangle$ is the N-body ground state. I.e., the lowest energy eigenfunction of Eq. (2.40). We next insert into Eq. (2.94) a complete set of states of the $N-1$ particle Hamiltonian[12] to find

$$\begin{aligned} G(\mathbf{x}, \mathbf{x}'\ t) &= i \left\langle 0 \right| \psi^\dagger(\mathbf{x}') \left| N-1; m \right\rangle \left\langle N-1; m \right| \psi(\mathbf{x}, t) \left| 0 \right\rangle \\ &= i \left\langle 0 \right| \psi^\dagger(\mathbf{x}') \left| N-1; m \right\rangle \left\langle N-1; m \right| \psi(\mathbf{x}) \left| 0 \right\rangle e^{i(E_{N-1;m} - E_{N;0})t} \\ &\equiv i \sum_m g_m(\mathbf{x}) g_m^*(\mathbf{x}) e^{i(\epsilon_m - \mu)t} \ , \end{aligned} \tag{2.95}$$

where we have defined the zero temperature chemical potential

$$\mu \equiv E_{N;0} - E_{N-1;0} \ ,$$

and the quasiparticle energy

$$\epsilon_m = E_{N-1,m} - E_{N-1;0} \ ,$$

both of which are positive. We have also defined the quasiparticle (hole) wavefunction[51, 42]

$$g_m(\mathbf{x}) = \left\langle N-1; m \right| \psi(\mathbf{x}) \left| 0 \right\rangle \ ,$$

which reduces to a single particle wavefunction in a non-interacting theory.[51]

Thus, because the density is given (in second quantized notation) by

$$n_0(\mathbf{x}) = \left\langle 0 \right| \psi^\dagger(\mathbf{x})\psi(\mathbf{x}) \left| 0 \right\rangle = -i \lim_{t \to 0^-} G(\mathbf{x}, \mathbf{x}; t) \ ,$$

we have

$$n_0(\mathbf{x}) = \sum_m |g_m(\mathbf{x})|^2 \ ,$$

[12] which is also given by Eq. (2.40) but where the sums over particles run from 0 to $N-1$ rather than N

which is an interesting equation to contrast with the Kohn-Sham density functional theory (DFT) expression for the density given later.

Indeed, we will see that DFT can serve as a useful starting point to attack the quantum many body excited-state problem.

2.4 Independent Particles and Density Functional Theory

2.4.1 Independent Particles

Other than the fact that we must start from somewhere, there is but little apology we can give for the independent particle treatment of a many-body system.

Here is what Hans Bethe said when asked, during an interview[52] conducted by David Mermin, why he felt that he and Sommerfeld and Peierls could ignore electron-electron interactions and treat the electrons as independent

> "I understand that the Russians found that very difficult. But to me it seemed quite obvious, because after all, it happened in the atom... so, we obviously would have a Hartree-Fock theory of electrons in a crystal... It didn't worry Peierls and me."
>
> –H. A. Bethe

Of course, it is usually necessary to go beyond the independent particle treatment. But, the point is that we may as well start from there.

The "independent particle" theory means that we can treat the many-body wavefunction as a Slater determinant of single-particle orbitals. Thus a N-body wavefunction is specified by giving N single-particle wavefunctions. In other words, our single N-body problem is effectively reduced to N single-body problems.

For example, the N-body ground state is specified in the independent particle picture by specifying N "occupied" orbitals. These "occupied" orbitals are the N eigenfunctions of some (rather arbitrary, in general) single-particle Hamiltonian which have the N lowest eigenvalues. Then, excited states are created from the ground state by swapping out the

occupied orbitals for other orbitals with higher eigenvalues of the single-particle Hamiltonian.

For example, consider Eq. (1.4) which gives the cross-section for x-ray absorption:

$$\sigma(\omega) = \frac{4\pi^2\omega}{c} \sum_m |\langle \Psi_m | \hat{\epsilon}^* \cdot \hat{\mathbf{d}} | \Psi_0 \rangle|^2 \delta(E_0 + \hbar\omega - E_m) \; .$$

In the independent particle approximation, the sum over the N different position operators within $\mathbf{d}$ can be replaced by a single position operator which acts on orbitals. This is because the dipole operator is a sum of single-body terms and it is sandwiched between two Slater determinants.[31] The non-zero matrix elements then are between Slater determinants which differ by exactly one orbital. Thus, the sum over final states reduces to a sum over "inital" or "occupied" orbitals and "final" or "unoccupied" orbitals. Finally, the differences in energies of the Slater determinants is just the difference in orbital energies. Thus Eq. (1.4) reduces, in the independent particle approximation as:

$$\sigma(\omega) \rightarrow \frac{4\pi^2\omega e^2}{c} \sum_{i,occ} \sum_{j,unocc} |\langle j | \hat{\epsilon}^* \cdot \hat{\mathbf{r}} | i \rangle|^2 \delta(\lambda_i + \hbar\omega - \lambda_j) \; ,$$

and cf., Eq. (1.10).

2.4.2 Density Functional Theory

Here we briefly discuss Kohn-Sham[53] (KS) density functional theory.[54, 55, 56, 57]

Density functional theory is based on the fact that the ground state density determines "everything".[56] That this is so can be seen from the first Hohenberg-Kohn (HK) theorem[54] which states that the Hamiltonian (up to an additive constant) is a unique functional of the ground-state density. But since the Hamiltonian knows about everything (i.e., all the states), then everything is a (albeit complicated) functional of the ground state density.

Even though the proof of the HK theorems was never "hard", the constrained search ideas of Levy[56, 58] make for a wonderful proof which seems trivial. These ideas also lead to an interesting definition of the ground-state as that antisymmetric wavefunction which yields the ground state density and minimizes the operator

$$\hat{T} + \hat{V}_{ee} \; , \tag{2.96}$$

where $\hat{T}$ is the kinetic energy operator

$$\hat{T} \equiv \sum_{i=1}^{N} \frac{\hat{p}_i^2}{2} \ , \tag{2.97}$$

and $\hat{V}_{ee}$ is the electron-electron interaction operator

$$\hat{V}_{ee} \equiv \frac{1}{2} \sum_{i \neq j=1}^{N} \frac{1}{|\hat{\mathbf{r}}_\mathbf{i} - \hat{\mathbf{r}}_\mathbf{j}|} \ . \tag{2.98}$$

That is, consider the following process: someone hands us a density (a non-negative function of a single variable) $n(\mathbf{r})$ for some N particle system. Then we go and find all antisymmetric N-particle wavefunctions

$$\left\{ \left|\Psi^1[n]\right\rangle, \left|\Psi^2[n]\right\rangle, \left|\Psi^3[n]\right\rangle, \ldots, \left|\Psi^{42}[n]\right\rangle, \ldots, \left|\Psi^{8473}[n]\right\rangle, \ldots \right\}$$

in the world for which

$$\left\langle \Psi^j[n] \right| \sum_{i=1}^{N} \delta(\mathbf{r} - \hat{\mathbf{r}}_\mathbf{i}) \left|\Psi^j[n]\right\rangle = n(\mathbf{r}) \ . \tag{2.99}$$

Then, we calculate the expectation value

$$A_n^j \equiv \left\langle \Psi^j[n] \right| T + V_{ee} \left|\Psi^j[n]\right\rangle \ , \tag{2.100}$$

which is a number, and we look through all those numbers and find the smallest one $A_n^{\min}$. That smallest number $A_n^{\min}$ is also called the (value of the) "universal functional" $F[n]$

$$F[n] \equiv A_n^{\min} = \left\langle \Psi^{j_{\min}}[n] \right| T + V_{ee} \left|\Psi^{j_{\min}}[n]\right\rangle \ , \tag{2.101}$$

where $\left|\Psi^{j_{\min}}[n]\right\rangle$ is a wavefunction (if there is more than one, it doesn't matter which one since we only care about the number $A_n^{\min}$) for which A_n^j has it's smallest value.

If the density someone hands us happens to be a ground-state density $n_0(\mathbf{r})$ then the wavefunction $\left|\Psi^{j_{\min}}[n_0]\right\rangle$ which gave the value $A_{n_0}^{\min}$ is the ground state $|\Psi_0\rangle$. If more than one gives the smallest value there is more than one ground state.

Similarly, we can define a "non-interacting kinetic energy functional" by searching for the minimum of just the kinetic energy operator over states which yield the density $n(\mathbf{r})$

$$T_s[n] \equiv \min_j \left\langle \Psi^j[n] \right| \hat{T} \left|\Psi^j[n]\right\rangle \ . \tag{2.102}$$

The state which yields the ground state density $n_0(\mathbf{r})$ and also minimizes just the kinetic energy operator is called the Kohn-Sham (KS) ground state $|\Phi_0\rangle$. Because the kinetic energy operator is a single particle operator, the KS ground state is usually a Slater determinant. The KS ground state determinant is made up of "KS orbitals" $\phi_i(\mathbf{r})$.

KS theory is based on the definition

$$F[n] = T_s[n] + \frac{1}{2}\int d^3r' \frac{n(\mathbf{r})n(\mathbf{r}')}{|\mathbf{r}-\mathbf{r}'|} + E_{xc}[n] \; , \tag{2.103}$$

which defines E_{xc}. Then, minimizing

$$E[n]-\mu N = F[n]+\int d^3r n(\mathbf{r})v_{\rm ext}(\mathbf{r})-\mu N = T_s[n]+\frac{1}{2}\int d^3r' \frac{n(\mathbf{r})n(\mathbf{r}')}{|\mathbf{r}-\mathbf{r}'|}+E_{xc}[n]+\int d^3r n(\mathbf{r})v_{\rm ext}(\mathbf{r})-\mu N \; , \tag{2.104}$$

with respect to the density gives

$$\frac{\delta T_s}{\delta n(\mathbf{r})} + \int d^3r' \frac{n(\mathbf{r}')}{|\mathbf{r}-\mathbf{r}'|} + \frac{\delta E_{xc}}{\delta n(\mathbf{r})} + v_{\rm ext}(\mathbf{r}) = \mu \; , \tag{2.105}$$

which is the same Euler equation as for (fictitious) non-interacting particles in a potential

$$v_s(\mathbf{r}) \equiv \int d^3r' \frac{n(\mathbf{r}')}{|\mathbf{r}-\mathbf{r}'|} + \frac{\delta E_{xc}}{\delta n(\mathbf{r})} + v_{\rm ext}(\mathbf{r}) \; . \tag{2.106}$$

The (KS) orbitals for these (fictitious) non-interacting particles obey the equation

$$\left(-\frac{1}{2}\nabla^2 + v_s(\mathbf{r})\right)\phi_i(\mathbf{r}) = \lambda_i \phi_i(\mathbf{r}) \; , \tag{2.107}$$

where λ_i is a Lagrange multiplier introduced to make the KS orbitals orthogonal. The KS ground state is made up of the N orbitals having the N smallest values of λ_i

$$\Phi_0(\mathbf{r}_1, \ldots, \mathbf{r}_N) = \frac{1}{\sqrt{N!}} \det(\phi_i(\mathbf{r}_j)) \; . \tag{2.108}$$

And the (exact) ground state density is

$$n_0(\mathbf{r}) = \sum_{i=1}^{N} |\phi_i(\mathbf{r})|^2 \; . \tag{2.109}$$

The only problem is that E_{xc} cannot be determined exactly.

But, the great power of KS density functional theory is that, for a variety of systems, E_{xc} can be approximated well enough to obtain good results. These results, of course,

officially only apply to the ground state. But, since we have so much luck in applying our approximations (for E_{xc}, for example) to the ground state we could just go ahead and try applying KS density functional theory to excited states.

For example, the KS orbitals look so much like quasiparticle states, one could hardly fault us for using their matrix elements and eigenvalues to compute spectra. Or, with the KS orbitals specifed, we could define the KS Green's function in a way that is most appropriate as a starting point for perturbation theory:

$$\begin{aligned} G^{KS}(\mathbf{x},\mathbf{x}';t) &\equiv i\left\langle\Phi_0\right|\mathcal{T}\left(e^{iH_{KS}t}\hat{\psi}(\mathbf{x})e^{-iH_{KS}t}\hat{\psi}^{\dagger}(\mathbf{x}')\right)\left|\Phi_0\right\rangle \\ &= -i\sum_{i=1}^{\infty}\phi_i(\mathbf{x})\phi_i{}^{*}(\mathbf{x}')e^{-i\lambda_i t}\left(\theta(t)(1-n_i)-\theta(-t)n_i\right)\ . \end{aligned} \tag{2.110}$$

Of course, it goes without saying that there will be corrections to DFT when applied to excited states. For example, DFT underestimates the optical band-gap for a number of materials. This is not at all surprising since the KS Lagrange multipliers are not quasiparticle energies. We can, however, systematically[51, 59] correct spectra within the overall framework of DFT, for example, by applying self-energy[60, 61, 62] corrections to KS Lagrange multipliers. But a full discussion of this point could fill another Ph.D. thesis.[63, 64]

Chapter 3

ELECTRON INELASTIC MEAN FREE PATHS AND STOPPING POWERS

3.1 Main Idea of Chapter

A method is presented for first-principles calculations of electron inelastic mean free paths and stopping powers in condensed matter over a broad energy range. The method is based on *ab initio* calculations of the dielectric function in the long wavelength limit using a real-space Green's function formalism, together with extensions to finite momentum transfer. From these results we obtain the energy-loss function (ELF) and related quantities such as optical-oscillator strengths and mean excitation energies. From a many-pole representation of the dielectric function we then obtain the electron self-energy and inelastic mean free paths (IMFP). Finally using our calculated dielectric function and the optical-data model of Fernández-Varea *et al.*, we obtain collision stopping powers (CSP) and penetration ranges. The results are consistent with semi-empirical approaches and with experiment.

3.2 Introduction

The effect of inelastic losses on fast electrons has long been of theoretical and experimental interest,[21, 7, 65] and continues to be an area of active development.[13, 6, 66] Theoretical calculations of such losses depend on the dielectric response of a material over a broad spectrum. Moreover, calculations of these losses are particularly sensitive to the excitation spectrum of a material. While first-principles approaches have been developed for calculations of losses at low energies, i.e., up to a few tens of eV,[67, 68] these methods are computationally intensive and may be difficult to implement. Thus detailed calculations of inelastic losses have generally been limited to semi-empirical approaches,[69, 13, 70, 71, 72, 73, 74] based on experimental optical data. On the other hand, experimental data over a sufficiently broad spectrum are not readily available for many materials of interest.

In an effort to overcome these difficulties, we present here a first-principles, real-space approach for general calculations of inelastic losses. The approach is applicable to both periodic and aperiodic condensed matter systems throughout the periodic table. Our calculations are based on *ab initio* calculations of the complex dielectric function $\epsilon(\omega) = \epsilon_1(\omega) + i\epsilon_2(\omega)$ as a function of the frequency ω, in the long-wavelength limit, together with extensions to finite momentum transfer.[75] The calculations of $\epsilon(\omega)$ are carried out using an all electron, real-space Green's function (RSGF) formalism as implemented in a generalization of the FEFF8 code [1, 2] for full-spectrum calculations of optical constants. This generalization of the FEFF8 code is referred to as FEFF8OP below.

We focus in this Chapter on several physical quantities which characterize the inelastic interactions of a fast probe electron, a photo-electron, or other charged particle in condensed matter. These include the inelastic mean-free-path (IMFP) and the collision stopping-power (CSP). Each of these quantities depends on the complex dielectric function $\epsilon(\omega)$ through the energy-loss function (ELF) for a given material $-[\mathrm{Im}\,\epsilon^{-1}(\omega)] = \epsilon_2(\omega)/[\epsilon_1(\omega)^2 + \epsilon_2(\omega)^2]$, which is calculated here up to x-ray energies. The ELF is directly related to the optical oscillator strength (OOS). From the OOS, which characterizes the distribution of excitations (e.g., plasmons, particle-hole excitations, etc.), we obtain values of the mean excitation energy I. Recently a comprehensive relativistic treatment of inelastic losses and scattering within the first Born approximation has been developed by Fernández-Varea *et al.* [13] Their semi-empirical approach requires experimental optical data as input, and is referred to here as the optical data model (ODM). This approach has the advantage that calculations of quantities such as the CSP are reduced to a single numerical integration. To facilitate precise comparisons, we have used their formulation for our CSP calculations, except for the substitution of our *ab initio* dielectric function. Our approach is therefore referred to as the "*ab initio* data model" (ADM). We have also compared IMFPs calculated using both the ADM and a one-particle *self-energy* approach.

Formally the IMFP and the CSP are related to energy moments of the differential cross-section (DCS) for inelastic collisions $d\sigma/d\omega$ of a fast probe electron (or other charged particle) of initial kinetic energy E with energy loss ω. The inverse IMFP is proportional

to the zeroth moment of the DCS

$$\frac{1}{\lambda(E)} = n_a \int d\omega \, \frac{d\sigma(\omega;E)}{d\omega} = n_a \sigma^{(0)}(E) \, , \tag{3.1}$$

where n_a is the atomic number density. Recall that here and elsewhere in this Chapter we use Hartree atomic units ($m = \hbar = e = 1$). Thus distances are in Bohr ($a_0 \approx 0.529$ Å) and energies are in Hartree (H ≈ 27.2 eV), unless otherwise specified. The CSP, here denoted by $S(E)$, is proportional to the first moment of the DCS

$$S(E) = n_a \int \omega \, d\omega \frac{d\sigma(\omega;E)}{d\omega} = n_a \sigma^{(1)}(E) \, . \tag{3.2}$$

Since $S(E) = -dE/dx$, this quantity has units of force. From an integral of $1/S(E)$ over energy we can then obtain the CSDA range[1] $R(E)$ as

$$R(E) = \int dx = \int_0^E \frac{dE}{S(E)} \, . \tag{3.3}$$

Implicit in Eqs. (3.1) and (3.2) are the kinematics of the colliding particles. In this Chapter we choose kinematics relevant for probe electrons. Regardless of the probe, the sample is characterized by the dielectric function $\epsilon(\mathbf{q},\omega)$. In this Chapter we consider cubic materials which we approximate as isotropic and homogeneous, i.e., in which the dielectric function depends only on the magnitude of the momentum transfer $q = |\mathbf{q}|$ and the energy-loss ω.

The DCS may be considered as the sum of longitudinal (instantaneous Coulomb) and transverse (virtual photon) contributions, denoted below with subscripts L and T respectively. The detailed relativistic form of the relationship between each contribution to the DCS and the ELF is obtained by integrating the double differential cross-section (DDCS) over the kinematically allowed values of momentum-transfer,[13]

$$\frac{d\sigma(\omega;E)}{d\omega} = \int dq \frac{d\sigma(q,\omega;E)}{dqd\omega} \, , \tag{3.4}$$

where

$$\frac{d\sigma(q,\omega)}{dqd\omega} = \frac{d\sigma_L(q,\omega)}{dqd\omega} + \frac{d\sigma_T(q,\omega)}{dqd\omega}. \tag{3.5}$$

[1] In actual calculations the lower limit in the definition of the CSDA range is usually taken as some small fraction of the incident energy, e.g., $0.1 \times E$, rather than zero. We could call such a definition the "CSDA range to lose ninty percent of the incident energy".

As an example of how the dielectric function determines the DDCS, we recall (see Eq. (2.71)) the familiar non-relativistic result:

$$\frac{d\sigma(q,\omega)}{dqd\omega} = \frac{d\sigma_L(q,\omega)}{dqd\omega} = -\frac{2}{\pi n_a q v^2}\,\mathrm{Im}\,\epsilon^{-1}(q,\omega) \tag{3.6}$$

where v is the velocity of the probe electron. The relativistic analog of Eq. (3.6) is similar and is given explicitly in Eqs. (8) and (9) of Ref. [13].

One of the main goals of this work is to calculate mean excitation energies I and IMFPs for general condensed matter systems over an energy range up to about 100 keV. Another goal is to calculate CSPs and penetration ranges over a range of order 10 MeV. We compare our results both with other semi-empirical approaches and with experimental data and tabulations.

3.3 Model Dielectric Function

Both the IMFP and the CSP can be computed as convolutions of the momentum-transfer and energy-loss dependent inverse dielectric function $\epsilon^{-1}(q,\omega)$, with relativistic weighting functions. The precise details of the weighting functions are discussed further below. In this Section we discuss the extension of our *ab initio* calculation of $\epsilon(q,\omega)$ in the long wavelength ($q \to 0$) limit to finite q.[13, 76, 69, 77, 78] In this work $\epsilon(\omega) \equiv \epsilon(0,\omega)$ is calculated from the UV to x-ray energies using the *ab initio* real-space Green's function code FEFF8OP [2, 79], which sums the contributions to the spectra over all occupied core and semi-core initial states. As an example, the calculated ELF for Ag is shown in Fig. 3.1.

We have chosen to discuss the extension to finite-q in terms of the ELF, but we could just as well have used the OOS $g(\omega)$, with differs by a factor proportional to ω, i.e.,

$$g(\omega) = -\frac{2}{\pi}\frac{Z}{\Omega_p^2}\,\omega\,\mathrm{Im}\big[\epsilon^{-1}(\omega)\big], \tag{3.7}$$

where $\Omega_p^2 = 4\pi n_a Z$ is the all-electron plasma frequency and Z is the atomic number. As an illustration of the quantitative agreement of our approach, three *ab initio* OOS calculations, spanning a range of atomic numbers, are compared to experiment in Fig. 3.2. Clearly the approximations in FEFF8 such as the use of atomic core initial states in the OOS calculation and muffin-tin scattering potentials are adequate to yield good agreement with experiment

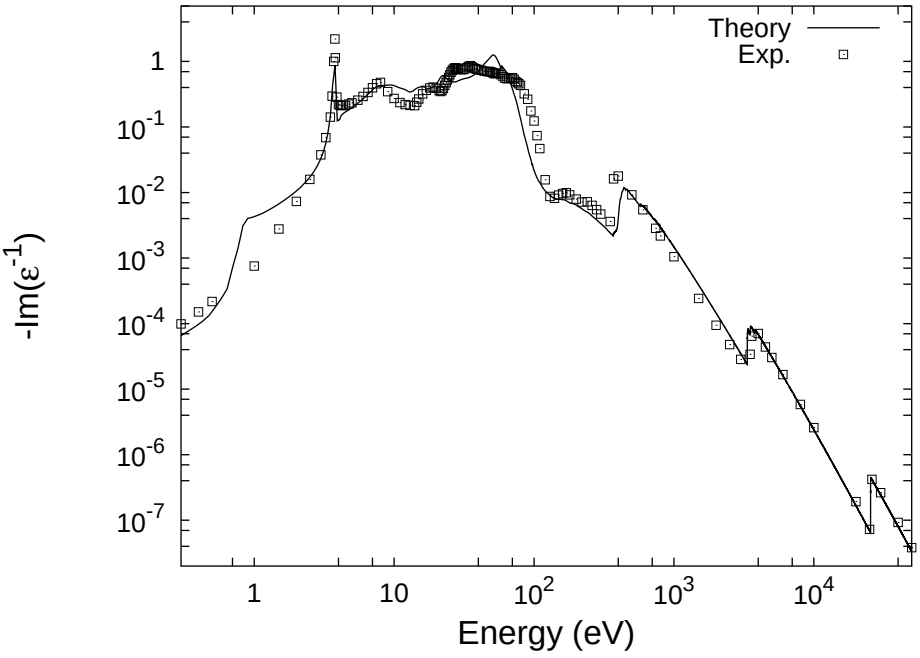

Figure 3.1: Energy-loss function $-[\mathrm{Im}\,\epsilon^{-1}(\omega)]$ of fcc silver as calculated by *ab intio* theory[2] (solid line) using the FEFFOP (see text) code and from experiment [3, 4] (points).

for UV energies and above. Additional examples are tabulated on the WWW.[80] For optical frequencies and below, however, the agreement is only semi-quantitative, but the errors tend to be suppressed in the OOS due to the overall factor of ω in Eq. (3.7). Further discussion of properties of our calculated OOS, encluding the f-sum rule, can be found elsewhere.[2, 79]

A global measure of the excitation spectra is given by the "mean excitation energy" $\ln I = \langle \ln \omega \rangle$, where the "mean" $\langle \ldots \rangle$ refers to an average with respect to the OOS weighting function, i.e.,

$$\ln I = \frac{\int d\omega\, g(\omega) \ln \omega}{\int d\omega\, g(\omega)}. \tag{3.8}$$

The quantity I appears in expressions for the collision stopping power, as shown in Sec. V. below. In Table 3.1 theoretical values of I, as calculated from our OOS spectra, are compared with those calculated from experimental optical constants,[4] and also with internationally recommended (ICRU) values for several elements. For low Z elements, the theoretical values of I are clearly in good agreement with measured values. For high Z elements I is predicted by Thomas-Fermi models to be proportional to Z. The proportion-

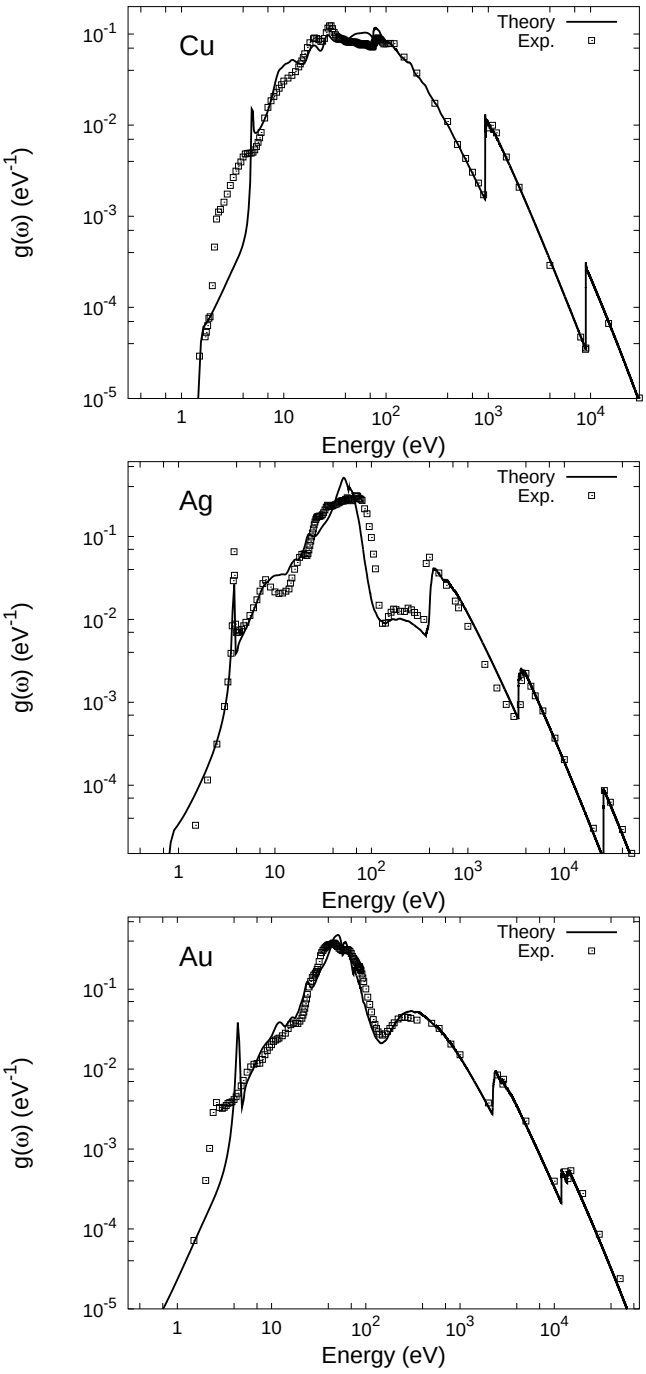

Figure 3.2: Optical oscillator strengths for Cu (upper), Ag (middle) and Au (lower) as calculated by *ab initio* theory[2] (solid line) using the FEFFOP code (see text) and compared to experiment [3, 4] (points).

Table 3.1: *Mean excitation energies* I for several elements as calculated in this work, and for comparison, results calculated from experimental [15, 4] optical constants, and recommended (ICRU [16]) values.

Element	I theory (eV)	I expt (eV)	ICRU (eV)
Aluminum	165	167 [15], 162 [4]	166
Silicon	174	173 [15]	173
Copper	312	319 [4]	322
Silver	420	382 [4]	470
Gold	662	752 [4]	790

ality constant can be determined experimentally to give a semi-empirical "rule of thumb" $I \approx 10\,Z$ (eV). In the high Z regime the agreement between theory and experiment appears to be only semi-quantitative, but it should be mentioned that the ratio of I to Z is not in fact constant but rather it varies from around 9 to around 11 and has been measured to be as low as 8.32 for lanthanum.[81] Furthermore, only the logarithm of I is needed for the determination of physical quantities, and typical errors in $\ln I$ from the values in Table I are only a few percent. For example, for a typical case of 100 keV electrons in gold, the error in stopping powers calculated using experimental versus theoretical values of I is only around 2%. Furthermore, this error decreases as the incoming electron energy increases. On the other hand, at the lowest energies of interest (e.g. $\sim$10 keV for Au) where the Bethe Formula (and the usefulness of $\ln I$ for calculating the CSP) breaks down, the percent difference between experimental and theoretical CSPs is still only around 6%. The method of calculating the CSP at lower energies without using $\ln I$ is described in Sec. V.

In the IMFP calculations presented here we consider two different extensions to finite q, as described below. Since our calculations show that both lead to similar results for the IMFP, we only present calculations of the CSP with one of these extensions. However, all our calculations use the same full-spectrum calculations of $\epsilon(\omega)$. For our IMFP calculations, we have used the many-pole representation of the dielectric function of Ref. [75], i.e. we approximate our calculated ELF $-\mathrm{Im}\,[\epsilon^{-1}(\omega)]$ as a sum of many (typically of order 100)

discrete poles. This "many-pole" model, denoted by $\epsilon_N^{-1}(\omega)$, has the standard analytic form for dielectric response,

$$\epsilon_N^{-1}(\omega) = 1 + \sum_{j=1}^{N} g_j \frac{\omega_j^2}{\omega^2 - \omega_j^2 + i\omega\delta}, \tag{3.9}$$

where $\delta\omega$ is a small damping term, comparable to the pole separations. Fig. 3.3 compares the IMFP for Cu as calculated using both our many-pole model and a single plasmon-pole model.[62] This single-pole model is essentially an Einstein-model for the response in which excitations (for a given momentum transfer q) occur at the plasmon excitation energy ω_q. Thus the single-pole model is a special case of the many-pole model in which all but one of the weights g_j appearing in Eq. (3.9) are set to zero. In our many-pole representation, the parameters ω_j are taken to be evenly spaced along the energy-loss axis, and the weights g_j are fixed by matching our calculation of $\mathrm{Im}\big[\epsilon^{-1}(\omega)\big]$ according to the formula

$$g_j = -\frac{2}{\pi}\frac{1}{\omega_j^2}\int_{\Delta_j} d\omega\, \omega\, \mathrm{Im}\big[\epsilon^{-1}(\omega)\big], \tag{3.10}$$

where the integration region Δ_j is from $(\omega_j + \omega_{j-1})/2$ to $(\omega_j + \omega_{j+1})/2$ and the similarity with Eq. (3.7) is apparent. Finally, the extension to finite q is obtained by shifting the pole locations via the substitution [62]

$$\omega_j^2 \quad \rightarrow \quad \omega_j^2 + \frac{{v_F}^2 q^2}{3} + \frac{q^4}{4}\,, \tag{3.11}$$

where v_F is the Fermi velocity as calculated at the mean interstitial electron density from the FEFF8 code. Further details of our approach, though not essential to our discussion here, are given in Refs. [75], [79] and [64]. The above substitution is sufficient to induce the so-called "Bethe ridge" for large momentum-transfer where the ELF is peaked about the point $\omega = q^2/2$. In other words, our model for large q satisfies the approximate relation

$$-\mathrm{Im}\big[\epsilon^{-1}(q,\omega)\big] \approx \pi\Omega_p^2\delta(\omega^2 - Q^2), \tag{3.12}$$

where $Q \equiv q^2/2$. Consequently the above extension can be regarded as an interpolation formula between small and large Q.

For CSP calculations, our aim here is to replace experimental optical data (which is used as input in the ODM of Ref. [13]) with theoretical "optical data" from our *ab initio*

calculation of $\epsilon(\omega)$, i.e., with an *ab initio* data model (ADM). Thus for consistency we follow the formulation of Ref. [13] as closely as possible in comparisons with their CSP results. In particular we have also implemented their delta-oscillator [76, 82] extension to finite q for our CSP calculations. For non-relativistic probe electrons the delta-oscillator model extends $\epsilon(\omega)$ to finite q according to the relation

$$\begin{aligned} -\mathrm{Im}\big[\epsilon^{-1}(q,\omega)\big] &= \pi\Omega_p^2 \frac{Z(Q)}{Z}\delta(\omega^2 - Q^2) \\ &- \mathrm{Im}\big[\epsilon^{-1}(\omega)\big]\theta(\omega - Q)\ , \end{aligned} \tag{3.13}$$

where $Z(Q)$ is the number of electrons that contribute to the zero momentum-transfer sum-rule with upper energy limit Q,

$$Z(Q) = -\frac{2Z}{\pi\Omega_p^2}\int_0^Q d\omega\,\omega\,\mathrm{Im}\big[\epsilon^{-1}(\omega)\big]\ . \tag{3.14}$$

Because $Z(Q)$ approaches Z for large q we see that the extension to finite q in Eq. (3.13) gives the Bethe ridge in much the same way as that of Eq. (3.12).

Although the finite-q extension algorithms in this Chapter differ somewhat, we do not expect our non-relativistic results to depend substantially on the details. The reason is that both algorithms reduce to the correct long-wavelength limit for low q, and both give the correct Bethe ridge dispersion for high q. This expectation is supported by the IMFP results in Sec. IV. Moreover our results for the q dependence are roughly consistent with the explicit real space calculations of $-\mathrm{Im}\big[\epsilon^{-1}(q,\omega)\big]$ at finite q of Soininen et al. [23].

3.4 Electron Self-Energy

Inelastic losses in the propagation of a fast charged particle can be expressed in terms of one-particle *self-energy* $\Sigma(E)$. This complex-valued quantity is a dynamically screened exchange-correlation contribution to the quasi-particle energy-momentum relation

$$E = \frac{p^2}{2} + \Sigma(E), \tag{3.15}$$

where p is the quasi-particle momentum. Our approach for calculating $\Sigma(E)$ is based on the "*GW*" approximation of Hedin,[51] together with our many-pole representation of the dielectric function, as summarized above [75]. In the GW method the vertex-corrections

to the electron self-energy are neglected, yielding an expression for $\Sigma(E)$ in terms of the electron propagator G and the screened Coulomb potential acting on an electron W, i.e.,

$$\Sigma(\mathbf{x},\mathbf{x}';E) = i\int \frac{d\omega}{2\pi} e^{-i\omega\eta} G(\mathbf{x},\mathbf{x}';E-\omega) W(\mathbf{x},\mathbf{x}';\omega), \tag{3.16}$$

where η is a positive infinitesimal and the $(\mathbf{x},\mathbf{x}')$ are spatial indices. Within the RSGF approach, the propagator G is calculated using a multiple-scattering expansion $G = G_0 + G_0 t G_0 + \cdots$ [1]. However, for simplicity in this work, we neglect the multiple-scattering terms (which would give rise to fluctuations in the self-energy) and simply use the free propagator G_0 for a homogeneous electron gas at the mean interstitial density. Then the screened Coulomb interaction for a spatially homogeneous system can be obtained from the Fourier transform $W(\mathbf{q},\omega) = \mathcal{F}\left[W(\mathbf{x}-\mathbf{x}',t)\right]$ and can be expressed in terms of the Coulomb potential $V_q = 4\pi/q^2$ and the dielectric function $\epsilon(\mathbf{q},\omega)$ as:

$$W(\mathbf{q},\omega) = \epsilon^{-1}(\mathbf{q},\omega)\, V_q. \tag{3.17}$$

The calculations of $\Sigma(E)$ are then carried out using the many-pole representation of Eq. (3.9) and (3.11). With this homogeneous model, our calculated $\Sigma(E)$ is then the average self-energy in the system. Further details are given in Ref. [64].

3.5 Inelastic Mean Free Path

We first calculate Eq. (3.1) for the IMFP in terms of the excited state *self-energy* $\Sigma(E)$ of the fast electron.

$$\lambda(E) = \sqrt{\frac{E}{2}}\frac{1}{|\mathrm{Im}\,\Sigma(E)|}\,. \tag{3.18}$$

Eq. (3.18) for the IMFP is consistent with the decay of a single electron wavefunction whose time dependence is given by $e^{-iE(p)t}$.[83] Eq. (3.18) is also equivalent to Eq. (3.1) because the self-energy is proportional to the forward scattering amplitude, i.e.,

$$\mathrm{Im}\,\Sigma(\mathbf{p}) = -2\pi n_a\,\mathrm{Im}\,f(\mathbf{p},\mathbf{p})\,. \tag{3.19}$$

The equivalence of Eq. (3.1) and Eq. (3.18) then follows from the optical theorem. It should be noted, however, that our calculations of the IMFP in terms of the self-energy via Eqn. (3.18) do not enclude relativistic effects, whereas Eqn. (3.1) is fully relativistic.

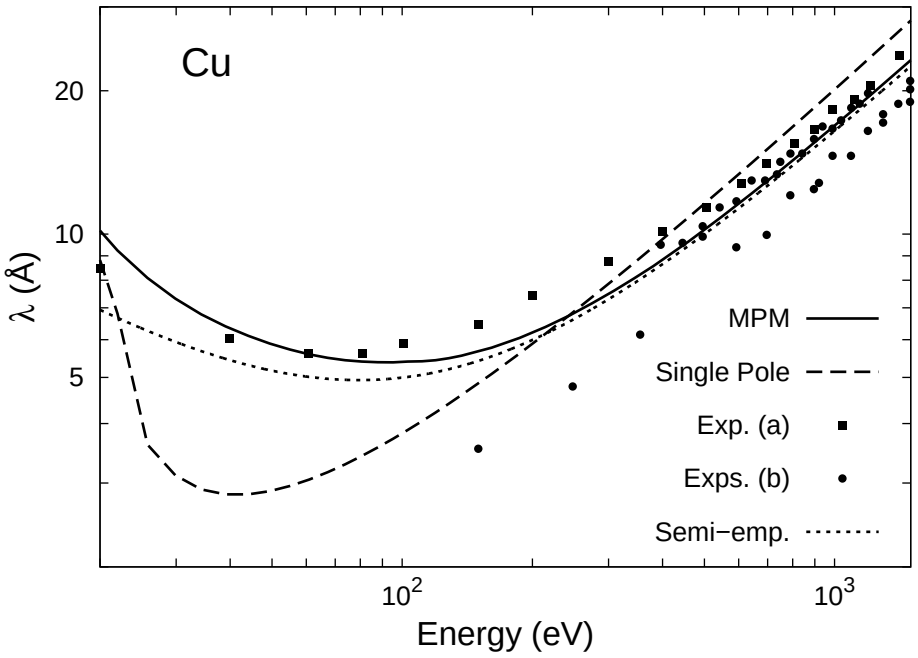

Figure 3.3: Inelastic mean free paths for copper calculated using the same *ab initio* dielectric function as the basis of two different theoretical models: The many-pole self-energy (MPM) model of Eq. (3.18) and the single-pole self-energy model (described in the text). These theoretical results are compared to: Exp. (a) [5] (squares), Exps. (b) (circles, the references for Exps. (b) are given in Ref. [6]), and a semi-empirical curve which is described in Ref. [6].

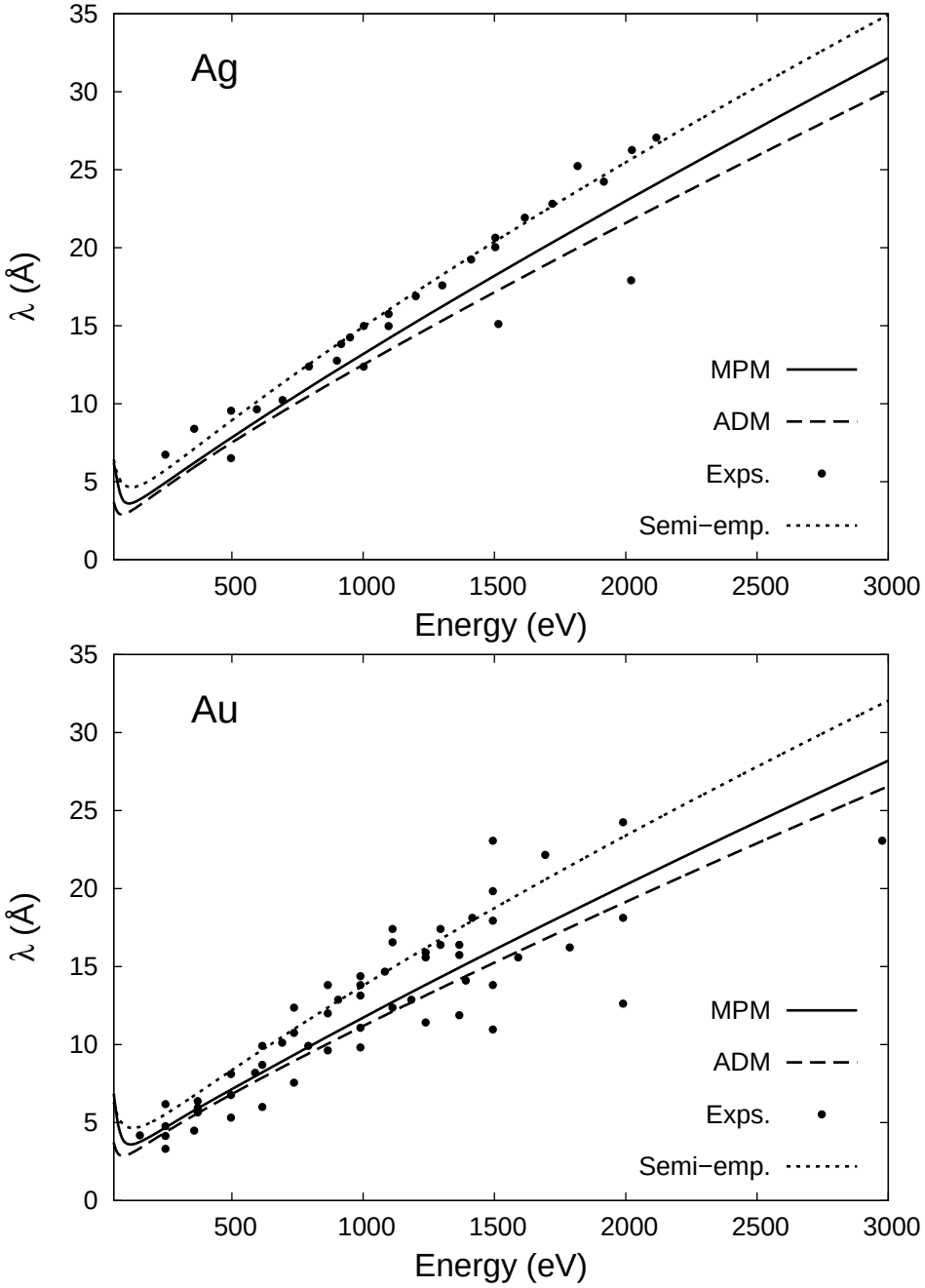

Figure 3.4: Inelastic mean free paths for Ag (upper) and Au (lower) calculated using the same *ab initio* dielectric function as the basis for two different theoretical models: the many-pole self-energy (MPM) model of Eq. (3.18), and the "*ab initio* data" model (ADM) described in the introduction. The theoretical results are compared to a semi-empirical curve [6] and to multiple experimental data sets. The references for the Exps. are given in Ref. [6]. The theoretical models are plotted over the expected range of validity of the semi-empirical curve.

The explicit dependence of the self-energy on the dielectric function in Eq. (3.17), the many-pole model of Eq. (3.9), and (3.11), and the full-spectrum FEFF8OP code are all that are needed to carry out *ab initio* calculations of IMFPs according to Eq. (3.18). Our many-pole model IMFP calculations (labeled MPM) are shown for several materials in Figs. 3.3 and 3.4, together with best fits [6] to currently available data. The fit lines in Figs. 3.3 and 3.4 are based on multiple data sets which were taken up to 3000 eV and are expected to accurately describe the IMFP as low as 50 eV. Fig. 3.4 also shows a calculation (labeled "ADM") which uses our *ab initio* $\epsilon(\omega)$ as input data to the semi-empirical optical-data model of Ref. [13]. Note that the MPM and ADM results are in in good agreement with each other, which verifies that the different extensions to finite q discussed in Sec. II. do not lead to substantially different results. Both theoretical models are plotted here over the expected range of validity of the fit line, but can be extended with our codes to energies up to about 100 keV. Although the agreement with experiment is reasonable, our calculations tend to underestimate the experimental IMFP somewhat for high Z materials.

3.6 Stopping Power

As noted in the introduction the CSP is the net reaction force $S(E) = -dE/dx$ due to electronic collisions at a given energy E that slows a fast probe electron. Over the range of energies from about 10 eV up to about 10 MeV the CSP is the main contribution to the total stopping power. Above this energy the total stopping power may be dominated by bremsstrahlung.[16] The CSP is calculated in this work using Eq. (3.2), where the DCS is related to our *ab initio* ELF using the formulation of Ref. [13]. This model is thought to be applicable with confidence for energies above about 100 eV, and appears to be applicable as low as about 10 eV. However, it is not obvious why a model based on the first Born approximation should be valid at such low energies. Furthermore, in the Born approximation the CSP is proportional to the square of the incoming particle charge and thus non-linear corrections such as the Barkas effect [84] are not encluded in this model. In the relativistic limit Eq. (3.2) reduces to the well-known Bethe-formula [21, 85, 65, 7] for the stopping

power

$$S(E) = \frac{\pi}{2}\frac{\Omega_p^2}{v^2}\left[\ln\left(\frac{E^2}{I^2}\frac{\gamma+1}{2}\right) + F(\gamma) - \delta_F(\gamma)\right], \tag{3.20}$$

where $\gamma = (1 - v^2/c^2)^{-1/2}$ is the relativistic dilation factor, and $F(\gamma)$ is given by

$$F(\gamma) = \left[\frac{1}{\gamma^2} - \frac{2\gamma-1}{\gamma^2}\ln 2 + \frac{1}{8}\left(\frac{\gamma-1}{\gamma}\right)^2\right]. \tag{3.21}$$

Also appearing in Eq. (3.20) are the "mean excitation energy" I defined in Sec. II., and Fermi's density correction [7] δ_F. The density correction δ_F is due solely to transverse interactions, and can be neglected for non-relativistic particles. A detailed description of how δ_F can be calculated as a functional of the ELF, is given in Ref. [13]. Fig. 3.5 shows the density correction $\delta_F(E)$ for copper as calculated using our *ab initio* dielectric function, and for comparison, the semi-empirical values used by ESTAR [8]. ESTAR is an on-line implementation of Eq. (3.20) which takes semi-empirical values of I as input. The mean excitation energy and the density correction have, heretofore, been difficult to calculate from first-principles, as they require accurate values of the OOS over a very large energy spectrum. However, our full-spectrum approach clearly gives reasonable agreement with experiment.

For relativistic probe electrons, the excellent agreement of the Bethe formula in Eq. (3.20) for the CSP is well known, so we have included data from ESTAR in lieu of experiment where necessary. The difference between Eq. (3.20) and Eq. (3.2) only appears in the non-relativistic regime, and can be seen in Fig. 3.6, where Eq. (3.20) begins to fail around 5000 eV. In order to calculate CSPs that are in good agreement with experiment for both non-relativistic and relativistic probe electrons we apply Eq. (3.2) with the more general form of $d\sigma/d\omega$ given in Ref. [13], but using our calculated dielectric function as input.

Figs. 3.6 and 3.7 show that the calculated CSPs for high energy electrons for the systems studied here (Cu, Ag and Au) are in good agreement with the ESTAR results. For lower energies the CSP calculations of this work show significantly better agreement with data than the Bethe formula.

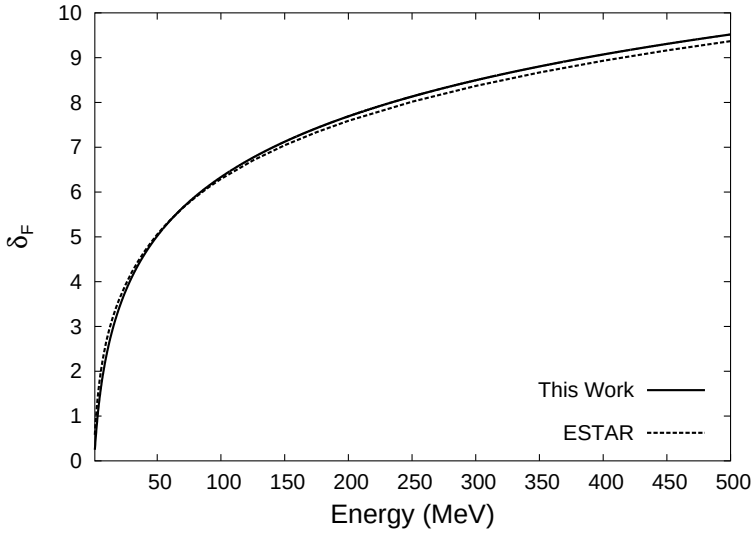

Figure 3.5: Fermi's density effect correction[7] to the stopping power from Eq. (3.20) as calculated in this work (solid), and compared to semi-empirical values [8] for copper (dashes).

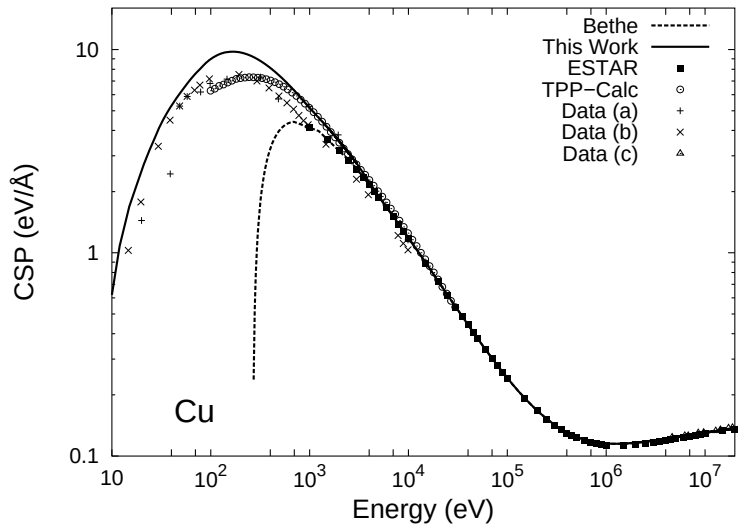

Figure 3.6: Collision stopping power for Cu as calculated using the *ab initio* dielectric function of Ref. [2] (solid) in the ADM (see text). Also shown are semi-empirical values of the CSP from ESTAR [8] (solid squares), and semi-empirical CSP values (labeled TPP-calc) based on the Penn model [9] (circles), and CSP values from experimental data: (+) [10], (x) [11], and (triangles) [12]. The Bethe formula of Eqn. (3.20) is shown as a dashed line.

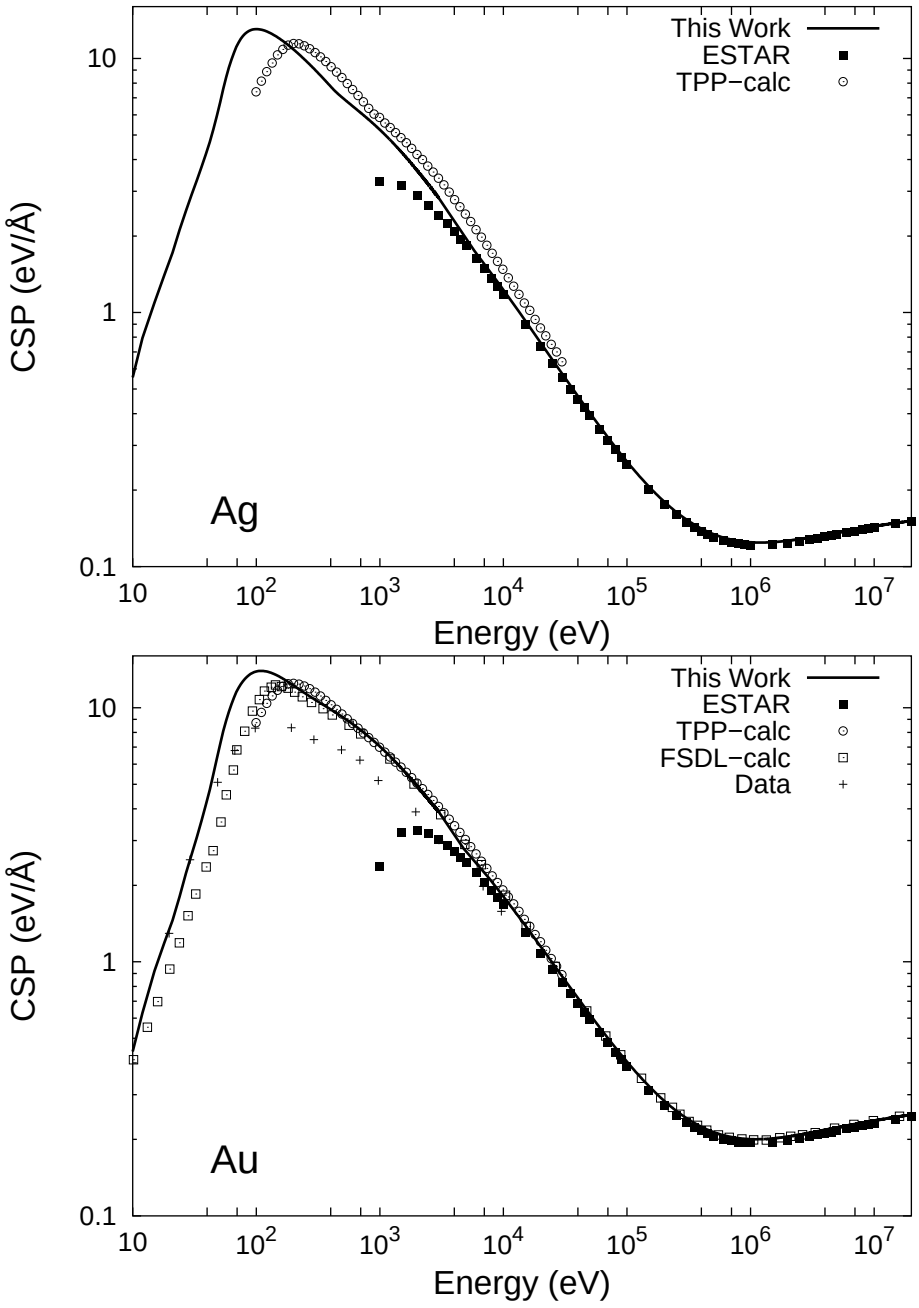

Figure 3.7: Collision stopping powers for Ag (upper) and Au (lower), with labels as in Fig. 3.6. Also shown for Au are the semi-empirical CSP values as calculated in Ref. [13] (labelled FSDL-calc), and CSP values from experiment.[10]

3.7 Conclusions

We have presented a general real-space Green's function approach for *ab initio* calculations of inelastic losses and stopping powers in condensed matter. Unlike most current approaches, our method is based on *ab initio* calculations of dielectric response, and does not rely on empirical optical data. We also find that accurate calculations of inelastic losses of probe electrons depend primarily on the quality of the calculated $q = 0$ dielectric function, and not on the details of the extension to finite q. Using our *ab initio* dielectric function, we also calculate the mean excitation energy and thus stopping powers for relativistic electrons, obtaining results in good agreement with experimental data. Furthermore, using the *ab initio* ADM we can extend the stopping power calculation down to energies of ~ 10 eV, i.e., much lower than the Bethe formula, while still maintaining reasonable agreement with experiment. Our approach for calculating inelastic losses of probe electrons can be easily extended to probe positrons. In conclusion, we believe our approach has the potential to complement or provide an alternative to semi-empirical approaches for calculations of IMFPs and stopping powers of electrons in condensed matter.

Chapter 4

EELS AND MAGIC ANGLE

4.1 Main Idea of The Chapter

Recently it has been demonstrated that a careful treatment of both longitudinal and transverse matrix elements in electron energy loss spectra can explain the mystery of relativistic effects on the *magic angle*. Here we show that there is an additional correction of order $(Z\alpha)^2$ where Z is the atomic number and α the fine structure constant, which is not necessarily small for heavy elements. Moreover, we suggest that macroscopic electrodynamic effects can give further corrections which can break the sample-independence of the magic angle.

4.2 Introduction: Magic Angle Mystery

The title of this Section is in reference to a recent work by Jouffrey *et al.* [86] with the title "The Magic Angle: A Solved Mystery." The *magic angle* in electron energy loss spectroscopy (EELS) is a special value of the microscope collection-angle α_c at which the measured spectrum "magically" becomes independent of the angle between the incoming beam and the sample "c-axis." The mystery, in the context of 200 keV electron microscopy, is that standard semi-relativistic quantum theory yields a ratio of the magic angle θ_M to "characteristic angle" θ_E of more than twice the observed [14] value. Unfortunately, time [87] and again,[14, 88] the theoretical justification of the factor of two turned out to be an errant factor of two elsewhere in the calculation. A key contribution of Jouffrey *et al.* was the observation that relativistic "transverse" effects, when properly included in the theory, naturally give a factor of two correction to the non-relativistic magic angle. Here we show that there are yet additional corrections to the theory which can even break the sample independence of the magic angle.

As in Ref. [86], we consider here the problem of a relativistic probe electron scattering

off of a macroscopic condensed matter sample. Similar problems have been solved long ago using both semi-classical [89] and fully quantum-mechanical approachs.[21, 90, 65] Indeed, the fully quantum-mechanical, relativistic case of scattering two plane-wave electrons has long been a textbook problem.[91, 49] This classic problem was revived recently in the works of Jouffrey *et al.* [86] and of Schattschneider *et al.*,[92] in which a "flaw" in the standard theory is pointed out. The flaw is the approximation that the so-called "longitudinal" and "transverse" matrix elements for the scattering process may be summed incoherently, as argued by Fano in a seminal paper.[90] In fact, this approximation is only valid when the sample under consideration posseses certain symmetries. In a later review article,[65] Fano states this condition explicitly; namely that his original formula for the cross-section is only applicable to systems of cubic symmetry. However, this caveat, seems to have been generally ignored, and hence turns out to be the source of the magic angle "mystery".[86] Jouffrey *et al.*, and later Schattschneider *et al.*, showed that if one correctly sums and squares the transition matrix elements then, in the dipole approximation, one finds the magic angle corrected by approximately a factor of two.

Our aim here is to examine the theory in more detail in order to derive both relativistic and material-dependent corrections to the magic angle. In Section 4.3 we consider relativistic electron scattering within the formalism of quantum electrodynamics (QED). Working in the Coulomb gauge, we show that one can almost reproduce the results of Jouffrey *et al.* and the theory of Schattschneider *et al.*, apart from a simple correction term of order $\hbar\omega/mc^2$, which is not always negligible. Here $\hbar\omega$ is the energy lost by the probe and mc^2 is the rest energy of an electron. In Section 4.4 we suggest the possibility of incorporating macroscopic electrodynamic effects into the theory, which can break the symmetry of sample independence of the magic angle.

4.3 Coulomb Gauge Calculation

An appealing aspect of the formalism of Schattschneider *et al.* is its simplicity. Their approach is similar to the semi-classical approach of Møller,[89] but with the added simplification of working with a probe and sample described by the Schrödinger equation, rather than the Dirac equation. They also find that the theory is simplified by choosing to work

in the Lorentz gauge. Unfortunately, however, the theory of Møller is somewhat *ad hoc* in that a classical calculation in the Lorentz gauge is modified by replacing the product of two classical charge densities by the product of four different wavefunctions in order to obtain the transition matrix element. For the Møller case this procedure is justified *a posteriori* by the fact that it reproduces the correct result, but is only rigorously justified by appealing to the method of second quantization.[91] Møller's procedure is physically reasonable *a priori*, because Møller was interested in the scattering of electrons in vacuum. However, the theory of Schattschneider *et al.,* which largely mimics Møller's theory, is less physically reasonable *a priori*, since the electrons are not scattering in vacuum, but are inside a solid which can screen the electrons. Nevertheless, since the discrepancy is small, the Schattschneider *et al.,* theory is justified *a posteriori* to a lesser extent by experiment.[14] We thus refer to the theory of Schattschneider et *al.* as a "vacuum-relativisitic theory." Consequently, in an effort to account for the discrepancy with experiment, we feel that it is useful to rederive the results of Jouffrey *et al.* from a more fundamental starting point.

It is easy to see that the theory of Schattschneider *et al.* is not formally exact, though for many materials the error in the vacuum relativistic limit is negligible. In fact, the discrepancy can be easily explained via single-particle quantum mechanics: although Schattschneider *et al.* work explicitly in the Lorentz gauge, they also make the assumption that the momentum and the vector potential commute,

$$\boldsymbol{p} \cdot \boldsymbol{A}(\boldsymbol{r}) \stackrel{?}{=} \boldsymbol{A}(\boldsymbol{r}) \cdot \boldsymbol{p}. \tag{4.1}$$

Of course, this commutation relation is only exact in the Coulomb gauge. In the end, however, the error in this approximation only effects the final results (e.g., matrix elements) by a correction of order $\hbar\omega/mc^2$ compared to unity, where $\hbar\omega$ is the energy lost by the probe. Since $\hbar\omega/mc^2$ is at most $(Z\alpha)^2$ for deep-core energy loss, the effect is usually negligible, except of course, for very heavy atoms. To see how corrections such as the above enter into the theory, and further to determine whether or not such corrections are meaningful or simply artifacts of the various approximations used in the theory of Schattschneider et *al.*, we find it useful to present a fully quantum-mechanical, relativistic many-body treatment along the lines of Fano,[65] but without any assumption of symmetry of the sample. Our

treatment is at least as general as that of Schattschneider *et al.* as far as the symmetry of the sample is concerned. Thus going beyond the formulations of Schattschneider *et al.* and Møller, we take as our starting point the many-particle QED Hamiltonian. We then show that in a single-particle approximation the theory yields the result of Schattschneider *et al.* together with the correction mentioned above.

Our starting point therefore is the Hamiltonian in Coulomb gauge [91]

$$H = H_{\rm el} + H_{\rm int} + H_{\rm rad} \ , \tag{4.2}$$

where the Hamiltonian has been split into three parts: i) the unperturbed electron part

$$H_{\rm el} = \int d^3x \, \psi^\dagger(\boldsymbol{x}) \left(c\boldsymbol{\alpha} \cdot \boldsymbol{p} + \boldsymbol{\beta} mc^2 \right) \psi(\boldsymbol{x}), \tag{4.3}$$

where $\psi(\boldsymbol{x})$ is the second-quantized Dirac field, $\boldsymbol{\alpha}_i$ and $\boldsymbol{\beta}$ are the usual Dirac matrices, m is the electron mass, and c is the speed of light;
ii) the unperturbed (transverse) radiation part

$$H_{\rm rad} = \sum_{\boldsymbol{k}} \sum_{i=1}^{2} a^\dagger_{\boldsymbol{k},i} a_{\boldsymbol{k},i} \hbar\omega_k, \tag{4.4}$$

where $a_{\boldsymbol{k},i}$ destroys a photon of momentum $\boldsymbol{k}$, polarization $\boldsymbol{\epsilon}_{\boldsymbol{k},i}$, and energy $\hbar\omega_k$; and
iii) the interaction part

$$\begin{aligned} H_{\rm int} &= + e \int d^3x \, \psi^\dagger(\boldsymbol{x}) \boldsymbol{\alpha} \cdot \boldsymbol{A}(\boldsymbol{x}) \psi(\boldsymbol{x}), \\ &+ \frac{e^2}{2} \int d^3x d^3y \frac{\psi^\dagger(\boldsymbol{x}) \psi^\dagger(\boldsymbol{y}) \psi(\boldsymbol{y}) \psi(\boldsymbol{x})}{|\boldsymbol{x} - \boldsymbol{y}|}, \end{aligned} \tag{4.5}$$

where

$$\boldsymbol{A}(\boldsymbol{x}) = \sum_{\boldsymbol{k},i} \sqrt{\frac{2\pi\hbar c^2}{V\omega_k}} \left(a_{\boldsymbol{k},i} \boldsymbol{\epsilon}_{\boldsymbol{k},i} e^{i\boldsymbol{k}\cdot\boldsymbol{x}} + a^\dagger_{\boldsymbol{k},i} \boldsymbol{\epsilon}^*_{\boldsymbol{k},i} e^{-i\boldsymbol{k}\cdot\boldsymbol{x}} \right), \tag{4.6}$$

$e = |e|$ is the charge of the proton, and V is the system volume.

Let us next specialize to the case of a fixed number $(N+1)$ of electrons where the $(N+1)$-th electron is singled out as the "fast probe" traveling with velocity $\boldsymbol{v}_0$, and the remaining N electrons make up the sample. We also introduce a lattice or cluster of ion-cores (below we consider only elemental solids of atomic number Z but the generalization

to more complex systems is obvious) which is treated classically, and which gives rise to a potential $v_{\text{e-core}}(\boldsymbol{x}) = \sum_{i=1}^{N/Z}(-Ze^2)/|\boldsymbol{x} - \boldsymbol{R}_i|$ as seen by the electrons. In this case our Hamiltonian becomes:

$$\begin{aligned} H &= \left[c\boldsymbol{\alpha}\cdot(\boldsymbol{p} + \frac{e}{c}\boldsymbol{A}(\boldsymbol{r})) + \boldsymbol{\beta}mc^2\right] + v_{\text{e-core}}(\boldsymbol{r}) \\ &+ \sum_{i=1}^{N}\left[c\boldsymbol{\alpha}^{(i)}\cdot(\boldsymbol{p}^{(i)} + \frac{e}{c}\boldsymbol{A}(\boldsymbol{r}^{(i)})) + \boldsymbol{\beta}^{(i)}mc^2\right] \\ &+ e^2\sum_{i=1}^{N}\frac{1}{|\boldsymbol{r} - \boldsymbol{r}^{(i)}|} + \frac{e^2}{2}\sum_{1=i\neq j=1}^{N}\frac{1}{|\boldsymbol{r}^{(i)} - \boldsymbol{r}^{(j)}|} \\ &+ \sum_{i=1}^{N} v_{\text{e-core}}(\boldsymbol{r}^{(i)}) + v_{\text{core-core}} + H_{\text{rad}}\ , \end{aligned} \tag{4.7}$$

where the coordinates which are not labelled by an index refer to the probe electron. The interaction $v_{\text{core-core}}$ between ion cores is a constant and is henceforth dropped.

To proceed to a single-particle approximation for the sample, the interaction of the sample electrons among themselves and with the potential of the ion cores may be taken into account by introducing a single-particle self-consistent potential $v(\boldsymbol{x})$ which includes both $v_{\text{e-core}}(\boldsymbol{x})$ and exchange-correlation effects. The interaction of the probe electron with the effective single electron of the sample will be considered explicitly. The difference between this interaction and the actual interaction between the probe and sample can be accounted for by introducing another potential $v'(\boldsymbol{x})$ which is not necessarily the same as $v(\boldsymbol{x})$; $v'(\boldsymbol{x})$ is, in theory, "closer" to the pure $v_{\text{e-core}}(\boldsymbol{x})$ potential than $v(\boldsymbol{x})$ though, in practice, this difference may not be of interest (see Section 4.6 for further explanation of this point). The potential $v'(\boldsymbol{x})$ leads to diffraction of the probe electron, which will not be considered in this Chapter in order to make contact with the theory of Schattschneider *et al.* It is also for this reason that we have introduced a single-particle picture of the sample, along with the fact that we want to apply this theory to real condensed matter systems in a practical way. The extension to the many-body case, in which the only single-body potential seen by the probe is due to the ion-cores, is given in Section 4.6. Thus using the single-particle

approximation for the sample,

$$\begin{aligned} H &= \left[c\boldsymbol{\alpha}\cdot[\boldsymbol{p}+\frac{e}{c}\boldsymbol{A}(\boldsymbol{r})]+\boldsymbol{\beta}mc^2\right] \\ &+ \left[c\boldsymbol{\alpha}_s\cdot[\boldsymbol{p}_s+\frac{e}{c}\boldsymbol{A}(\boldsymbol{r}_s)]+\boldsymbol{\beta}_s mc^2\right] \\ &+ v'(\boldsymbol{r})+e^2\frac{1}{|\boldsymbol{r}-\boldsymbol{r}_s|}+v(\boldsymbol{r}_s)+H_{\rm rad}, \end{aligned} \tag{4.8}$$

where the quantities labeled by the letter s refer to the sample electron and the unlabeled quantites refer to the probe electron. In the remainder of this Chapter we set $v' \to 0$, though the generalization of the theory to include diffraction is not expected to be difficult.

As it turns out,[93] we may start from an effective Schrödinger treatment of both the sample *and the probe* rather than a Dirac treatment. Working with a Schrödinger equation treatment facilitates contact with the "vacuum-relativistic" magic-angle theory of Schattschneider *et al.*

The treatment of the probe by a "relativistically corrected" Schrödinger equation is standard practice [94] in much of EELS theory, and is appropriate [93] for modern microscope energies of interest here (*e.g.,* a few hundred keV). However, in order to correctly treat the probe via a "relativistically corrected" Schrödinger equation we must also neglect the effects of spin. In particular, the results which we will "reproduce" correspond to the Dirac treatment averaged over initial spins and summed over final spins. The essential point of our interest presently is just that, assuming spins are ignored, a "relativistically-corrected" Schrödinger equation reproduces the correct first Born approximation results, including transverse response. There is no reason to expect that correct results (obtained from the Dirac equation) will be obtained at higher order by starting from a Schrödinger-type equation. As stated above, the only real motivation for working with a Schrödinger equation is to make our formal developments resemble those of Schattschneider *et al* for ease of comparison.

The relativistic correction to the Schrödinger equation of the probe consists in simply replacing the mass of the probe m by the relativistic mass $m' = m\gamma$ where $\gamma = 1/\sqrt{1-v_0^2/c^2}$. We will indicate later how the results change if we retain a full Dirac treatment of the

electrons. Thus we may start with the Hamiltonian

$$\begin{aligned} H &= \frac{[\boldsymbol{p}+(e/c)\boldsymbol{A}(\boldsymbol{r})]^2}{2m'} + \frac{[\boldsymbol{p}_s+(e/c)\boldsymbol{A}(\boldsymbol{r}_s)]^2}{2m} \\ &+ v(\boldsymbol{r}_s) + \frac{e^2}{|\boldsymbol{r}_s-\boldsymbol{r}|} + H_{\rm rad} \\ &\equiv H_0 + \frac{e}{m'c}\boldsymbol{p}\cdot\boldsymbol{A}(\boldsymbol{r}) + \frac{e}{mc}\boldsymbol{p}_s\cdot\boldsymbol{A}(\boldsymbol{r}_s) \\ &+ \frac{e^2}{|\boldsymbol{r}_s-\boldsymbol{r}_p|} + O(A^2)\ . \end{aligned} \tag{4.9}$$

In this theory the unperturbed states are then direct products of unperturbed sample electron states (which in calculations can be described, for example, by the computer code FEFF8,[1]) unperturbed probe electron states (plane-waves, ignoring diffraction), and the free (transverse) photon states. Also, from now on we ignore the interaction terms which are $O(A^2)$. Thus our perturbation is

$$U = \frac{e^2}{|\boldsymbol{r}-\boldsymbol{r}_s|} + \frac{e}{m'c}\,\boldsymbol{p}\cdot\boldsymbol{A}(\boldsymbol{r}) + \frac{e}{mc}\,\boldsymbol{p}_s\cdot\boldsymbol{A}(\boldsymbol{r}_s), \tag{4.10}$$

and we are interested in matrix elements of

$$U + UG_0U + \ldots \tag{4.11}$$

where the one-particle Green's function is

$$G_0(E) = \frac{1}{E - H_0 + i\eta} \tag{4.12}$$

and η is a postive infinitesimal. The matrix elements are taken between initial and final states (ordered as: probe, sample, photon)

$$|I\rangle = |k_I\rangle\,|i\rangle\,|0\rangle \quad \text{and} \quad |F\rangle = |k_F\rangle\,|f\rangle\,|0\rangle\ . \tag{4.13}$$

To lowest order (e^2) there will be a "longitudinal" (instantaneous Coulomb) contribution to the matrix element, and a "transverse" (photon mediated) contribution, as illustrated in Fig. 1.

Instead of elaborating the details from standard perturbation theory, we simply write down the result for the matrix element

$$\begin{aligned} M &= \frac{4\pi e^2}{V}\left[\frac{1}{q^2}\,\langle f|\,e^{i\boldsymbol{q}\cdot\boldsymbol{r}_s}\,|i\rangle\right. \\ &+ \left.\frac{1}{\omega^2-c^2q^2}\frac{k_T^j}{m'}\,\langle f|\,\frac{p_s^j}{m}e^{i\boldsymbol{q}\cdot\boldsymbol{r}_s}\,|i\rangle\right]\ , \end{aligned} \tag{4.14}$$

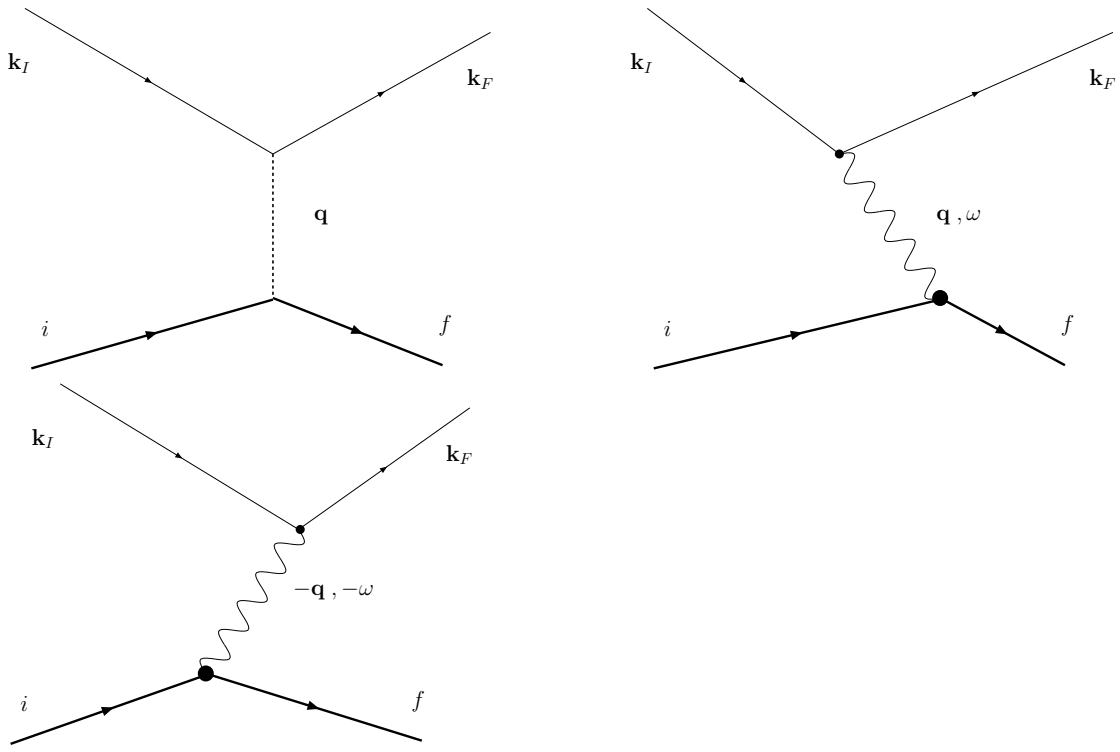

Figure 4.1: Feynman diagrams for the scattering process due to both the instantaneous Coulomb interaction (upper) and the transverse photon interaction (middle, lower). The solid lines labeled by momenta $\mathbf{k}_I$ and $\mathbf{k}_F$ represent the probe particle; thick solid lines labeled by the letters i and f represent the sample particle; the dashed line is the instantaneous Coulomb interaction; and the wiggly lines are transverse photons. Time flows to the right.

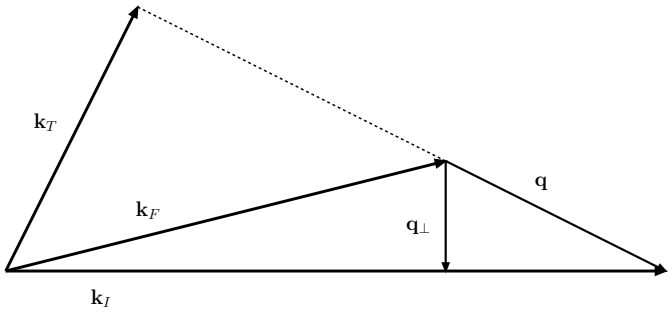

Figure 4.2: The relevant momenta: $\boldsymbol{k}_I$ is the initial momentum of the probe particle, $\boldsymbol{k}_F$ is the final momentum of the probe particle, $\boldsymbol{q}$ is the momentum transfer $\boldsymbol{k}_I - \boldsymbol{k}_F$ and $\boldsymbol{k}_T$ is the part of both the initial of final momenta which is perpendicular to the momentum transfer.

where $\boldsymbol{k}_T$ (see Fig. 2) is the part of the initial (or final) momentum which is perpendicular to the momentum transfer $\hbar\boldsymbol{q}$. In the remainder of this Chapter we will choose our units such that $\hbar = 1$.

$$k_T^j = \left(\delta_{lj} - \frac{q_l q_j}{q^2}\right) k_F^l = \left(\delta_{lj} - \frac{q_l q_j}{q^2}\right) k_I^l \,. \tag{4.15}$$

The result of Eq. (4.14) is easy to understand diagramatically. For example, to each wiggly line of momentum $\boldsymbol{q}$ and energy ω we may assign a value

$$\frac{1}{\omega - c|\boldsymbol{q}|}\left(\delta_{ij} - \frac{q_i q_j}{q^2}\right)\frac{2\pi c}{V|\boldsymbol{q}|}\,. \tag{4.16}$$

At this point we note that the relativistic many-body version of Eq. (4.14) can be obtained by making intuitively reasonable replacements such as $\boldsymbol{p}/m \to c\boldsymbol{\alpha}$, $e^{i\boldsymbol{q}\cdot\boldsymbol{r}_s} \to \sum_i e^{i\boldsymbol{q}\cdot\boldsymbol{r}^{(i)}}$. See Section 4.6 for further details.

Eq. (4.14) is equivalent to the matrix elements given by Fano in Eq. (12) of Ref. [65]. The cross-section given by Fano in Eq. (16) of Ref. [65], in which the matrix elements have been summed incoherently, is not generally correct and is the source of the magic angle "mystery".[92]

Before continuing to the dipole approximation it is useful to rewrite Eq. (4.14) using the

definition

$$\boldsymbol{k}_T = \boldsymbol{k}_I - \boldsymbol{q}\frac{\boldsymbol{q}\cdot\boldsymbol{k}_I}{q^2} \tag{4.17}$$

to eliminate $\boldsymbol{k}_T$ in favor of $\boldsymbol{k}_I$ (or equivalently $\boldsymbol{v}_0 = \boldsymbol{k}_I/m'$). Making this replacement we obtain

$$\begin{aligned} M &= \frac{4\pi e^2}{V}\left[\frac{1}{q^2}\langle f|\, e^{i\boldsymbol{q}\cdot\boldsymbol{r}}\,|i\rangle - \frac{\boldsymbol{q}\cdot\boldsymbol{v}_0}{mq^2}\frac{\langle f|\,\boldsymbol{q}\cdot\boldsymbol{p}e^{i\boldsymbol{q}\cdot\boldsymbol{r}}\,|i\rangle}{\omega^2-c^2q^2}\right. \\ &+ \left.\frac{\langle f|\,\boldsymbol{v}_0\cdot(\boldsymbol{p}/m)e^{i\boldsymbol{q}\cdot\boldsymbol{r}}\,|i\rangle}{\omega^2-c^2q^2}\right]\ , \end{aligned} \tag{4.18}$$

which can be rewritten as:

$$\begin{aligned} M &= \frac{4\pi e^2}{V}\frac{1}{q^2-(\omega^2/c^2)}\langle f|\, e^{i\boldsymbol{q}\cdot\boldsymbol{r}}\times \\ &\left[1-\frac{\boldsymbol{v}_0\cdot\boldsymbol{p}}{mc^2}-\frac{\omega^2}{q^2c^2}(1-\frac{\boldsymbol{q}\cdot\boldsymbol{p}}{m\omega})\right]|i\rangle\ , \end{aligned} \tag{4.19}$$

where we have made use of $\boldsymbol{q}\cdot\boldsymbol{v}_0 = \omega$ in order to cancel certain terms which appear after commuting the exponential through to the far left. Also, we have removed the label s from the position and momentum of the sample electron. This change in notation will be used throughout the remainder of this Chapter.

Eq. (4.19) is the same as Eq. (6) of Schattschneider *et al.*, except for an "extra" term

$$\langle f|\, e^{i\boldsymbol{q}\cdot\boldsymbol{r}}\left(1-\frac{\boldsymbol{q}\cdot\boldsymbol{p}}{m\omega}\right)|i\rangle\ . \tag{4.20}$$

Fortunately, this term may be simplified by considering the commutator

$$[e^{i\boldsymbol{q}\cdot\boldsymbol{r}}, H_0] = [e^{i\boldsymbol{q}\cdot\boldsymbol{r}}, \frac{p^2}{2m}] = e^{i\boldsymbol{q}\cdot\boldsymbol{r}}\left(-\frac{\boldsymbol{p}\cdot\boldsymbol{q}}{m}-\frac{q^2}{2m}\right)\ , \tag{4.21}$$

where the first equals sign follows from the fact that $e^{i\boldsymbol{q}\cdot\boldsymbol{r}}$ commutes with everything in H_0 except for the kinetic term of the sample electron (by its definition H_0 explicitly contains only local potentials). Then, using the fact that for any operator O,

$$\langle f|\,[O, H_0]\,|i\rangle = \langle f|\,O\,|i\rangle\,(E_i - E_f) = \langle f|\,O\,|i\rangle\,(-\omega) \tag{4.22}$$

we have

$$\langle f|\, e^{i\boldsymbol{q}\cdot\boldsymbol{r}}\,|i\rangle\,(-\omega) = -\langle f|\, e^{i\boldsymbol{q}\cdot\boldsymbol{r}}(\frac{\boldsymbol{p}\cdot\boldsymbol{q}}{m}+\frac{q^2}{2m})\,|i\rangle \tag{4.23}$$

and thus

$$\langle f|\, e^{i\boldsymbol{q}\cdot\boldsymbol{r}}(1-\frac{\boldsymbol{p}\cdot\boldsymbol{q}}{m\omega})\,|i\rangle = \langle f|\, e^{i\boldsymbol{q}\cdot\boldsymbol{r}}\frac{q^2}{2m\omega}\,|i\rangle\ . \tag{4.24}$$

Making the above replacement in Eq. (4.19) we find

$$\begin{aligned} M &= \frac{4\pi e^2}{V}\frac{1}{q^2-\omega^2/c^2} \\ &\times \langle f|\, e^{i\boldsymbol{q}\cdot\boldsymbol{r}}\left(1-\frac{\boldsymbol{v}_0\cdot\boldsymbol{p}}{mc^2}-\frac{\omega^2}{q^2c^2}\frac{q^2}{2m\omega}\right)|i\rangle \end{aligned} \tag{4.25}$$

and we see that the "extra" term only changes the result by order ω/mc^2 where mc^2 is the rest energy of an electron and ω is the energy lost;

$$\begin{aligned} M &= \frac{4\pi e^2}{V}\frac{1}{q^2-\omega^2/c^2}\,\langle f|\, e^{i\boldsymbol{q}\cdot\boldsymbol{r}}\left(1-\frac{\boldsymbol{v}_0\cdot\boldsymbol{p}}{mc^2}-\frac{\omega}{2mc^2}\right)|i\rangle \\ &= \frac{4\pi e^2}{V}\frac{1}{q^2-\omega^2/c^2}\,\langle f|\, e^{i\boldsymbol{q}\cdot\boldsymbol{r}}\left(1-\frac{\boldsymbol{v}_0}{mc^2}\cdot(\boldsymbol{p}+\frac{\boldsymbol{q}}{2})\right)|i\rangle\,. \end{aligned} \tag{4.26}$$

Eq. (4.26) is the same as what Schattschneider *et al.* would have obtained if they had not neglected the commutator $[\boldsymbol{p},\boldsymbol{A}]$.

That a term proportional to $\boldsymbol{p}+\boldsymbol{q}/2$ rather than simply $\boldsymbol{p}$ appears in Eq. (4.26) is correct and can be understood from the following simple example: The interaction Hamiltonian for a point particle with an external field is given by $e\phi - e\boldsymbol{v}\cdot\boldsymbol{A}/c$, or rather

$$H_{\rm int} \sim \int d^3x\left(n(\boldsymbol{x})\phi(\boldsymbol{x})-\frac{1}{c}\boldsymbol{j}(\boldsymbol{x})\cdot\boldsymbol{A}(\boldsymbol{x})\right)\ , \tag{4.27}$$

where $n(\boldsymbol{x})$ is the density and $\boldsymbol{j}(\boldsymbol{x})$ is the current, and where the above integral, with the potentials considered as functions of the source location, is a convolution in space and thus a product in Fourier space–the rough correspondence indicated by the "$\sim$" symbol in Eq. (4.27) is considered more rigorously in the Section 4.6. Next, we note that the Fourier transform of the current density (in second-quantization) is given for a free particle by [95]

$$\boldsymbol{j}(\boldsymbol{q}) = \frac{1}{mV}\sum_{\boldsymbol{k}}\left(\boldsymbol{k}+\frac{\boldsymbol{q}}{2}\right)c^\dagger_{\boldsymbol{k}+q}c_{\boldsymbol{k}}\ , \tag{4.28}$$

where

$$\psi(\boldsymbol{x}) = \sum_{\boldsymbol{k}} c_{\boldsymbol{k}}e^{i\boldsymbol{k}\cdot\boldsymbol{x}}\ , \tag{4.29}$$

and where $\mathbf{q}$ is considered to be the momentum transferred *to* the sample. This is in agreement with the usual conventions of EELS

$$\boldsymbol{q} = \boldsymbol{k}_I - \boldsymbol{k}_F \ . \tag{4.30}$$

Thus we see that Eq. (4.26) is indeed correct, in both sign and magnitude of the "extra" term.

4.3.1 Dipole Approximation and the Magic Angle

In the dipole approximation Eq. (4.26) reduces to

$$\frac{4\pi e^2}{V}\frac{1}{q^2-\omega^2/c^2}\left\langle f\right|\left(i\boldsymbol{q}\cdot\boldsymbol{r}-\frac{\boldsymbol{v}_0\cdot\boldsymbol{p}}{mc^2}\right)\left|i\right\rangle \ . \tag{4.31}$$

The term $(1-\boldsymbol{v}_0\cdot\boldsymbol{q}/2mc^2)$ does not contribute because $\langle i|f\rangle = 0$. Now, we make use of the replacement $\boldsymbol{p}/m \to i\omega\boldsymbol{r}$ which is appropriate within the matrix element to find

$$\frac{4\pi e^2}{V}\frac{i}{q^2-\omega^2/c^2}\left\langle f\right|\left(\boldsymbol{q}-\frac{\boldsymbol{v}_0(\boldsymbol{q}\cdot\boldsymbol{v}_0)}{c^2}\right)\cdot\boldsymbol{r}\left|i\right\rangle \ . \tag{4.32}$$

We have thus found the same "shortened q-vector" that appears in Eq. (15) of Schattschneider *et al.* and Eq. (2) of Jouffrey *et al.* Specifically, for an initial electron velocity $\boldsymbol{v}_0$ in the z-direction, we have found the replacement $q_z \to q_z(1-v_0^2/c^2)$ which in turn leads to a significant correction (on the order of 100 percent for typical electron microscopes) to the magic angle.

The magic angle θ_M is defined for materials with a "c-axis" by the equality of two functions of collection angle α_c:

$$F(\alpha_c) \equiv \int_0^{\alpha_c} d\theta\theta\frac{\theta^2}{\left[\theta^2+\theta_E^2/\gamma^4\right]^2} \ , \tag{4.33}$$

and

$$G(\alpha_c) \equiv 2\frac{\theta_E^2}{\gamma^4}\int_0^{\alpha_c} d\theta\theta\frac{1}{\left[\theta^2+\theta_E^2/\gamma^4\right]^2} \ . \tag{4.34}$$

where $\gamma = (1-v_0^2/c^2)^{-1/2}$, θ_E is the so-called "characteristic angle" given in terms of the energy-loss ω, the initial probe speed v_0, and $k_I\theta_E = \omega/v_0$. Both of the above integrals may easily be evaluated in terms of elementary functions, but we leave them in the above-form for comparison with the theory of the Section 4.4. Eqs. (4.33) and (4.34) both make

use of the approximation $\sin(\theta) \approx \theta$. Since typical scattering angles are on the order of milli-radians this small angle approximation is highly accurate.

The expressions for $F(\alpha_c)$ and $G(\alpha_c)$ are easily derived within the framework of the Schattschneider "vacuum theory"[92] and result in a ratio of magic angle to characteristic angle which is independent of the material which makes up the sample. The factors of $(1 - v_0^2/c^2)$ which appear in Eqs. (4.33) and (4.34) come from including the transverse effects (as in Section 4.2) and thus the non-relativistic ($c \to \infty$) result for the ratio of magic angle to characteristic angle is independent of transverse effects. The "transverse" correction to the magic angle is on the order of 100 percent. This corrected theoretical magic angle is in much better agreement with the experimentally observed magic angle, although the experimentally observed magic angle seems be somewhat larger (on the order of 30 percent) and sample dependent.[14] These further discrepancies between theory and experiment are addressed in Section 4.4.

4.4 Macroscopic Electrodynamic Effects

As discussed above, the result of Schattschneider *et al.* is nearly in agreement with that obtained in Section 4.3 of this Chapter in the vacuum relativistic limit. However, because of the residual discrepancy between these results and experiment we now consider how macroscopic electrodynamic effects can be incorported into the quantum mechanical single-particle formalism. We find that the corrections to the magic angle which result can be quite substantial at low energy-loss. However, we are unaware of any experimental data in this regime with which to compare the theory. Nevertheless, the inclusion of dielectric response introduces a sample dependence of the theoretical magic angle which is consistent with the sign of the observed discrepancy.

Certain condensed matter effects are already present in the existing formalism via the behavior of the initial and final single-particle states in the sample, and in many-electron effects which are neglected in the independent electron theory. However, the macroscopic response of the sample can be taken into account straightforwardly within a dielectric formalism. This procedure is similar to the well-known "matching" procedure between atomic calculations and macroscopic-dielectric calculations of the stopping power.[29, 13, 24] That

is, the fast probe may interact with many atoms at once, as long the condition $v_0 >> \omega_0 a$ (where ω_0 is a typical electronic frequency and a a typical length scale) is fulfilled. Under these conditions the sample can be treated using the electrodynamics of continuous media.[29]

Effects due to the macroscopic response of the system can be included within a formalism that parallels that of Schattschneider *et al.* simply by choosing the "generalized Lorentz gauge"[29] for a given dielectric function $\epsilon(\omega)$, instead of the Lorentz gauge of the vacuum-relativistic theory. In the generalized Lorentz gauge, most of the formal manipulations of Schattschneider *et al.* carry through in the same way, except that instead of Eq. (4.19) we end up with

$$\begin{aligned} M &= \frac{4\pi e^2}{\epsilon(\omega) V} \frac{1}{q^2 - \epsilon(\omega)\omega^2/c^2} \times \\ &\quad \langle f | \, e^{i\boldsymbol{q}\cdot\boldsymbol{r}} \left[1 - \frac{\epsilon(\omega)\boldsymbol{v}_0}{mc^2} \cdot (\boldsymbol{p} + \frac{\boldsymbol{q}}{2}) \right] | i \rangle \ . \end{aligned} \tag{4.35}$$

The factors of ϵ in Eq. (4.35) can be understood physically as due to the fact that $c \to c/\sqrt{\epsilon}$ in the medium, and also to the fact that the sample responds to the electric field $\boldsymbol{E}$ rather than the electric displacement $\boldsymbol{D}$. Eq. (4.35) is derived in the following subsection.

4.4.1 Generalized Lorentz Gauge calculation

We consider a probe electron which passes through a continuous medium characterized by a macroscopic frequency-dependent dielectric constant $\epsilon(\omega)$ and magnetic permeability $\mu = 1$. It is appropriate to ignore the spatial dispersion of the dielectric constant at this level of approximation.[96] Then Maxwell's equations are

$$\nabla \cdot \boldsymbol{D} = 4\pi \rho_{\text{ext}}, \tag{4.36}$$

with $\boldsymbol{D} = \epsilon \boldsymbol{E}$. And

$$\nabla \times \boldsymbol{B} = \frac{4\pi \boldsymbol{j}_{\text{ext}}}{c} + \frac{1}{c} \frac{\partial \boldsymbol{D}}{\partial t}, \tag{4.37}$$

where the charge/current densities ρ_{ext} and $\boldsymbol{j}_{\text{ext}}$ refer only to the "external" charge and current for a probe electron shooting through the material at velocity $\boldsymbol{v}_0$. The other two

Maxwell equations refer only to $\boldsymbol{E}$ and $\boldsymbol{B}$, and can be satisfied exactly using the definitions

$$\boldsymbol{E} = -\nabla\phi - \frac{1}{c}\frac{\partial \boldsymbol{A}}{\partial t} \ , \tag{4.38}$$

and

$$\boldsymbol{B} = \nabla \times \boldsymbol{A} \ . \tag{4.39}$$

We next insert Eqs. (4.38) and (4.39) into Eqs. (4.36) and (4.37) and choose the generalized Lorentz gauge [29]

$$\nabla \cdot \boldsymbol{A} + \frac{1}{c}\frac{\partial}{\partial t}\int dt' \, \epsilon(t-t')\phi(t') = 0 \ . \tag{4.40}$$

This gauge choice leads to the momentum space ($\boldsymbol{q}$,ω) equations

$$\left[-q^2 + \epsilon(\omega)\frac{\omega^2}{c^2}\right]\phi(\boldsymbol{q},\omega) = 4\pi\frac{\rho_{\rm ext}(\boldsymbol{q},\omega)}{\epsilon(\omega)}, \tag{4.41}$$

and

$$\left[-q^2 + \epsilon(\omega)\frac{\omega^2}{c^2}\right]\boldsymbol{A}(\boldsymbol{q},\omega) = 4\pi\,\frac{\boldsymbol{j}_{\rm ext}(\boldsymbol{q},\omega)}{c}. \tag{4.42}$$

We now write $\rho_{\rm ext}(\boldsymbol{q},\omega) = (-2\pi e)\delta(\omega - \boldsymbol{q}\cdot\boldsymbol{v}_0)$ and $\boldsymbol{j}_{\rm ext} = \boldsymbol{v}_0\rho_{\rm ext}$ to find explicit expressions for ϕ and $\boldsymbol{A}$:

$$\epsilon(\omega)\phi(\boldsymbol{q},\omega) = \frac{4\pi(-2\pi e)\delta(\omega - \boldsymbol{q}\cdot\boldsymbol{v}_0)}{[\epsilon(\omega)\omega^2/c^2] - q^2}, \tag{4.43}$$

and

$$\boldsymbol{A}(\boldsymbol{q},\omega) = \frac{\boldsymbol{v}_0}{c}\epsilon(\omega)\phi(\boldsymbol{q},\omega) \ . \tag{4.44}$$

Then, proceeding roughly in analogy with Schattschneider *et al.*, we have

$$\begin{aligned} H &= H_0 + \frac{e}{2mc}\left(\boldsymbol{p}\cdot\boldsymbol{A} + \boldsymbol{A}\cdot\boldsymbol{p}\right) - e\phi + O(A^2) \\ &= H_0 + \frac{e}{2mc}\left(2\boldsymbol{A}\cdot\boldsymbol{p} - i\nabla\cdot\boldsymbol{A}\right) - e\phi + O(A^2). \end{aligned} \tag{4.45}$$

Next, evaluating the perturbation $U \equiv H - H_0$ with $\boldsymbol{A} = (\boldsymbol{v}_0/c)\epsilon(\omega)\phi$, we find

$$U = \frac{e}{mc}\left(\phi\frac{\epsilon(\omega)}{c}\boldsymbol{v}_0\cdot\boldsymbol{p} - i\epsilon\frac{\boldsymbol{v}_0}{2c}\cdot\nabla\phi\right) - e\phi \ . \tag{4.46}$$

In calculating the matrix element of U it is appropriate to replace $\nabla\phi$ by $i\boldsymbol{q}\phi$ for the case when the final states are on the *left* in the matrix element. Thus

$$\begin{aligned} M &\equiv \langle f|\,\langle k_f|\,U\,|k_i\rangle\,|i\rangle = -e\phi(\boldsymbol{q},\omega) \\ &\times \langle f|\,e^{i\boldsymbol{q}\cdot\boldsymbol{r}}\left[1 - \frac{\epsilon(\omega)}{mc^2}\boldsymbol{v}_0\cdot(\boldsymbol{p}+\boldsymbol{q}/2)\right]|i\rangle \ . \end{aligned} \tag{4.47}$$

Alternatively, since

$$\phi(\boldsymbol{q},\omega) = \frac{-4\pi e}{\epsilon(\omega)\left(q^2 - \omega^2\epsilon(\omega)/c\right)} \ , \tag{4.48}$$

we have

$$\begin{aligned} M &= \frac{4\pi e^2}{\epsilon(\omega)(q^2 - \epsilon(\omega)\omega^2/c^2)} \langle f| \, e^{i\boldsymbol{q}\cdot\boldsymbol{r}} \\ &\times \left[1 - \frac{\epsilon(\omega)}{mc^2}\boldsymbol{v}_0 \cdot (\boldsymbol{p} + \boldsymbol{q}/2)\right] |i\rangle \ . \end{aligned} \tag{4.49}$$

In the dipole approximation Eq. (4.49) reduces to

$$\frac{4\pi e^2}{\epsilon(\omega)V}\frac{1}{q^2 - \epsilon(\omega)\omega^2/c^2} \langle f| \, i\left[\boldsymbol{q} - \epsilon(\omega)\frac{\boldsymbol{v}_0(\boldsymbol{q}\cdot\boldsymbol{v}_0)}{c^2}\right]\cdot\boldsymbol{r} \, |i\rangle \ , \tag{4.50}$$

where $\epsilon(\omega)$ is the generally complex valued macroscopic dielectric constant as which can be calculated, for example, by the FEFFOP [97] code. Consequently we find that that instead of the longitudinal q-vector replacement

$$q_z \to q_z(1 - \beta^2) \tag{4.51}$$

found by Jouffrey *et al.* and Schattschneider *et al.*, we obtain the replacement

$$q_z \to q_z[1 - \epsilon(\omega)\beta^2], \tag{4.52}$$

which is appropriate for an electron traversing a continuous dielectric medium. In the same way that Eq. (4.51) can be understood classically as being due to a charge in uniform motion in vacuum,[7] Eq. (4.52) can be understood as due to a charge is in uniform motion in a medium. Because the motion is uniform, the time dependence can be eliminated in favor of a spacial derivative opposite to the direction of motion and multiplied by the speed of the particle. For motion in the z-direction

$$\frac{\partial}{\partial t} \to -v_0\frac{\partial}{\partial z} \tag{4.53}$$

Therefore, if we consider the electric field

$$\boldsymbol{E} = -\nabla\phi - \frac{1}{c}\frac{\partial \boldsymbol{A}}{\partial t} \to -\nabla\phi + \frac{v_0}{c}\frac{\partial \boldsymbol{A}}{\partial z}, \tag{4.54}$$

Eq. (4.51) follows from the substitution $A_z = (v_0/c)\phi$, whereas Eq. (4.52) follows by making the correct substitution in the presence of a medium

$$A_z = \frac{v_0}{c}\epsilon\phi \ , \tag{4.55}$$

which in Fourier space gives

$$\boldsymbol{E}(\boldsymbol{q},\omega) \quad = \quad \left[-i\boldsymbol{q} + \hat{z}\frac{\epsilon(\omega)v_0^2}{c^2}iq_z\right]\phi(\boldsymbol{q},\omega) \ , \tag{4.56}$$

which is equivalent to Eq. (4.52).

Because Eq. (4.52) depends on the macroscopic dielectric function the ratio θ_M/θ_E, which formerly was a function only of v_0, will now show material dependence. This is seen from the generalization of Eqs. (4.33) and (4.34), the equality of which gives the magic angle. Instead of Eq. (4.33) for $F(\alpha_c)$ we now have

$$F(\alpha_c) \equiv \int_0^{\alpha_c} d\theta\theta \frac{\theta^2}{\left|\theta^2 + \theta_E^2 g\right|^2} \ , \tag{4.57}$$

and, instead of Eq. (4.34) we now have

$$G(\alpha_c) \equiv 2\theta_E^2|g|^2 \int_0^{\alpha_c} d\theta\theta \frac{1}{\left|\theta^2 + \theta_E^2 g\right|^2} \ , \tag{4.58}$$

where

$$g = 1 - \epsilon(\omega)v_0^2/c^2 \tag{4.59}$$

is a complex number which replaces $1/\gamma^2$ in the vacuum relativistic theory.

If one can calculate the macroscopic dielectric function of the sample by some means [97] then the material dependent magic angle can be determined theoretically and compared to experiment. Furthermore, the correction to the magic angle given by the introduction of the macroscopic dielectric constant relative to the relativistic macroscopic "vacuum value" of Jouffrey *et al.* is seen to be typically positive (since $\mathrm{Re}[\epsilon] \lesssim 1$ and $0 \lesssim \mathrm{Im}\,[\epsilon]$), in rough agreement with observation.[14] In fact, it turns out that the correction is always positive for the materials we consider and is substantial only for low energy-loss where the dielectric function differs substantially from its vacuum value. For modern EELS experiments which use relativistic microscope energies and examine low energy-loss regions, the effect of the dielectric correction on the magic angle should be large.

Example calculations using our relativistic dielectric theory compared to both the relativistic vacuum theory of Schattschneider *et al.* and to the non-relativistic vacuum theory are shown in Fig. (4.3) for the materials boron nitride and graphite. The data of Daniels et *al.* [14] is also shown in the figures. We have not attempted to estimate the true error bars for the data; the error bars in the figure indicate only the error resulting from the unspecified finite convergence angle.

4.5 Conclusions

We have developed a fully relativistic theory of the magic angle in electron energy loss spectra starting from the QED Hamiltonian of the many body system. As with the single-particle theory of Jouffrey *et al.* and Schattschneider *et al.* we find a factor of two "transverse" correction to the non-relativistic ratio θ_M/θ_E. We have also shown how macroscopic electrodynamic effects can be incorporated into the relativistic single-particle formalism of Schattschneider *et al.* In particular we predict that these dielectric effects can be important for determining the correct material-dependent magic angle at low energy-loss, where the difference between the dielectric function relative to its vacuum value is observed to be substantial.

Several other factors may be important for correctly describing the energy loss dependence of the magic angle in anisotropic materials. In particular, we believe that further study of the many body effects (beyond a simple macroscopic dielectric model) via explicit calculations of the *microscopic* dielectric function and including time-dependant density functional/Bethe-Salpeter theory TDDFT/BSE[98] are an important next step in the description of all EELS phenomena, including the magic angle.

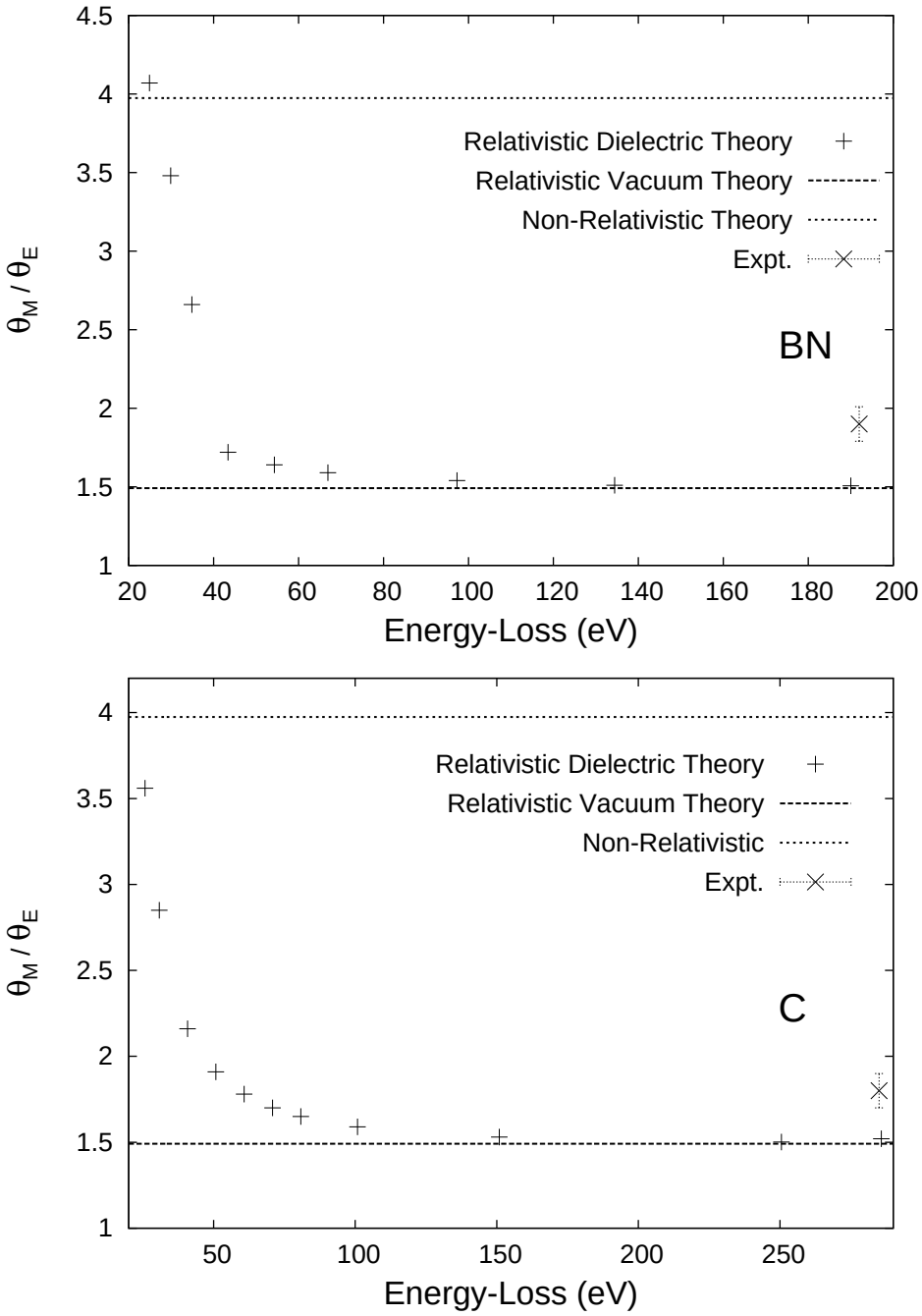

Figure 4.3: The magic angle to characteristic angle ratio θ_M/θ_E is compared for three differing theories and one experiment.[14] The materials considered in the figure are boron nitride (top figure) and graphite (bottom). The microscope voltage is fixed at 195 keV. Both the non-relativistic and relativistic vacuum theories show no dependence on the energy-loss and no dependence on the material. The relativistic dielectric theory shows that the magic angle should deviate from the vacuum value by a significant amount in regions where the macroscopic dielectric response is substantial.

4.6 Relativistic Effects

Starting from Eq. (4.7) we write (the notation H_0 in this Section differs from that in the main body of the text):

$$\begin{aligned} H_0 &= c\boldsymbol{\alpha}\cdot\boldsymbol{p} + \boldsymbol{\beta}mc^2 + v_{\text{e-core}}(\boldsymbol{r}) \\ &+ \sum_{i=1}^{N}\left[c\boldsymbol{\alpha}^{(i)}\cdot\boldsymbol{p}^{(i)} + \beta^{(i)}mc^2 + v_{\text{e-core}}(\boldsymbol{r}^{(i)})\right] \\ &+ \frac{1}{2}\sum_{1=i\neq j=1}^{N}\frac{e^2}{|\boldsymbol{r}^{(i)}-\boldsymbol{r}^{(j)}|} + H_{\text{rad}}, \end{aligned} \tag{4.60}$$

and

$$U = e\boldsymbol{\alpha}\cdot\boldsymbol{A}(\boldsymbol{r}) + \sum_{i=1}^{N}\frac{e^2}{|\boldsymbol{r}-\boldsymbol{r}^{(i)}|} + \sum_{i=1}^{N}e\boldsymbol{\alpha}^{(i)}\cdot\boldsymbol{A}(\boldsymbol{r}^i)\ . \tag{4.61}$$

We are interested in matrix elements of the perturbation

$$U + UG_0U + \ldots \tag{4.62}$$

between eigenstates of the unperturbed Hamiltonian

$$|I\rangle = |k_i\rangle\,|\Psi_i\rangle\,|0\rangle \quad \text{and} \quad |F\rangle = |k_f\rangle\,|\Psi_f\rangle\,|0\rangle\ . \tag{4.63}$$

The difference between the many-body case and the single-particle theory of the sample is that the wavefunction of the sample now depends on N electron coordinates, instead of one effective coordinate. Also we see that the only potential "seen" by the probe (i.e., included in the unperturbed probe Hamiltonian) is the $v_{\text{e-core}}$ potential. This is to be contrasted with the "unperturbed" sample Hamiltonian which includes not only the $v_{\text{e-core}}$ but also the Coulomb interactions between all the sample electrons.

Consequently, working with a unit volume and proceeding exactly as in the single-particle case, we find a "longitudinal" contribution to the matrix element

$$M_L = \frac{4\pi e^2}{q^2}u^\dagger(\boldsymbol{k}_f)u(\boldsymbol{k}_i)\,\langle\Psi_f|\sum_{i=1}^{N}e^{i\boldsymbol{q}\cdot\boldsymbol{r}^{(i)}}\,|\Psi_i\rangle\,, \tag{4.64}$$

and a "transverse" contribution

$$M_T = \frac{4\pi e^2}{\omega^2/c^2-q^2}u^\dagger(\boldsymbol{k}_f)\boldsymbol{\alpha}_T u(\boldsymbol{k}_i)\cdot\langle\Psi_f|\sum_{i=1}^{N}\boldsymbol{\alpha}^{(i)}e^{i\boldsymbol{q}\cdot\boldsymbol{r}^{(i)}}\,|\Psi_i\rangle\ , \tag{4.65}$$

where

$$\boldsymbol{\alpha}_T = \boldsymbol{\alpha} - \boldsymbol{q}\frac{\boldsymbol{q}\cdot\boldsymbol{\alpha}}{q^2}\ , \tag{4.66}$$

and where the $u(\boldsymbol{p})$ are the usual free-particle Dirac spinors, normalized such that

$$u^\dagger(\boldsymbol{p})u(\boldsymbol{p}) = 1\ . \tag{4.67}$$

The two matrix elements M_L and M_T are to be summed and then squared, but before proceeding with this plan we make the following useful definitions: The transverse Kronecker delta function (transverse to momentum-transfer)

$$\delta_T^{ij} = \delta^{ij} - \frac{q^i q^j}{q^2}\ ; \tag{4.68}$$

the (Fourier transformed) density operator

$$n(\boldsymbol{q}) = \sum_i^N e^{-i\boldsymbol{q}\cdot\boldsymbol{r}^{(i)}}\ ; \tag{4.69}$$

and the (Fourier transformed) current operator

$$\boldsymbol{j}(\boldsymbol{q}) = \sum_i^N c\boldsymbol{\alpha}^{(i)} e^{-i\boldsymbol{q}\cdot\boldsymbol{r}^{(i)}}\ . \tag{4.70}$$

Next, we recall some properies of the Dirac spinors $u(\boldsymbol{p})$ and of Dirac matrices which we will presently find useful: i) There are four independent spinors $\left\{u^{(1)}, u^{(2)}, u^{(3)}, u^{(4)}\right\}$, the first two of which will refer to positive energy solutions, and the second two of which will refer to negative energy solutions (and are not used in this calculation);

ii) the positive energy spinors satisfy a "spin sum"

$$\begin{aligned}\sum_{s=1}^{2} u^{(s)}(\boldsymbol{p}){u^{(s)}}^\dagger(\boldsymbol{p}) &= \frac{1}{2E(p)}\left(E(p) + c\boldsymbol{\alpha}\cdot\boldsymbol{p} + \boldsymbol{\beta}mc^2\right) \\ &\equiv \frac{1}{2E(p)}\left(E(p) + h_D(\boldsymbol{p})\right)\ ,\end{aligned} \tag{4.71}$$

where $E(p) = \sqrt{p^2c^2 + m^2c^4}$;

iii) the Dirac matrices satisfy the trace identities

$$\mathrm{Tr}(\boldsymbol{\alpha}_i\boldsymbol{\alpha}_j) = 4\delta_{ij}, \tag{4.72}$$

$$\mathrm{Tr}(\boldsymbol{\alpha}_i\boldsymbol{\alpha}_j\boldsymbol{\alpha}_k\boldsymbol{\alpha}_l) = 4\left(\delta_{ij}\delta_{kl} - \delta_{ik}\delta_{jl} + \delta_{il}\delta_{jk}\right), \tag{4.73}$$

$$\mathrm{Tr}(\boldsymbol{\alpha}_T^i\boldsymbol{\alpha}^j) = \mathrm{Tr}(\boldsymbol{\alpha}_T^i\boldsymbol{\alpha}_T^j) = 4\delta_T^{ij}, \tag{4.74}$$

$$\mathrm{Tr}(\boldsymbol{\alpha}^i\boldsymbol{\alpha}_T^j\boldsymbol{\alpha}^k\boldsymbol{\alpha}_T^l) = 4\left(\delta_T^{ij}\delta_T^{kl} - \delta^{ik}\delta_T^{jl} + \delta_T^{il}\delta_T^{jk}\right); \tag{4.75}$$

iv) Finally, we note that in this calculation there are many simplifications due to the fact that $\omega << mc^2 < E(\boldsymbol{k}_I) \approx E(\boldsymbol{k}_F)$. For example,

$$\frac{1}{2E_iE_j}(E_iE_j + m^2c^4 + c^2\boldsymbol{k}_i \cdot \boldsymbol{k}_j) \quad = \\ 1 - \frac{\omega}{E(k_i)} + O(\frac{\omega^2}{E(k_i)^2}) \approx 1 \; ;$$

throughout the calculation we ignore terms of order $\omega/E(\boldsymbol{p}_I)$ Using these identities it is easy to see that

$$\frac{1}{2}\sum_{s_i=1}^{2}\sum_{s_f=1}^{2}|M_L|^2 = \left(\frac{4\pi e^2}{q^2}\right)^2 |\left\langle \Psi_F \right| n_q^\dagger \left| \Psi_I \right\rangle|^2 \tag{4.76}$$

which has the same form as in the non-relativistic case (up to order ω/E_i); the squared matrix element is much simplified by the sum over final probe-spin and average over initial probe-spin. Of course, the matrix element itself is completely general in terms of probe-spin, but many simplification arise from ignoring the probe-spin and exploiting the spin-sums.

Continuing on to the transverse matrix element–and including a few more of the details (a, b, c, and d are Dirac indices)–we find

$$\frac{1}{2}\sum_{s_i=1}^{2}\sum_{s_f=1}^{2}|M_T|^2 = \frac{1}{2}\sum_{s_i=1}^{2}\sum_{s_f=1}^{2}\left(\frac{4\pi e^2}{\omega^2/c^2 - q^2}\right)^2 \\ \times u(\boldsymbol{k}_f)_a^{(s_f)^*}\boldsymbol{\alpha}_T^{mab}u(\boldsymbol{k}_i)_b^{(s_i)}u(\boldsymbol{k}_i)_c^{(s_i)^*}\boldsymbol{\alpha}_T^{n\,cd}u(\boldsymbol{k}_f)_d^{(s_f)} \\ \times \left\langle \Psi_F \right| j_m(\boldsymbol{q})^\dagger \left| \Psi_I \right\rangle \left\langle \Psi_I \right| j_n(\boldsymbol{q}) \left| \Psi_F \right\rangle$$

$$= \left(\frac{4\pi e^2}{\omega^2/c^2 - q^2}\right)^2 \left\langle \Psi_F \right| j_m(\boldsymbol{q})^\dagger \left| \Psi_I \right\rangle \left\langle \Psi_I \right| j_n(\boldsymbol{q}) \left| \Psi_F \right\rangle \\ \times \mathrm{Tr}\left((E(k_f) + h_D(\boldsymbol{k}_f))\boldsymbol{\alpha}_T^m(E(k_i) + h_D(\boldsymbol{k}_i))\boldsymbol{\alpha}_T^n\right) \\ = \left(\frac{4\pi e^2}{\omega^2/c^2 - q^2}\right)^2 \left|\left\langle \Psi_I \right| \frac{\boldsymbol{v}_T \cdot \boldsymbol{j}(\boldsymbol{q})}{c^2} \left| \Psi_F \right\rangle\right|^2 . \tag{4.77}$$

For the cross term we find

$$\frac{1}{2}\sum_{s_i=1}^{2}\sum_{s_f=1}^{2}M_L M_T^* = \left(4\pi e^2\right)^2 \frac{1}{q^2(\omega^2/c^2 - q^2)} \\ \times \left\langle \Psi_F \right| n^\dagger(\boldsymbol{q}) \left| \Psi_I \right\rangle \left\langle \Psi_I \right| \frac{\boldsymbol{j}(\boldsymbol{q}) \cdot \boldsymbol{v}_T}{c^2} \left| \Psi_F \right\rangle \; . \tag{4.78}$$

Thus we have finally derived an expression for the relativistic many-body summed-then-squared matrix elements summed and averaged over spins,

$$\begin{aligned}\frac{1}{2}\sum_{s_i}\sum_{s_f}|M_L+M_T|^2 &= \left(\frac{4\pi e^2}{V}\right)^2 \\ &\times\left|\frac{\langle\Psi_I|\,n(\boldsymbol{q})\,|\Psi_F\rangle}{q^2}+\frac{\langle\Psi_I|\,\boldsymbol{v}_T\cdot\boldsymbol{j}(\boldsymbol{q})\,|\Psi_F\rangle}{\omega^2-q^2c^2}\right|^2 \\ &= \left[\frac{4\pi e^2}{V(\omega^2/c^2-q^2)}\right]^2\left|\langle\Psi_I|\,n(\boldsymbol{q})-\frac{\boldsymbol{v}_0\cdot\boldsymbol{j}(\boldsymbol{q})}{c^2}\,|\Psi_F\rangle\right|^2 .\end{aligned} \tag{4.79}$$

The last equality follows from

$$\boldsymbol{q}\cdot\langle\Psi_I|\,\boldsymbol{j}(\boldsymbol{q})\,|\Psi_F\rangle=\omega\,\langle\Psi_I|\,n(\boldsymbol{q})\,|\Psi_F\rangle\,, \tag{4.80}$$

which itself follows by considering the commutator analogous to that of Eq. (4.21).

The final line of Eq. (4.79) is quite pleasing since we have found that if we can "ignore" the spin of the probe particle, we may as well have started by taking matrix elements between electronic states only of the much simpler interaction Hamiltonian

$$U'=\int d^3x\left[n(\boldsymbol{x})\phi_\omega(\boldsymbol{x}-\boldsymbol{x}_p)-\frac{\boldsymbol{j}(\boldsymbol{x})\cdot\boldsymbol{A}_\omega(\boldsymbol{x}-\boldsymbol{x}_p)}{c^2}\right]\,, \tag{4.81}$$

where the fields $\{\phi_\omega,\boldsymbol{A}_\omega\}$ are just the $e^{-i\omega t}$ components of the *classical* field of a point charge of velocity $\boldsymbol{v}_0$ in the Lorentz gauge, and where

$$n(\boldsymbol{x})=\sum_i^N\delta(\boldsymbol{x}-\boldsymbol{x}^{(i)})\,, \tag{4.82}$$

and

$$\boldsymbol{j}(\boldsymbol{x})=\sum_i^N c\boldsymbol{\alpha}^{(i)}\delta(\boldsymbol{x}-\boldsymbol{x}^{(i)})\,. \tag{4.83}$$

That is, if we take Eq. (4.81) as our starting point and proceed in the usual way, we will find that our squared matrix elements are exactly the same as what we know to be correct from Eq. (4.79). The photons have dropped out entirely!

Chapter 5

MIXED DYNAMIC FORM FACTOR

5.1 Main Idea of Chapter

We present real-space multiple-scattering calculations of the mixed dynamic form factor (MDFF) which is the imaginary part of the retarded density-density correlation function. Our calculations are based on an extension of the x-ray scattering code `FEFFq`[23] and the x-ray absorption code `FEFF`[1]. The MDFF of a given system contains all the available system information within the framework of linear response. For example, the information contained in the MDFF is equivalent to that contained in the complex inhomogeneous space and time dependent dielectric function. Knowledge of the MDFF is important for the correct description of scattering experiements regardless of the nature of the probe particle, but here we concentrate in particular on electron scattering. The numerical calculations presented here are quite time-consuming which may explain the paucity of other MDFF calculations in the literature. To our knowledge these are the first calculations of the MDFF which are based on real-space multiple scattering methods.

5.2 Introduction

For the purpose of describing scattering experiments (this applies equally well to electrons, photons, or neutrons) one is often interested in computing matrix elements between unperturbed states of some perturbation operator V. In many cases of interest the unperturbed states can be factorized into a "probe" part and a "sample" part. Typically, the treatment of the probe is easy, but the treatment of the sample (even in a single-particle approximation) is difficult. In this Chapter we consider a quantity known as the mixed dynamic form factor (MDFF) which must be used to describe the sample in the most general kinds of scattering experiments. The MDFF is the main topic of this Chapter and it is defined in Section (5.3).

Throughout this Chapter we work within the independent-particle approximation and we choose units such that $\hbar = e = m = 1$ where $\hbar$ is the reduced Planck constant, e is the charge of the proton, and m is the mass of the electron. With these conventions the unit of energy is the Hartree (≈ 27.2 electron Volts) and the unit of length is the Bohr (≈ 0.529 Angstroms).

For orientation, and also to introduce the role of form factors in scattering, we first consider the scattering of a plane-wave probe electron (i.e., the probe is described before and after the scattering by a single plane-wave) off of a sample electron with momentum-transfer $\mathbf{q}$ and energy-loss ω;

$$|\mathbf{k}_i\rangle\,|\text{Sample}_I\rangle \longrightarrow |\mathbf{k}_f\rangle\,|\text{Sample}_F\rangle$$

where $\mathbf{k}_i = \mathbf{k}_f + \mathbf{q}$ and the energy-gain of the sample is ω; for the case of electrons we may also write $k_i^2/2 = k_f^2/2 + \omega$.

Because the interaction operator V depends only on the difference in positions of the sample and probe, it is well known[99] that the double differential cross section (DDCS) factors into a simple or "classical" part (which depends on the probe and interaction) and a difficult or "quantum" part (which depends on the sample). The DDCS can be written as

$$\frac{d\sigma}{d\Omega d\omega} = \left(\frac{d\sigma}{d\Omega}\right)_{\text{Cl}} S(\mathbf{q},\mathbf{q};\omega) \tag{5.1}$$

where we have introduced the notation $d\sigma/d\Omega_{\text{Cl}}$ to describe the part of the DDCS which depends only on the probe and the interaction; for fast electrons, where $k_f/k_i \approx 1$ we see from Eq. (2.91) that $d\sigma/d\Omega_{\text{Cl}} = 4/q^4$. We have also introduced the notation $S(\mathbf{q},\mathbf{q}';\omega)$ for the MDFF which describes the sample.

Only the diagonal part of the MDFF, known as the dynamic form factor (DFF), appears in Eq. (5.1) for the scattering of a single plane-wave. Off-diagonal elements of the MDFF must be taken into account if the initial or final probe states are coherent superpostions of more than one plane-wave (e.g., Bloch waves). Roughly speaking, for a coherent superposition of plane-wave initial states

$$\left(|\mathbf{k}_i + \Delta\mathbf{k}\rangle + \left|\mathbf{k}_i + \Delta\mathbf{k}'\right\rangle\right)|\text{Sample}_I\rangle \longrightarrow |\mathbf{k}_f\rangle\,|\text{Sample}_F\rangle\ ,$$

we find a cross section that depends on both diagonal and off-diagonal elements of the MDFF:

$$\sigma(k_i \to k_f) \sim S(\mathbf{q},\mathbf{q};\omega) + S(\mathbf{q}',\mathbf{q}';\omega) + S(\mathbf{q},\mathbf{q}';\omega) + S(\mathbf{q}',\mathbf{q};\omega) \ .$$

An experiment which involves the scattering of coherent superpositions of electrons and which thus measures the diagonal and off-diagonal elements of the MDFF has recently been proposed.[100]

Further motivation for studying the MDFF comes not only from direct applications like that mentioned above, but also from indirect applications such as the description of Kikuchi Bands which are observed in electron diffraction experiements. That is, account must be taken of the fact that the electron within the sample is necessarily a coherent superposition of plane waves (a Bloch wave). The interference of these Bloch waves can only be taken into account using the MDFF.

5.3 Theory

The MDFF is defined[101, 102, 94] within the single-particle approximation, and for a fixed single-electron initial state $|i\rangle$ of energy E_i, by

$$S_i(\mathbf{q},\mathbf{q}';\omega) = \sum_f \langle i|\, e^{i\mathbf{q}\cdot\mathbf{r}}\, |f\rangle \, \langle f|\, e^{-i\mathbf{q}'\cdot\mathbf{r}}\, |i\rangle \, \delta(E_i + \omega - E_f) \ , \tag{5.2}$$

where $|f\rangle$ is a state of energy E_f and $\mathbf{r}$ is the position operator of the electron. When the quantity defined by Eq. (5.2) is summed over occupied initial states it is equal to the quantity denoted by "S" in Eq. (5.1). Eq. (5.1) is an approximation for the cross-section which, amoung other things, is only correct when the speed of light is taken to be infinte; transverse effects are neglected in this approximation. For all cases considered in this Chapter that approximation is very good. An account of transverse effects has already been given in Chapter (4). For the sake of definiteness, therefore, we take Eq. (5.2) as our definition of the MDFF for a given initial state.

As mentioned in Section (5.2), the vectors $\mathbf{q}$ and $\mathbf{q}'$ will be interpreted in the context of scattering as momentum-transfers and the number ω will be interpreted as energy-loss.

In anticipation of scattering experiments which are tuned for energy-losses near to a given initial state energy, Eq. (5.2) considers only the contribution of one given initial state

to the MDFF. The total MDFF is a sum over initial states. Furthermore, we assume that our given initial-state is an angular momentum eigenstate (labelled by $L_I = \{\ell_I, m_I\}$), but that we give up knowledge of the initial-state's azimuthal angular momentum. That is, we assume we are scattering off of a given angular momentum "shell" which only specifies total angular momentum. Thus, we should average Eq. (5.2) over initial azimuthal angular momenta by letting

$$S_I \longrightarrow \frac{1}{2\ell_I + 1} \sum_{m_I} S_I \equiv S(\mathbf{q}, \mathbf{q}'; \omega) \; .$$

This change in notation is used throught the remainder of the Chapter.

The sum over final-states in Eq. (5.2) can be formally evaluated by introducing a single-particle Green's function

$$G(E) = \frac{1}{E - H' + i\delta} \; .$$

where H' is the effective single-particle Hamiltonian of the final-states, and δ is a positive infinitesimal. Thus we find

$$S(\mathbf{q}, \mathbf{q}'; \omega) = \frac{-1}{2\ell_I + 1} \sum_{m_I} \langle I | \, e^{i\mathbf{q}\cdot\mathbf{r}} \frac{1}{\pi} \frac{G(E_I + \omega) - G^\dagger(E_I + \omega)}{2i} e^{i\mathbf{q}'\cdot\mathbf{r}} \, | I \rangle \tag{5.3}$$

where the † symbol stands for Hermitian conjugation.

On arriving at Eq. (5.3) we have reduced most of the problem of calculating the MDFF to the evaluation of a Green's function. The importance of the Green's function stems from the fact that it has an easy physical interpretation. This leads to a physically motivated method for its calculation known as the real-space multiple-scattering (RSMS) approach[103, 104, 105, 106]. Such a RSMS calculation of the Green's function can be done using the computer program FEFF[1, 23], which utilizes this Green's function in simulations of x-ray absorption and x-ray scattering spectra.

Along with the Green's function, we also need matrix elements of the operator $e^{i\mathbf{q}\cdot\mathbf{r}}$ in order to compute the MDFF. The calculation of these matrix elements for use in modeling inelastic x-ray scattering was recently included in an extension of the FEFF code known as FEFFq[23]. The FEFFq code can be used to obtain diagonal elements of the MDFF (i.e., the DFF) matrix in momentum-transfer space. The main aim of this Chapter is the

description of a new code which extends FEFFq beyond the diagonal calculation to the calculation of all matrix elements of the MDFF.

As described in detail elsewhere[23] the density-matrix

$$\rho(\mathbf{r},\mathbf{r}';E) \equiv -\frac{1}{\pi}\left\langle \mathbf{r}\right| \frac{G(E)-G^{\dagger}(E)}{2i}\left|\mathbf{r}'\right\rangle = -\frac{1}{\pi}\mathrm{Im}G(\mathbf{r},\mathbf{r}';E)$$

which appears in Eq. (5.3) can be written in an angular momentum basis as

$$\rho(\mathbf{r},\mathbf{r}';E) = \sum_{L,L'} R_L(\mathbf{r})\rho_{L,L'}(E)R_{L'}(\mathbf{r})$$

where $R_L(\mathbf{r}) = R_\ell(r)i^\ell Y_L(r)$ and $R_\ell(r)$ is the regular solution to the radial Schrödinger equation in the presence of the potential centered on the absorbing atom (central-atom potential). Here we use the symbol $L = (\ell, m)$ as a double index.

Thus we may write

$$S(\mathbf{q},\mathbf{q}';\omega) = \frac{1}{2\ell_I+1}\sum_{m_I}\sum_{L,L'}\left\langle I\right| e^{i\mathbf{q}\cdot\mathbf{r}}\left|L\right\rangle \rho_{L,L'}(E)\left\langle L'\right| e^{-i\mathbf{q}'\cdot\mathbf{r}}\left|I\right\rangle \ . \tag{5.4}$$

Here we have written $E \equiv E_I + \omega$ for simplicity of notation, and $\langle\mathbf{r}|L\rangle = R_L(\mathbf{r})$.

To make use of our angular momentum basis expansion for the density matrix, we next insert the well-known expansion of the exponential in terms of spherical harmonics

$$e^{i\mathbf{q}\cdot\mathbf{r}} = \sum_L 4\pi i^\ell j_\ell(qr)Y_L(\hat{r})Y_L^*(\hat{q})$$

into Eq. (5.4) and we find

$$\begin{aligned} S(\mathbf{q},\mathbf{q}';\omega) &= (4\pi)\sum_{LL'}\sum_{L_1L_2}\left\langle \ell_I\right| j_{\ell_1}(qr)\left|\ell\right\rangle \left(\left\langle \ell_I\right| j_{\ell_2}(q'r)\left|\ell'\right\rangle\right)^* \rho_{L,L'}Y_{L_1}^*(\hat{q})Y_{L_2}(\hat{q}') \\ &\times \sqrt{(2\ell_1+1)(2\ell+1)}\begin{pmatrix}\ell_1 & \ell & \ell_I\\ 0 & 0 & 0\end{pmatrix}\sqrt{(2\ell_2+1)(2\ell'+1)}\begin{pmatrix}\ell_2 & \ell' & \ell_I\\ 0 & 0 & 0\end{pmatrix} \\ &\times \sum_{m_I}\begin{pmatrix}\ell_1 & \ell & \ell_I\\ m_1 & m & -m_I\end{pmatrix}\begin{pmatrix}\ell_2 & \ell' & \ell_I\\ m_2 & m' & -m_I\end{pmatrix}\ , \end{aligned} \tag{5.5}$$

where $L_1 = (\ell_1, m_1)$, etc are double indices, and where

$$\left\langle \ell_I\right| j_{\ell'}(qr)\left|\ell\right\rangle = \int_0^\infty dx x^2\phi_I(x)j_{\ell'}(qx)R_\ell(x)i^\ell$$

is the reduced matrix element of the order ℓ' spherical regular Bessel function. The Wigner-3J symbols appear as the result integrating products of three spherical harmonics.

For the case of poly-crystaline solids we must average the MDFF over sample orientations. This procedure reduces the density-matrix to diagonal form in angular momentum indices $\rho_{L,L'} \rightarrow \delta_{L,L'}\rho_\ell$ where $\rho_\ell = 1/(2\ell+1)\sum_m \rho_{\ell m,\ell m}$. This averaging over sample orientations does not effect the initial-states because of the sum (average) over initial azimuthal quantum numbers. Thus, in the polycrystaline case, we may write

$$S(\mathbf{q},\mathbf{q}';\omega) = \sum_\ell (2\ell+1)\rho_\ell(E)N_\ell(q,q',\hat{q}\cdot\hat{q}') \tag{5.6}$$

where

$$N(q,q',\hat{q}\cdot\hat{q}') = \sum_{\ell'}(2\ell'+1)P_{\ell'}(\hat{q}\cdot\hat{q}')\begin{pmatrix} \ell' & \ell & \ell_I \\ 0 & 0 & 0 \end{pmatrix}^2 \langle \ell_I|\, j_{l'}(qr)\,|\ell\rangle \langle \ell_I|\, j_{\ell'}(q'r)\,|\ell\rangle^* \tag{5.7}$$

and P_ℓ is a Legendre polynomial.

On comparing Eq. (5.7) with Eq. (17) of Ref. ([23]), we see that the main difference between a calculation of the DFF and a calculation of the MDFF is simply the insertion of a single Legendre polynomial which depends on the relative angle between **q** and **q'**

5.4 Relativistic Central-Atom Example

The FEFF code uses fully relatistic (Dirac) initial states and thus the Green's function and the scattering states must be considered as, respectively, matrices and vectors in dirac-component space and an appropriate *total* angular momentum basis. In Section II we considered an *orbital* angular momentum basis to facilitate the comparison of our results with previous theories.

In order to be clear about the generalization of RSMS to relativistic systems we present an explicit MDFF calculation for the relativistic central-atom case. "Central-atom" means that we consider only the potential located at the obsorbing atom rather than the total potential. The manipulations involved in obtaining the total poly-crystaline MDFF are quite similar to the central-atom case.

The central-atom MDFF, summed over the initial-state azimuthal quantum numbers m_I, is given by:

$$\sum_{m_I} S_c(\mathbf{q},\mathbf{q}';\omega) = \frac{2k}{\pi}\sum_{m_I}\sum_{\kappa,m} \langle \kappa_I, m_I|\, e^{i\mathbf{q}\cdot\mathbf{r}}\, |\kappa, m\rangle \langle \kappa, m|\, e^{-i\mathbf{q}'\cdot\mathbf{r}}\, |\kappa_I, m_I\rangle \ . \tag{5.8}$$

As in Section II, the exponentials may be expanded using

$$e^{i\mathbf{q}\cdot\mathbf{r}} = \sum_{\ell,m} 4\pi i^\ell j_\ell(qr) Y_L^*(\hat{q}) Y_L(\hat{r}) \ . \tag{5.9}$$

Matrix elements of the operators appearing in Eq. (5.9) can be written in terms of an integral over the large (P) and small (Q) Dirac components

$$\langle \kappa_I|\, j_\ell(qr)\, |\kappa\rangle = \int_0^\infty \left(P_{\kappa_I}(r)P_\kappa(r) + Q_{\kappa_I}(r)Q_\kappa(r)\right) j_\ell(qr)$$

according to the formula[107]

$$\begin{aligned}\langle \kappa_I m_I|\, j_{\ell_1}(qr) Y_{L_1}\, |\kappa m\rangle &= \sqrt{\frac{(2\ell_1+1)(2j_I+1)(2j+1)}{4\pi}}(-1)^{m_I+1/2} \begin{pmatrix} j_I & \ell_1 & j \\ 1/2 & 0 & -1/2 \end{pmatrix} \\ &\times \begin{pmatrix} j_I & \ell_1 & j \\ -m_I & m_1 & m \end{pmatrix} \langle \kappa_I|\, j_{\ell_1}(qr)\, |\kappa\rangle \ . \end{aligned} \tag{5.10}$$

Thus we find

$$\begin{aligned}\sum_{m_I} S_c(\mathbf{q},\mathbf{q}';\omega) &= \frac{2k}{\pi}\sum_{\kappa\ell_1 m_1 \ell_2 m_2} 4\pi i^{\ell_1-\ell_2} \langle \kappa_I|\, j_{\ell_1}(qr)\, |\kappa\rangle \left(\langle \kappa_I|\, j_{\ell_2}(q'r)\, |\kappa\rangle\right)^* Y_{L_1}^*(\hat{q}) Y_{L_2}(\hat{q}') \\ &\times \begin{pmatrix} j_I & \ell_1 & j \\ 1/2 & 0 & -1/2 \end{pmatrix} \begin{pmatrix} j_I & \ell_2 & j \\ 1/2 & 0 & -1/2 \end{pmatrix} \sqrt{(2\ell_1+1)(2\ell_2+1)} \\ &\times (2j_I+1)(2j+1) \sum_{m,m_I} \begin{pmatrix} j & j_I & \ell_1 \\ m & -m_I & m_1 \end{pmatrix} \begin{pmatrix} j & j_I & \ell_2 \\ m & -m_I & m_2 \end{pmatrix} \end{aligned} \tag{5.11}$$

Next, we exploit the orthogonality of the Wigner-3J symbols

$$\sum_{m,m_I} \begin{pmatrix} j & j_I & \ell_1 \\ m & -m_I & m_1 \end{pmatrix} \begin{pmatrix} j & j_I & \ell_2 \\ m & -m_I & m_2 \end{pmatrix} = \delta_{L_1 L_2} \frac{1}{2\ell_1+1}$$

to find

$$\begin{aligned}\sum_{m_I} S_c(\mathbf{q},\mathbf{q}';\omega) &= \frac{2k}{\pi}\sum_{\kappa\ell_1} 4\pi \langle\kappa_I|\, j_{\ell_1}(qr)\,|\kappa\rangle \left(\langle\kappa_I|\, j_{\ell_1}(q'r)\,|\kappa\rangle\right)^* \\ &\times \begin{pmatrix} j_I & \ell_1 & j \\ 1/2 & 0 & -1/2 \end{pmatrix}^2 (2j_I+1)(2j+1)\sum_{m1} Y^*_{L1}(\hat{q})Y_{L1}(\hat{q'}) \\ &= \frac{2k}{\pi}\sum_{\kappa}(2j+1)\left\{(2j_I+1)\sum_{\ell_1}(2\ell_1+1)\,\langle\kappa_I|\, j_{\ell_1}(qr)\,|\kappa\rangle\right. \\ &\times \left.\left(\langle\kappa_I|\, j_{\ell_1}(q'r)\,|\kappa\rangle\right)^* \begin{pmatrix} j_I & \ell_1 & j \\ 1/2 & 0 & -1/2 \end{pmatrix}^2 P_{\ell_1}(\hat{q}\cdot\hat{q'})\right\}. \qquad (5.12)\end{aligned}$$

In the above equation, the quantity within the $\{\ldots\}$ reduces to

$$|N_\kappa(q,E)|^2 \equiv (2j_I+1)\sum_{\ell_1}(2\ell_1+1)|\,\langle\kappa_I|\, j_{\ell_1}(qr)\,|\kappa\rangle\,|^2 \begin{pmatrix} j_I & \ell_1 & j \\ 1/2 & 0 & -1/2 \end{pmatrix}^2$$

for the case of $\mathbf{q} = \mathbf{q}'$. This $|N_\kappa(q,E)|^2$ is seen to be the relativistic equivalent of the $|M_\ell(q,E)|^2$ quantities defined in Eq. (17) of Soininen et al.[23]

5.5 Case of equal magnitude momentum transfers

For the case of $|\mathbf{q}| = |\mathbf{q}'|$ we see that the only difference between the MDFF and the DFF comes from the factor of $P_{\ell_1}(\hat{q}\cdot\hat{q'})$ which appears in the sum over reduced matrix elements in Eq. (5.7).

For the case of K-shell or L1-shell $|\mathbf{q}| = |\mathbf{q}'|$ scattering, the problem of calculating the MDFF simplifies a great deal further; given a DFF (i.e., diagonal elements only)

$$S(q,\omega) = \sum_\ell S_\ell(q,\omega)$$

which is a sum of angular contributions of the type already available in the output of FEFFq, the generalization to the MDFF (i.e., all off-diagonal and diagonal elements) is obtained by the simple replacement

$$S_\ell \rightarrow S_\ell P_\ell(\hat{q}\cdot\hat{q'})\,. \qquad (5.13)$$

For the general case of non-spherically symetric initial states (non K-shell or L1-shell) the above simplifying trick will not work and one must calculate with Eq. (5.7) directly. An example calculation for a non-spherically symmetric initial state is shown in Fig. (5.4).

Also shown are the MDFF for K-shell scattering off of copper, K-shell GeCl4, and L1-shell nickel calculated using the simplified form of Eq. 5.13. These results are shown in Figs. (5.1,5.2,5.3).

5.6 Results and Discussion.

We have included some figures showing the MDFF for nickel, copper, and GeCl4 evaluated for equal magnitudes of momentum-transfers and for all angles between momentum transfers. In Figs. (5.1,5.2,5.3) the axis which runs from -1 to 1 is the variable $(\hat{q} \cdot \hat{q}')$. The other "horizontal" axis is energy-loss (in eV) and the last axis is the value of the MDFF (in eV^{-1}).

In Fig. (5.4) we plot in two dimensions for clarity and the third dimension (angle between q and q') has been demoted to a graph key label. In Fig. (5.4) the term "old code" refers to the FEFFq DFF code, and thus should be equivalent to our MDFF calculation when $\vec{q}$ and $\vec{q}'$ point in the same direction.

5.7 Conclusions.

We have presented *ab initio* calculations of the MDFF for a variety of condensed matter systems.

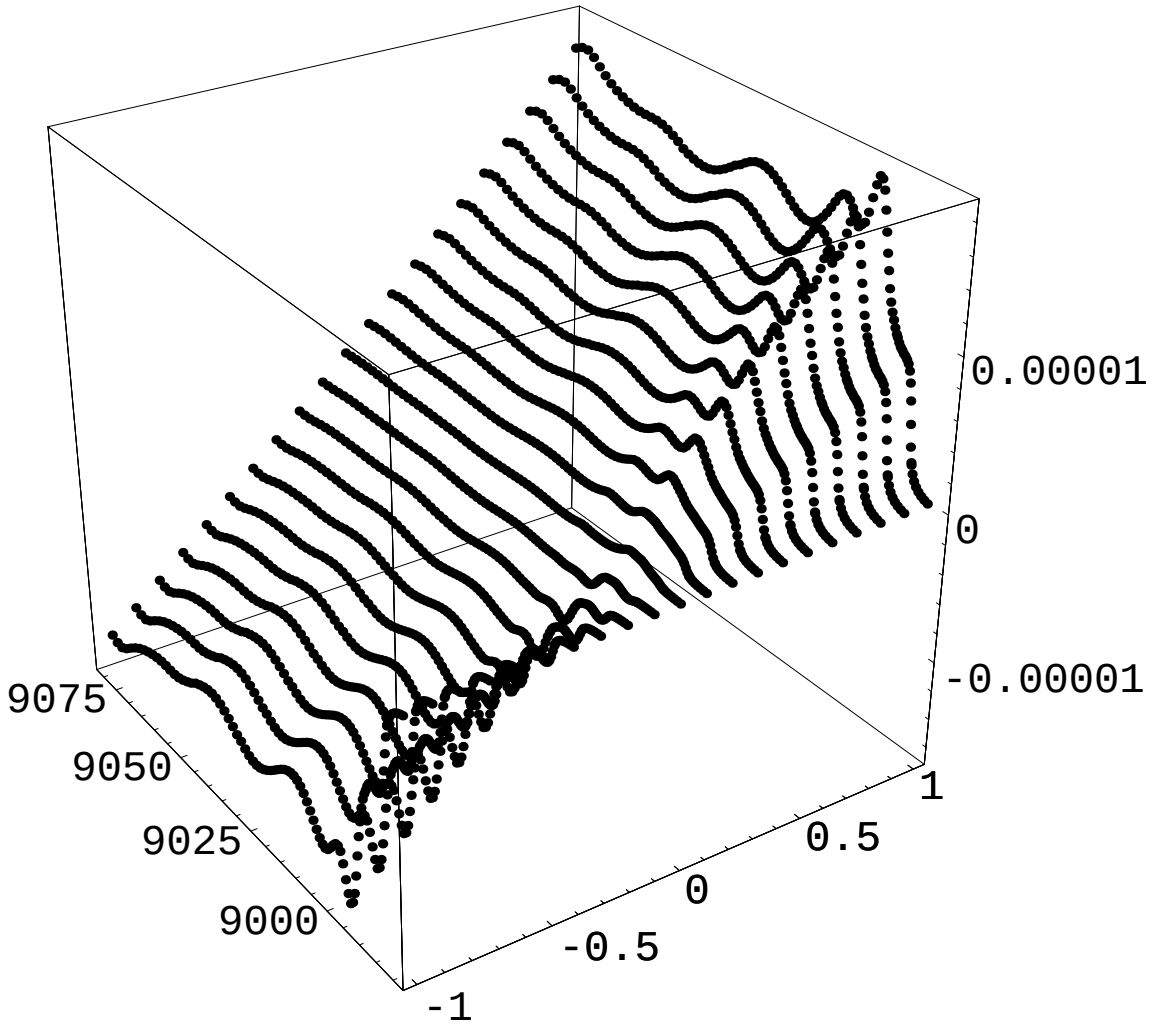

Figure 5.1: MDFF for Copper near K-shell energies. The MDFF is plotted versus energy-loss (in eV) and the cosine of the angle between $\mathbf{q}$ and $\mathbf{q}'$.

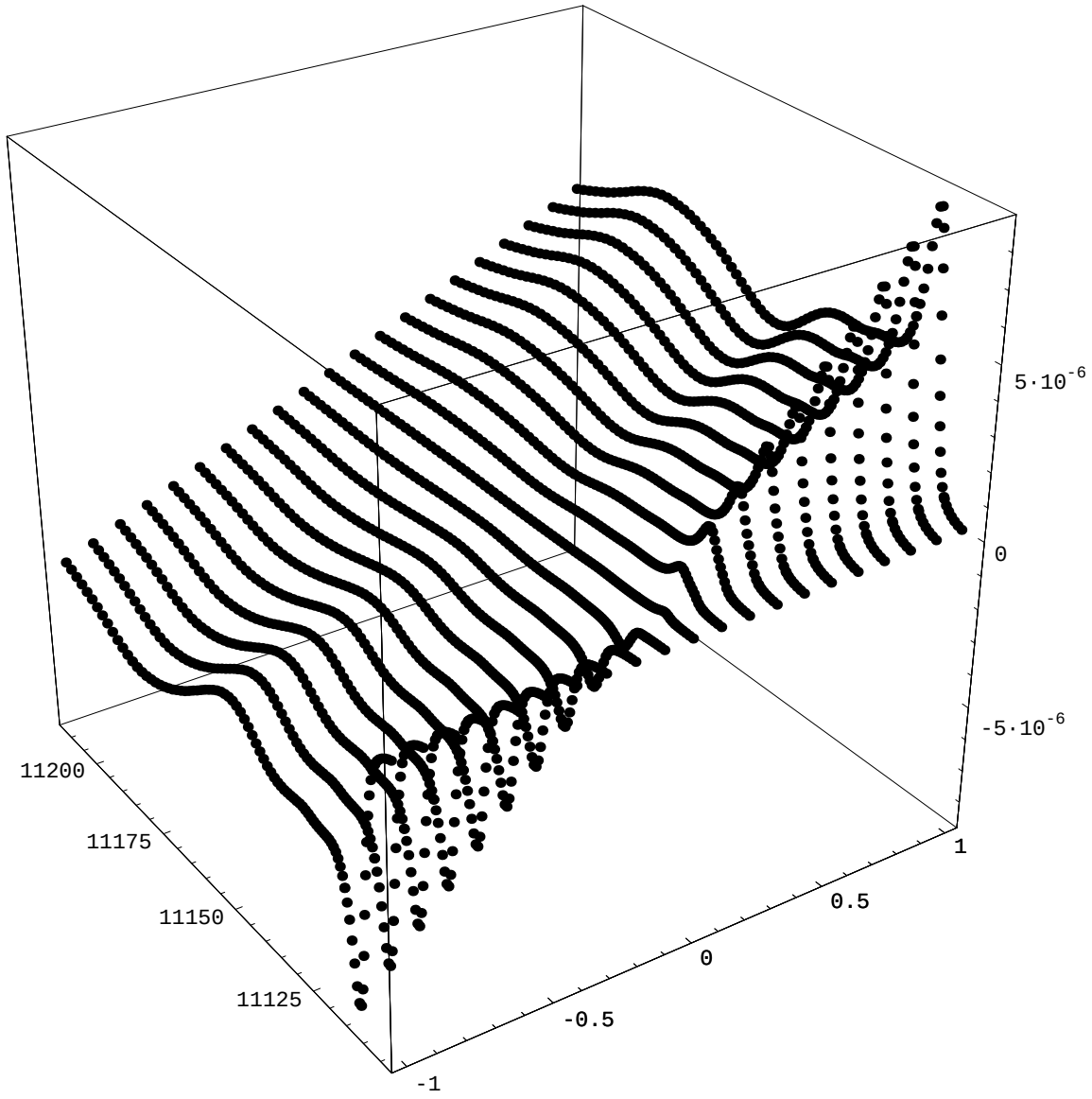

Figure 5.2: MDFF for GeCl4 near K-shell energies. The MDFF is plotted versus energy-loss (in eV) and the cosine of the angle between $\mathbf{q}$ and $\mathbf{q}'$.

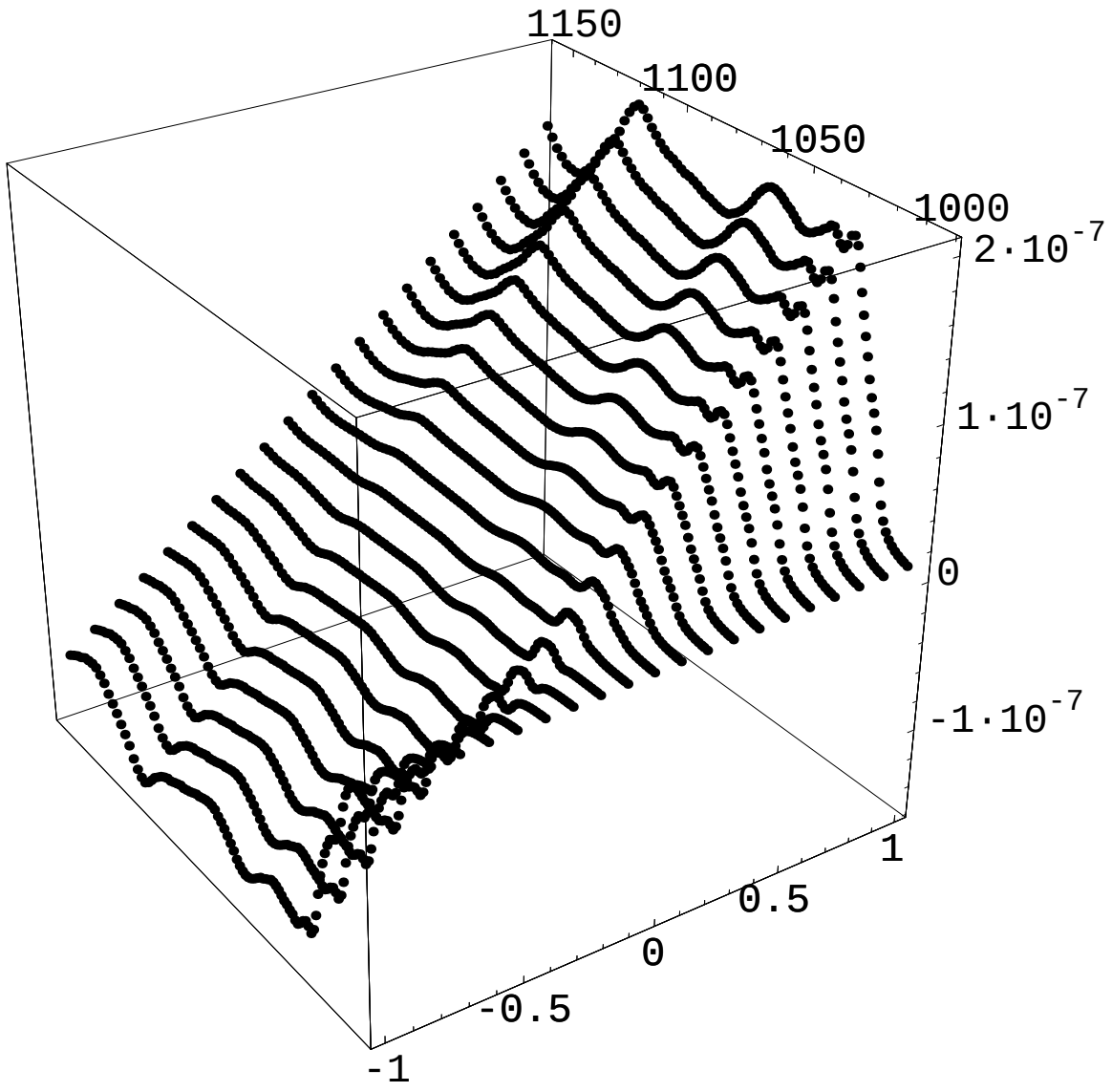

Figure 5.3: MDFF for nickel near L1-shell energies. The MDFF is plotted versus energy-loss (in eV) and the cosine of the angle between $\mathbf{q}$ and $\mathbf{q}'$.

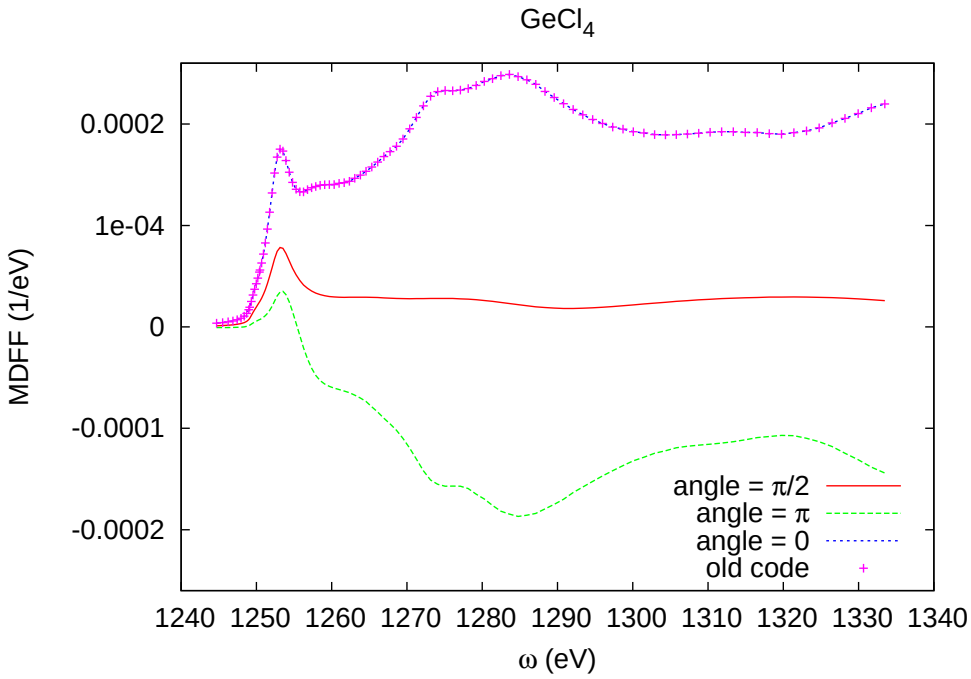

Figure 5.4: MDFF for GeCl4 near L2-shell energies. The MDFF is plotted versus energy-loss (in eV). The "angle" specified in the key is the angle between $\mathbf{q}$ and $\mathbf{q}'$. The label "Old Code" refers to `FEFFq`.

Chapter 6

CONCLUSIONS

The work presented in this thesis builds on previous theory that is now nearly 100 years old. The progress that we have been able to make in recent years is, to a large part, based on the exploitation of modern computing power and recent advances[75, 64] in theory and efficient theoretical techniques. Using this power we have been able to start from first principles and calculate theoretical results in agreement with experiment for many kinds of materials. In particular, this work relies heavily on the availability of *ab initio* calculations of optical dielectric response over a broad spectral range. We obtained our dielectric functions from a generalization[2, 79] of the real-space multiple-scattering Green's function code `FEFF8`[1]. We then used this dielectric function in two different ways. In Chapter 3 we combined our *ab initio* dielectric function with a relativistic "optical data" model[13] in order to obtain relativistic *ab initio* stopping powers, mean free paths, and mean excitations energies. In Chapter 4 we utilized our *ab initio* dielectric function by modifiying a relativistic theory[108] of the EELS magic angle to include dielectric response via the generalized Lorenz gauge. This allowed us, since we knew the dielectric response from the begining, to obtain material-dependent magic angle ratios for high energy transmission electron microscopes.

In Chapter (3) we presented *ab initio* calculations, based on a real-space Green's function approach implemented in the `FEFF8`[1] computer program, of relativistic stopping powers and inelastic mean free paths in real condensed matter systems. Also, we calculated the "mean excitation energy" $\log(I)$ which is a parameter in the relativistic Bethe formula. This parameter is interesting because it can not be calculated for a solid without recourse to intensive numerics. This is so because $\log(I)$ depends on the details of the response over a broad spectrum. We have presented calculations for aluminum, silicon, copper, silver, and gold. We have found that accurate calculations of these parameters depend on the quality of

the optical loss function $-\mathrm{Im}(1/\epsilon)$, but not on the details of extension to finite wavelength. In order to perform these calculations we used an optical loss function calculated with the computer program FEFF8[1] as input into our "optical data model". This method allowed us to obtain *ab initio* inelastic parameters in good agreement with experimental data over a broad range of incident electron energies. For example, our *ab initio* stopping power calculation can be extended down to energies on the order of 10 eV, while still maintaining reasonable agreement with experiment. This lower limit is much better than the limit of applicability of the Bethe formula. In light of the broad spectral range of applicability of these calculations, our *ab initio* approach has the potential to compliment or provide an alternative to semi-empirical approaches for calculations of IMFP and stopping power of electrons in condensed matter.

In Chapter (4) we have developed a fully relativistic theory of the EELS magic angle starting from the QED Hamiltonian of the many body system. We find approximately a factor-of-two "transverse" correction to the non-relativistic magic angle ratio. We have shown how the effects of macroscopic electrodynamic response (screening) can be incorporated into a relativistic independent-particle formalism via the generalized Lorenz gauge. In particular, we predict that dielectric screening effects are important for determining the correct, material-dependent, magic angle at low energy-loss. We used our screened theory in conjunction with *ab initio* calculations of the dielectric function to calculate the relativistic and dielectric corrections to the EELS magic angle for boron nitride and graphite.

In Chapter (5), we have presented a number of calculations of the mixed dynamic form factor. Quantitative calculations of the MDFF are important for a proper description of a variety of new EELS techniques[109]. Our work on the MDFF was accomplished by modifying a recent[23] extension of the `FEFF8` program which was developed to simulate NRIXS spectra.

6.0.1 Future Goals

One practical goal for the immediate future, which builds on work presented in this thesis, is the smooth integration of our codes with the next generation `FEFF9` computer code.

In particular, our calculations of relativistic stopping powers, mean free paths, and mean excitation energies can be further automated and integrated into the `FEFF9` full-spectrum technology. In addition, the work done in this thesis on the MDFF should also be extended. Currently, the non-dipole MDFF can only be calculated for equal magnitudes of momentum transfer $q = q'$. The dipole MDFF has already[22] been integrated into the `FEFF` code system for arbitrary values of $\mathbf{q}$ and $\mathbf{q}'$ (trivially, since the transfered momenta "factor out" in the dipole case) subject, of course, to the condition that q and q' are small enough that the dipole approximation is valid.

Further theoretical work on the DFF is also an important future goal. In particular, the inclusion of screening should be important in many of the same cases where it is important for x-ray absorption[110]. We should emphasise that this screening effect should not be handled in the same way that we screened relativistic electrons in Chapter 4. Rather, in this case a time-dependent density functional theory (TDDFT) approach is more appropriate.

Formally, one can see how to include screening for the MDFF and the DFF as follows: The MDFF is closely related to the off-diagonal density response function $\chi(\mathbf{q}, \mathbf{q}', \omega)$. That is, given an external field of the form

$$\phi^{\mathbf{q}'}_{\text{ext}}(\mathbf{r}) = e^{i(\mathbf{q}'\cdot\mathbf{r}' - \omega t)} = e^{-i\omega t} \left|\mathbf{q}'\right\rangle \ , \tag{6.1}$$

then the density response $\rho(\mathbf{q}, \omega)$ at wavevector[1] $\mathbf{q}$ is equal to $\chi(\mathbf{q}, \mathbf{q}'; \omega)$. We thus write,

$$\chi(\mathbf{q}, \mathbf{q}'; \omega) = \langle \mathbf{q}| \, \chi_0(\omega) \left|\mathbf{q}'_{\text{SCF}}\right\rangle = \langle \mathbf{q}_{\text{SCF}}| \, \chi_0(\omega) \left|\mathbf{q}'_{\text{SCF}}\right\rangle - \langle \mathbf{q}_{\text{SCF}}| \, \chi_0^\dagger(\omega) K(\omega) \chi_0(\omega) \left|\mathbf{q}'_{\text{SCF}}\right\rangle \ , \tag{6.2}$$

where $\chi_0(\omega)$ is the independent particle density response function, and

$$|\mathbf{q}_{\text{SCF}}\rangle = (1 + K\chi) \, |\mathbf{q}\rangle = |\mathbf{q}\rangle + K\chi_0 \, |\mathbf{q}_{\text{SCF}}\rangle \ , \tag{6.3}$$

and the kernal $K(\omega)$ relates the induced (screening) field to the density response. This kernal has well-known[111] approximations within TDDFT.

In order to obtain the DFF we may set $\mathbf{q} = \mathbf{q}'$ and take the imaginary part of Eq. (6.2) to find

$$S(\mathbf{q}, \omega) = -\frac{1}{\pi} \text{Im}(\chi(\mathbf{q}, \mathbf{q}; \omega)) = -\frac{1}{\pi} \langle \mathbf{q}_{\text{SCF}}| \, \text{Im}(\chi_0(\omega)) \, |\mathbf{q}_{\text{SCF}}\rangle \ . \tag{6.4}$$

[1] recall that $\mathbf{q}$ may be different from $\mathbf{q}'$ in an (spatially) inhomogeneous system.

Thus the DFF takes the same form as in the independent particle picture, cf. Eq. (5.4), but with screened (SCF) matrix elements. These screened matrix elements should be calculated using currently available `FEFF` technology and used in DFF calculations in place of the unscreened matrix elements.

BIBLIOGRAPHY

[1] A. L. Ankudinov, B. Ravel, J. J. Rehr, and S. D. Conradson *Phys. Rev. B*, vol. 58, p. 7565, 1998.

[2] M. Prange, J. Rehr, G. Rivas, and J. Kas unpublished.

[3] H. J. Hagemann, W. Gudat, and C. Kunz *J. Opt. Soc. Am.*, vol. 65, p. 7421, 1975.

[4] H. J. Hagemann, W. Gudat, and C. Kunz, *Optical Constants from the Far Infrared to the X-ray Region: Mg, Al, Cu, Ag, Au, Bi, C and Al_2O_3, DESY SR-7417.* Desy, Hamburg, W. Germany, 1974.

[5] W. S. M. Werner *Surf. Interface Anal.*, vol. 31, p. 141, 2001.

[6] C. J. Powell and A. Jablonski *J. Phys. Chem. Ref. Data*, vol. 28, p. 19, 1999.

[7] E. Fermi *Phys. Rev.*, vol. 57, p. 485, 1940.

[8] M. J. Berger, J. S. Coursey, M. A. Zucker, and J. Chang, *ESTAR, PSTAR, and ASTAR: Computer Programs for Calculating Stopping-Power and Range Tables for Electrons, Protons, and Helium Ions (version 1.2.3).* National Institute of Standards and Technology, Gaithersburd, MD.

[9] S. Tanuma, C. J. Powell, and D. R. Penn *Surf. Interface Anal.*, vol. 37, p. 978, 2005.

[10] S. Luo, X. Zhang, and D. C. Joy *Radiat. Eff. Def. Solids*, vol. 117, p. 235, 1991.

[11] P. Hovington, D. C. Joy, R. Gauvin, and N. Evans *Scanning Microsc.*, vol. 10, p. 653, 1996.

[12] M. S. Macpherson, *Accurate Measurements of the Collision Stopping Powers for 5 to 30 MeV Electrons, Ph.D. Thesis.* PhD thesis, NRC Report PIRS-0626, 1998.

[13] J. M. Fernández-Varea, F. Salvat, M. Dingfelder, and D. Liljequist *Nucl. Instr. and Meth. B*, vol. 229, p. 187, 2005.

[14] H. Daniels, A. Brown, A. Scott, T. Nichells, B. Rand, and R. Brydson *Ultramicroscopy*, vol. 96, p. 523, 2003.

[15] C. Tschalar and H. Bichsel *Phys. Rev.*, vol. 175, p. 476, 1968.

[16] ICRU, *ICRU Report 37, Stopping Powers and Ranges for Protons and Alpha Particles.* International Commission of Radiation Units and Measurements., 1984.

[17] N. Bohr, *Niels Bohr Collected Works (Volume 2).* North-Holland, 1981.

[18] N. Bohr *Phil. Mag.*, vol. 25, p. 10, 1913.

[19] N. Bohr *Mat. Fys. Medd. Dan. Vidensk. Selsk.*, vol. 18, p. 1, 1948.

[20] N. Bohr, *Niels Bohr Collected Works (Volume 8).* North-Holland, 1987.

[21] H. Bethe, "Theory of passage of swift corpuscular rays through matter," *Ann. Phys.*, vol. 5, pp. 325–400, 1930.

[22] K. Jorissen, *The Ab Initio Calculation of Relativistic Electron Energy Loss Spectroscopy.* PhD thesis, University of Antwerp, 2007.

[23] J. A. Soininen, A. L. Ankudinov, and J. J. Rehr *Phys. Rev. B*, vol. 72, p. 045136, 2005.

[24] A. P. Sorini, J. J. Kas, J. J. Rehr, M. P. Prange, and Z. H. Levine *Phys. Rev. B*, vol. 74, p. 165111, 2006.

[25] A. P. Sorini, J. J. Rehr, and Z. H. Levine *Phys. Rev. B*, vol. 77, p. 115126, 2008.

[26] E. Fermi, *Nuclear Physics.* University of Chicago Press, 1950.

[27] H. Frohlich, *Theory of Dielectrics.* Oxford University Press, 1958.

[28] J. D. Jackson, *Classical Electrodynamics (Third Edition).* Wiley, 1999.

[29] L. D. Landau, E. M. Lifshitz, and L. P. Pitaevskii, *Electrodynamics of Continuous Media, Second Edition.* Permagon Press, 1984.

[30] J. Schwinger, J. L. L. DeRaad, K. A. Milton, and W. Tsai, *Classical Electrodynamics.* Perseus Books, 1998.

[31] H. A. Bethe and R. W. Jackiw, *Intermediate Quantum Mechanics (Second Edition).* W. A. Benjamin, Inc., 1968.

[32] N. F. Nott and H. S. W. Massey, *The Theory of Atomic Collisions (Third Edition).* Oxford, 1965.

[33] O. V. Dolgov, D. A. Kirzhnits, and E. G. Maksimov *Rev. Mod. Phys.*, vol. 53, p. 81, 1981.

[34] D. Pines and P. Nozieres, *The Theory of Quantum Liquids (vol. 1)*. W. A. Benjamin, Inc., 1966.

[35] A. Messiah, *Quantum Mechanics (Volume 1)*. North-Holland, 1961.

[36] A. Messiah, *Quantum Mechanics (Volume 2)*. North-Holland, 1962.

[37] H. A. Bethe and E. E. Salpeter, *Quantum Mechanics of One- and Two-Electron Atoms*. Plenum, 1957.

[38] C. Cohen-Tannoudji, B. Diu, and F. Laloe, *Quantum Mechanics*. John Wiley and Sons, 1977.

[39] D. Pines, *The Many-Body Problem*. W. A. Benjamin, 1961.

[40] M. Gell-Mann and F. Low *Phys. Rev.*, vol. 84, pp. 350–354, 1951.

[41] G. D. Mahan, *Many-Particle Physics*. Plenum Press, 1981.

[42] A. A. Abrikosov, L. P. Gorkov, and I. E. Dzyaloshinski, *Methods of Quantum Field Theory in Statistical Physics*. Dover, 1963.

[43] P. C. Martin, *Measurements and Correlation Functions*. Gordon and Breach, 1968.

[44] M. L. Goldberger and K. M. Watson, *Collision Theory*. John Wiley & Sons, Inc., 1964.

[45] J. R. Taylor, *Scattering Theory*. Wiley, 1972.

[46] R. G. Newton, *Scattering Theory of Waves and Particles*. Springer-Verlag, 1982.

[47] C. J. Joachain, *Quantum Collision Theory*. North-Holland, 1975.

[48] L. S. Brown, *Quantum Field Theory*. Cambridge University Press, 1992.

[49] M. E. Peskin and D. V. Schroeder, *An Introduction to Quantum Field Theory*. Westview, 1995.

[50] A. L. Fetter and J. D. Walecka, *Quantum Theory of Many-Particle Systems*. McGraw-Hill, 1971.

[51] L. Hedin and S. Lundqvist *Solid State Phys.*, vol. 23, p. 1, 1969.

[52] H. A. Bethe and N. D. Mermin *Physics Today*, vol. 57, p. 53, 2004.

[53] W. Kohn and L. J. Sham *Phys. Rev.*, vol. 140, p. A1133, 1965.

[54] P. Hohenberg and W. Kohn *Phys. Rev.*, vol. 136, p. B864, 1964.

[55] R. O. Jones and O. Gunnarsson *Rev. Mod. Phys.*, vol. 61, p. 698, 1989.

[56] S. B. Trickey, ed., *Advances in Quantum Chemistry*, vol. 21. Academic Press, Inc., 1990.

[57] K. Burke, *The ABC of DFT*. http://dft.uci.edu/book/gamma/g1.pdf, 2007.

[58] M. Levy *Proc. Natl. Acad. Sci. USA*, vol. 76, p. 6062, 1979.

[59] L. Hedin *Phys. Rev.*, vol. 139, p. A796, 1965.

[60] M. S. Hybertson and S. G. Louie *Phys. Rev. B*, vol. 34, p. 5390, 1986.

[61] L. J. Sham and W. Kohn *Phys. Rev.*, vol. 145, p. 561, 1966.

[62] B. I. Lundqvist *Phys. kondens. Materie*, vol. 6, p. 206, 1967.

[63] J. J. Kas unpublished.

[64] J. J. Kas, A. P. Sorini, M. P. Prange, , L. W. Campbell, and J. Rehr *Phys. Rev. B*, vol. 76, p. 195116, 2007.

[65] U. Fano *Ann. Rev. Nucl. Sci.*, vol. 13, p. 1, 1963.

[66] H. Bichsel in *Atomic, Moecular, and Optical Physics Handbook* (G. W. F. Drake, ed.), AIP Press, Woodbury, N.Y., 1996.

[67] I. Campillo, J. M. Pitarke, A. Rubio, E. Zarate, and P. M. Echenique *Phys. Rev. Lett.*, vol. 83, p. 2230, 1999.

[68] J. A. Soininen, J. J. Rehr, and E. L. Shirley *J. Phys.: Condens. Matter*, vol. 15, p. 2572, 2003.

[69] D. R. Penn *Phys. Rev. B*, vol. 35, p. 482, 1987.

[70] R. M. Sternheimer, S. M. Seltzer, and M. J. Berger *Phys. Rev. B*, vol. 26, p. 6067, 1982.

[71] R. M. Sternheimer, S. M. Seltzer, and M. J. Berger *Phys. Rev. B*, vol. 27, p. 6971, 1983.

[72] I. Abril, R. Garcia-Molina, C. D. Denton, F. J. Perez-Perez, and N. R. Arista *Phys. Rev. A*, vol. 58, p. 357, 1998.

[73] S. Heredia-Avalos, R. Garcia-Molina, J. M. Fernandez-Varea, and I. Abril *Phys. Rev. A*, vol. 72, p. 052902, 2005.

[74] C. C. Montanari and J. E. Miraglia *Phys. Rev. A*, vol. 73, p. 024901, 2006.

[75] J. J. Rehr, J. J. Kas, M. P. Prange, F. D. Vila, A. L. Ankudinov, L. W. Campbell, and A. P. Sorini unpublished, arXiv:cond-mat/0601242v1, 2006.

[76] D. Liljequist *J. Phys. D: Appl. Phys.*, vol. 16, p. 1567, 1983.

[77] J. C. Ashley, J. J. Cowan, R. H. Ritchie, V. E. Anderson, and J. Hoelzl *Thin Solid Films*, vol. 60, p. 361, 1979.

[78] J. C. Ashley *J. Electron Spectrosc. Relat. Phenom.*, vol. 46, p. 199, 1988.

[79] M. Prange, G. Rivas, and J. J. Rehr, *Table of Optical Constants for Mg, Al, Cu, Ag, Au, Bi and C.* World Wide Web, 2008. http://leonardo.phys.washington.edu/feff/opcons/.

[80] A. P. Sorini, J. Kas, J. J. Rehr, and M. P. Prange, *Tables of mean free paths and stopping powers.* World Wide Web, 2005. http://leonardo.phys.washington.edu/feff/loss/.

[81] H. Bichsel *Phys. Rev. A*, vol. 46, p. 5761, 1992.

[82] F. Salvat, J. M. Fernández-Varea, and J. Sempau, *PENELOPE - A Code System for Monte Carlo Simulation of Electron and Photon Transport.* OECD/Nuclear Energy Agency, Issy-les-Moulineaux, France.

[83] J. J. Quinn *Phys. Rev.*, vol. 126, p. 1453, 1962.

[84] P. Sigmund and A. Schinner *Nucl. Instrum. Methods Phys. Res. B*, vol. 212, p. 110, 2003.

[85] M. Inokuti *Rev. Mod. Phys.*, vol. 43, p. 297, 1971.

[86] B. Jouffrey, P. Schattschneider, and C. Herbert *Ultramicroscopy*, vol. 102, p. 61, 2004.

[87] A. T. Paxton, M. van Schilfgaarde, M. Mackenzie, and A. J. Craven *J. Phys.: Condens. Matter*, vol. 12, p. 729, 2000.

[88] C. Hebert, B. Jouffrey, and P. Schattschneider *Ultramicroscopy*, vol. 101, p. 271, 2004.

[89] C. M. Moller *Ann. Phys.*, vol. 14, p. 531, 1932.

[90] U. Fano *Phys. Rev.*, vol. 102, p. 385, 1956.

[91] W. Heitler, *The Quantum Theory of Radiation, Third Edition.* Clarendon Press, Oxford, 1954.

[92] P. Schattschneider, C. Hérbert, and H. Franco *Phys. Rev. B*, vol. 72, p. 045142, 2005.

[93] K. Fujiwara *J. Phys. Soc. Japan*, vol. 16, p. 2226, 1961.

[94] L.-M. Peng, S. Dudarev, and M. Whelan, *High-Energy Electron Diffraction and Microscopy.* Oxford University Press, 2004.

[95] G. D. Mahan, *Many-Particle Physics.* Plenum Press, New York, 1981.

[96] E. Cockayne and Z. H. Levine *Phys. Rev. B*, vol. 74, p. 235107, 2006.

[97] M. Prange, G. Rivas, J. Rehr, and A. Ankudinov unpublished.

[98] A. L. Ankudinov, Y. Takimoto, and J. J. Rehr *Phys. Rev. B*, vol. 71, p. 165110, 2005.

[99] L. V. Hove *Phys. Rev.*, vol. 95, p. 249, 1954.

[100] P. Schattschneider, S. Rubino, C. Hebert, J. Rusz, J. Kunes, P. Novak, E. Carlino, M. Fabrizioli, G. Panaccione, and G. Rossi *Nature*, vol. 441, p. 486, 2006.

[101] H. Kohl and H. Rose *Advances in Electronics and Electron Physics*, vol. 65, p. 173, 1985.

[102] P. Schattschneider, M. Nelhiebel, and B. Jouffrey *Phys. Rev. B*, vol. 59, p. 10959, 1999.

[103] P. A. Lee and J. B. Pendry *Phys. Rev. B*, vol. 11, p. 2795, 1975.

[104] J. J. Rehr and R. C. Albers *Phys. Rev. B*, vol. 41, p. 8139, 1990.

[105] J. J. Rehr and R. C. Albers *Rev. Mod. Phys.*, vol. 72, p. 621, 2000.

[106] A. Gonis and W. H. Butler, *Multiple scattering in solids*. Springer, New York, 2000.

[107] I. P. Grant *Advances in Physics*, vol. 19, p. 747, 1970.

[108] P. Schattschneider, C. Hebert, and H. Franco, "Anisotropic relativistic cross sections for inelastic electron scattering, and the magic angle," *Phys. Rev. B*, vol. 72, p. 045142, 2005.

[109] P. Schattschneider, S. Rubino, C. Hebert, J. Rusz, J. Kunes, P. Novak, E. Carlino, M. Fabrizioli, G. Panaccione, and G. Rossi *Nature*, vol. 441, p. 486, 2006.

[110] A. Zangwill and P. Soven *Phys. Rev. A*, vol. 21, p. 1561, 1980.

[111] E. K. U. Gross and W. Kohn, *Advances in Quantum Chemistry Volume 21*, pp. 255–291. Academic Press, 1990.

Appendix A

NEW AND MODIFIED COMPUTER CODES

The purpose of this Appendix is to describe in detail the computer codes used in the numerical calculations presented in this thesis. In order to accomplish the work presented in this thesis we wrote three programs and modified four `FEFFq`[23] program modules.

The first two programs we discuss are named `lamb.x` and `tot2.x`. These programs were used to calculate stopping powers and mean free paths via the relativistic formalism presented in Chapter 3. The program `lamb.x` calculates both inelastic mean free paths and stopping powers in the non-relativistic region. The program `tot2.x` calculates the stopping power in the relativistic region as well as auxilliary parameters such as the density-effect correction.

The third program we wrote is named `magic.x`. This program was used to calculate the relativistic and dielectric corrections to the EELS magic angle presented in Chapter 4.

A.1 Stopping Power Code: `lamb.x` *and* `tot2.x`

A.1.1 Introduction

These computer programs were written to calculate the inelastic mean free path (IMFP) and the collision stopping power (CSP) of a relativistic probe electron within a solid.

A.1.2 Input

The input for the code `lamb.x` is the $q = 0$ complex dielectric function $\epsilon(\omega)$, where ω is the angular frequency. This input file is a text file consisting of 8 columns of numbers and it must be named `opconsKK.dat`. The input text file may have a header of comments. Comments may only be in the head of the file. Comments are here defined as lines of text which begin with either `#`, or `!`, or `c`, or `*`.

The first column of numbers in the input text file must contain the value of the angular-frequency in eV; the second column must contain the real part of $\epsilon(\omega) - 1$; the third column must contain the imaginary part of $\epsilon(\omega)$; the eighth column must contain the imaginary part of $-1/\epsilon(\omega)$; the other columns of `opconsKK.dat` are not used by the code `lamb.x`.

The input for the code `tot2.x` is also the $q = 0$ dielectric function given as a text file named `opconsKK.dat` in the same format as described above. The code `tot2.x` also requires that the user enter the square of the all-electron plasma frequency, and the logarithm of the numerical value the mean excitation energy in Hartree.

A.1.3 Output

The output of the code `lamb.x` are the files `lamb.dat` and `lowsp.dat`. The file `lamb.dat` is a text file containing three columns. The first column gives the energy in units of eV. The second column is set to zero. The third column gives the value of the inelastic mean free path in inverse Angstroms.

The output of the code `tot2.x` is the file `sp.dat` containing the relativistically correct stopping power. The file is a two-column text file. The first column gives the energy in eV. The second column gives the stopping power in eV/Angstroms.

A.1.4 Example Program Usage

Once we have obtained the file `opconsKK.dat` running the code is very simple. In the following we assume that the files `opconsKK.dat`, `lamb.x`, and `tot2.x` are all in the same directory. Change directories to the directory containing our files and then run the codes. When running `tot2.x` we will be prompted to enter the plasma frequency (squared) and the log of the mean excitation energy. The following example illustrates this for a material with $\Omega_p^2 = 1077$ and $\log(I) = 1.9$:

```
[asorini@botticelli test]$ ls
lamb.x opconsKK.dat tot2.x
[asorini@botticelli test]$ ./lamb.x
[asorini@botticelli test]$ ls
```

```
lamb.dat  lamb.x  lowsp.dat  opconsKK.dat  tot2.x
[asorini@botticelli test]$ ../tot2.x
 enter omega_p**2.
 further info in putit.f code
1077
 enter lni
1.9
 making F(L) from opconsKK.dat...
 FL.dat created.
 making delta_f from opconsKK.dat and FL.dat...
 deltafF.dat created.
 making sp.dat...
 done.
[asorini@botticelli test]$ ls
lamb.dat  lamb.x  lowsp.dat  opconsKK.dat  sp.dat  tot2.x
```

A.2 Magic Angle Code: `magic.x`

A.2.1 Introduction

This computer program was written in order to calculate the relativistically correct EELS magic angle for a material, specified by its dielectric function. The EELS magic angle also depends on the transmission electron microscope's operating voltage (incident electron energy).

A.2.2 Input

The input for the code `magic.x` is the $q = 0$ complex dielectric function $\epsilon(\omega)$. The dielectric function must be contained in a file named `opconsKK.dat`. The form of this input file is exactly as specified in the previous Section.

A.2.3 Output

The output of the code `magic.x` is the file `magic.dat`. The output file is a plain text file consisting of a header followed by three columns of data. Column one gives the energy-loss in eV; column two gives the value of the relativistically correct EELS magic angle θ_M; column three gives the value of the microscope characteristic angle θ_E.

A.2.4 Example Program Usage

Once we have the file `opconsKK.dat`, running the code is very simple. In the following we assume that the files `opconsKK.dat` and `magic.x` are both in the same directory (called test2 in the following). In this example we take the TEM voltage to be 100 keV:

```
[asorini@botticelli test2]$ ls
magic.x  opconsKK.dat
[asorini@botticelli test2]$ ./magic.x
 Enter microscope voltage in eV:
100000
   100000.000000000
 reading opconsKK.dat ...
 calculating ...
  ... done!
[asorini@botticelli test2]$ ls
magic.dat  magic.x  opconsKK.dat
```

A.3 Modified Subroutines of `FEFFq`

The MDFF calculations presented in this thesis are based on modifcations made to the computer program `FEFFq`[23]. That program, in turn, is an extension of the computer program `FEFF8`[1]. The computer program `FEFFq` calculates the diagonal elements of the MDFF. Our extension of `FEFFq` calculates the off-diagonal elements of the MDFF for equal magnitudes of momentum transfers $q = q'$. In this case, one must specify the angle between

$\mathbf{q}$ and $\mathbf{q}'$

$$\hat{q} \cdot \hat{q}' = \cos(\theta) \ .$$

Within the code this number is refered to as `cosleg`.

Once this angle has been read in by our modified `FEFFq` code, the formula given in Eq. (5.6) can easily be implemented as an extension of the current `FEFFq` subroutines. More precisely, we list below the modified subroutines of `FEFFq` and our modifications:

A.3.1 COMMON: itoken

This subroutine was modified in order to recognize the `ADAM` card in the `feff.inp` input file. This card corresponds to itoken=55 in `FEFFq`. The value of $\hat{q} \cdot \hat{q}'$ is given as the argument of the `ADAM` card.

A.3.2 RDINP: rdinp

This subroutine was modified by adding token 55 corresponding to the `ADAM` card in order to read in the value of $\hat{q} \cdot \hat{q}'$ to a variable named `cosleg` in the code. This is the numerical value of the cosine of the angle between $\mathbf{q}$ and $\mathbf{q}'$. For example, if we want to specify that $\mathbf{q}$ and $\mathbf{q}'$ are perpendicular we would add the line

```
ADAM 0
```

to the `feff.inp` input file. Or, if we wish to reproduce the results of `FEFFq` (for which $\mathbf{q}$ and $\mathbf{q}'$ are parallel) we would instead specify

```
ADAM 1
```

in the `feff.inp` input file.

A.3.3 RDINP: iniall

The variable `cosleg` is initalized to (double precision) zero.

A.3.4 RDINP: allinp.h

The variable `cosleg` is put in the common block `qveci`.

A.3.5 RDINP: wrtall

The value of `cosleg` read from the input file is written to the standard input files for the modules `mod2.inp` and `mod3.inp`.

A.3.6 FMS: ffmod3

This subroutine calls the subroutine `reafms` and the call to `reafms` was modified by adding the variable `cosleg`.

A.3.7 FMS: reafms

This subroutine was modified to read in the variable `cosleg` from the standard input file `mod2.inp`.

A.3.8 FMS: fmstot

This subroutine was modified by adding a call to `cpl0` in order to obtain the Legendre polynomials P_ℓ(`cosleg`) for $\ell = 0$ to `ljmax`. `ljmax` is a variable used in `FEFFq` to specify the maximum angular momentum. The P_ℓ(`cosleg`) are stored in the double precision array `pleg(1:ljmax+1)`. The array `pleg` was then used to multiply the code variables `gtr` and `gtrl`.

A.3.9 XSPH: rexsph

This subroutine was modified to read in the value of `cosleg` from the file `mod3.inp`

A.3.10 XSPH: specupd

This subroutine was modified by adding a call to `cpl0` to obtain the appropriate Legendre polynomials (exactly as in the modifications of FMS). The array `pleg` was then use to multiple the code variable `aa`.

A.3.11 XSPH: specupdatom

This subroutine was modified in the same way as `specupd`.

A.3.12 XSPH: specuplg

This subroutine was modified in the same way as `specupd`.

A.3.13 Input and Output

The input file for our modified version of `FEFFq` is a standard `FEFFq` input file, but now with the `ADAM` card available for specifying the angle between $\mathbf{q}$ and $\mathbf{q}'$. For example, if we want to calculate the MDFF for $q = q' = 6.0$/Bohr and $\hat{q} \cdot \hat{q}' = -0.42$ at the GeCl4 K-edge, we would use put the text

```
TITLE GeCl_4 MDFF
ADAM -0.42
QVEC -1 6.0
LJMAX 10
LDEC 2

CONTROL 1 1 1 1 1 1
NOHOLE
HOLE 1 1.0
RSIGMA
SCF 3.0 1
FMS 3.0 1
RPATH 1.0
XANES 8.0 0.05
AFOLP 1.30
POTE
* ipot z   label
    0  32  Ge  3  3
    1  17  Cl  3  3
ATOMS
   0.0      0.0       0.0      0   Ge
```

```
   1.210    1.210     1.210    1   Cl
   1.210   -1.210    -1.210    1   Cl
  -1.210    1.210    -1.210    1   Cl
  -1.210   -1.210     1.210    1   Cl
END
```

into the file `feff.inp`.

The output is contained in the file `xmu.dat` and the format is the same as for `FEFFq` except that the DFF is replaced by the MDFF. I.e., `xmu.dat` consists of six columns of data. Column one is the energy-loss, column two is photoelectron energy relative to the Fermi energy, column three is photoelectron wavenumber relative to the Fermi momentum, column four is the MDFF, column five is the MDFF atomic background, column six is the MDFF atomic background times the MDFF fine-structure.

VITA

Adam Sorini was born in Ann Arbor, Michigan. He is the great-grandson of a copper miner. He was told that his Vita must include the following sentence. In 2008, Adam graduated from the University of Washington with a Ph.D. in Physics.